

DISSERTATION

IMPORTANCE OF BOUNDARY LAYER ENTRAINMENT FOR SURFACE FLUXES
OVER LAND

Submitted by

Erica L. McGrath-Spangler

Department of Atmospheric Science

In partial fulfillment of the requirements

For the Degree of Doctor of Philosophy

Colorado State University

Fort Collins, Colorado

Fall 2011

Doctoral Committee:

Advisor: A. Scott Denning

David A. Randall

Colette Heald

Dusanka Zupanski

Jennifer A. Hoeting

ABSTRACT

IMPORTANCE OF BOUNDARY LAYER ENTRAINMENT FOR SURFACE FLUXES OVER LAND

An idealized experiment examined the impacts of entrainment in a coupled ecosystem-atmosphere model by implementing an enhanced entrainment parameterization based on the assumption that the heat flux at the top of the PBL is negatively proportional to the heat flux at the surface. This experiment found that entrainment produced a warmer, drier, and deeper PBL and that the surface fluxes of heat and moisture were modified by the vegetative response to the altered atmospheric conditions. A realistic simulation for the summer of 1999 found that enhanced entrainment produced stronger early morning growth of the PBL and a deeper midday depth. This better captured the monthly mean diurnal cycle of PBL depth from observations by a radar sounding system in northern Wisconsin. Additionally, the complex land-atmosphere interactions produced a time-mean spatial CO₂ gradient of 7 ppm over 1000 km. A sensitivity analysis performed for June 2007 to the strength of the PBL-top entrainment flux found subtle spatial variations in the time mean. The addition of entrainment from overshooting thermals weakened the Bermuda high circulation and weakened the spatial gradients between the warm, dry semiarid southwestern United States and cooler, moister locations in eastern North America. These subtle variations

produced a 3.5 ppm CO₂ change in the time mean across 280 km. One possible explanation for these more subtle results is that additional changes to the coupled model resulted in persistent cloud cover that produced relatively cold and dark conditions.

In order to evaluate and improve model simulations, PBL depth has been estimated using the backscatter from the LIDAR onboard the Cloud-Aerosol Lidar and Infrared Pathfinder Satellite Observation (CALIPSO) satellite. Using an automated method, millions of estimates have been derived to which model results can be compared. This method evaluates the maximum vertical variance of the backscatter in order to identify backscatter features associated with the top of the PBL and helps to identify the vertical extent of turbulent mixing. This analysis sheds some light on the spatial heterogeneity of boundary layer processes. The derived depths are shallower over water than over land and show a local minimum along the Mississippi River valley. Deeper features are found over the desert Southwest and deeper than expected values are retrieved over the Boreal forests.

ACKNOWLEDGMENTS

I would like to thank my advisor, Dr. Scott Denning, for his understanding and enthusiasm. His constant reminders to enjoy the journey and never accept the first attempt have made me a better scientist and hopefully a better person. I would also like to thank my committee members, Drs. Dave Randall, Colette Heald, Dusanka Zupanski, and Jennifer Hoeting for taking the time to read and review this dissertation. It is by far the longest thing I've ever written and I'm glad someone did read it.

Thank you to all of the Denning group members. Matt Bishop and Ammon Redman have yet to fail me when it comes to keeping the computers running and answering my various IT questions. Thank you to my officemate Biljana Orescanin. We've listened to each other's trials and tribulations and she has helped me tremendously these last few months. Thank you to Andrew Schuh who was an unexpected source of encouragement and always pushed me to do better. I would not have been able to complete this dissertation without the help of Ian Baker and Mark Branson. Their willingness to help me when I need it the most has supported me so many times.

I am forever grateful to my husband Tim. He has been my best friend through all the ups and downs of graduate school while his trust in me and loving support have allowed me to succeed where I never thought it possible.

The data providers were invaluable to this research. I wish to thank Ken Davis and Liza Diaz at The Pennsylvania State University for the West Branch, Iowa rawinsondes and the WLEF data and Oak Ridge National Laboratory for providing public

access to these data. The Department of Energy ARM program supported the rawinsondes. The NARR data for this study are from the Research Data Archive (RDA), which is maintained by the Computational and Information Systems Laboratory (CISL) at the National Center for Atmospheric Research (NCAR). NCAR is sponsored by the National Science Foundation (NSF). The original data are available from the RDA (<http://dss.ucar.edu>) in data set number ds608.0. The MERRA data for this study are from the Global Modeling and Assimilation Office (GMAO) and the Goddard Earth Sciences Data and Information Services Center (GES DISC). The original data are available from the RDA (<http://dss.ucar.edu>) in data set number ds608.0. I would also like to thank Nikisa Jordan and Mark Vaughan for their assistance with the CALIPSO data and the PBL depth algorithm and the opportunity to attend the CALIPSO science team meeting. I would also like to thank the anonymous reviewers for their work on the two published chapters of this manuscript. This research was supported by National Aeronautics and Space Administration grants NNG05GD15G and NNX08AV04H

TABLE OF CONTENTS

| | |
|--|-----------|
| 1. Introduction..... | 1 |
| 2. Idealized Case Study..... | 6 |
| Summary..... | 6 |
| 2.1 Introduction..... | 7 |
| 2.2 Model setup..... | 12 |
| 2.3 Entrainment parameterization and implementation..... | 14 |
| 2.4 Results..... | 17 |
| 2.4a Physical effects..... | 17 |
| 2.4b Physiological effects..... | 23 |
| 2.4c Parameterization magnitude effects..... | 28 |
| 2.5 Conclusions..... | 29 |
| 3. 1999 Case Study..... | 31 |
| Summary..... | 31 |
| 3.1 Introduction..... | 32 |
| 3.2 Methods..... | 35 |
| 3.2a Model description..... | 35 |
| 3.2b Entrainment parameterization..... | 36 |
| 3.3 Observations..... | 38 |
| 3.4 Results..... | 39 |

| | |
|--|----|
| 3.4a WLEF comparison..... | 39 |
| 3.4b NARR comparison..... | 46 |
| 3.4c Regional comparison..... | 49 |
| 3.5 Conclusions..... | 58 |
| 4. Sensitivity of Coupled Simulations to the Magnitude of Entrainment Fluxes...60 | |
| Summary..... | 60 |
| 4.1 Introduction..... | 61 |
| 4.2 Methods..... | 64 |
| 4.3 Results..... | 67 |
| 4.4 Conclusions..... | 80 |
| 5. PBL Depth from Space.....82 | |
| Summary..... | 82 |
| 4.1 Introduction..... | 82 |
| 4.2 Methods..... | 86 |
| 4.3 Results and discussion..... | 90 |
| 4.4 Conclusions..... | 97 |
| 6. Conclusions.....99 | |
| References.....103 | |

Chapter 1

Introduction

Exchanges of energy, moisture, momentum, and trace gases between the Earth's surface and atmosphere are absolutely fundamental to the climate system. All of these exchanges are mediated by turbulent processes in a layer of the atmosphere near the lower boundary, which is commonly referred to as the planetary boundary layer (PBL). PBL processes are important for air pollution, cloud formation, and precipitation among many other land-atmosphere interactions and atmospheric processes. The transport of water vapor in order to form clouds and momentum in order to dissipate at the Earth's surface must pass through the PBL. Capped by an overlying temperature inversion, scalars with surface sources and sinks are trapped within the daytime PBL, producing a gradient between the PBL and the overlying free troposphere. Such scalars include aerosols and carbon dioxide (CO₂).

CO₂ is the most important anthropogenic greenhouse gas and is the largest contributor to human-induced climate change (Solomon, et al., 2007). CO₂ has multiple sources and sinks near the surface that alter its concentration in the atmosphere. Anthropogenic sources such as fossil fuel burning and land use changes (Houghton, 1999; Davis et al., 2003) account for the recent warming trend and the rate of CO₂ increase of 1-2 ppmv yr⁻¹ over the past half-century (Conway et al., 1994; Davis et al., 2003). However, only about half of the carbon being released into the atmosphere by

humans remains there (e.g. Schimel et al., 1994; Denning et al., 1995). The remainder is taken up by the oceans and the terrestrial biosphere (e.g. Tans et al., 1990; Sarmiento et al., 1992; Sarmiento and Sundquist 1992; Schimel et al., 1994; Denning et al., 1995). In order to understand how CO₂ concentrations are going to change in the future, it is necessary to understand the processes that control the natural surface sources and sinks and how they will evolve in the future (e.g. Denning et al., 1996a; Gurney et al., 2003; Friedlingstein et al., 2006).

Fluxes of carbon at the surface occur into and out of the planetary boundary layer (PBL) (Wofsy et al., 1988; Baker et al., 2003) and are mixed by turbulent eddies to produce a nearly homogeneous vertical profile of CO₂ concentration (Stull 1976; 1988). Understanding the processes that govern the PBL is thus important in determining the vertical and horizontal distribution of CO₂ concentrations (Wofsy et al., 1988; Denning et al., 1995; Yi et al., 2001; 2004; Chen et al., 2005). The response of CO₂ concentration to fluxes is inversely proportional to the depth of the PBL (Denning et al., 1995; Yi et al., 2001; 2004) due to the dilution of CO₂ fluxes by turbulent mixing (Yi et al., 2004). An error in the PBL depth therefore relates linearly to an error in the simulated CO₂ concentration (Denning et al., 1995; 1996b; 1999; 2008; Zhang, 2002; Gerbig et al., 2003).

Most measurements of CO₂ concentration are made within the PBL (Chen et al., 2005) using flasks and continuous towers and so observation to model comparisons will produce a mismatch when the PBL depth is not simulated correctly. Although extremely important for simulating CO₂ concentrations, few models accurately determine the PBL depth and vertical turbulent mixing (Denning et al., 1995; 1996a; 2008; Gurney et al.,

2003; Yi et al., 2004). Many of the processes that control PBL development are small-scale and unresolved by models (Ayotte et al., 1996; Gerbig et al., 2003). During the daytime, the depth of the PBL is typically several kilometers, making it difficult to observe fluxes and processes at the top.

Entrainment at the top of the boundary layer, an important process governing PBL development, involves the mixing of turbulent PBL air with free tropospheric air aloft that has not recently been in contact with the surface. Entrainment may result from shear at the top of the PBL or as a result of rising surface thermals that overshoot their neutral level and continue into the overlying inversion. During their subsequent descent, the thermals drag down free tropospheric air and grow the boundary layer through the insertion of energy and mass (Stull, 1988; Sullivan et al., 1998). The thermals also distort the boundary separating the PBL and the free troposphere (Stull, 1976), directly incorporating the free troposphere into the boundary layer. The overshooting thermals play a crucial role in entrainment mechanics (Sayler and Breidenthal, 1998; Sullivan et al., 1998; Stevens and Bretherton, 1999), one of the most important processes of any model to represent (Ayotte et al., 1996). Turbulent entrainment is generally represented in numerical models as downgradient diffusion by unresolved eddies, with an “eddy diffusivity” parameterized according to shear and buoyancy at grid resolution. But since convective daytime boundary layers are typically capped by strongly stable inversions, eddy diffusivity becomes very weak near the PBL top, inhibiting mixing between the PBL and overlying free atmosphere. This has been shown to lead to systematic underestimation of both morning growth rates and maximum mixing depth and is the result of processes (overshooting thermals) that are orders of magnitude smaller than grid

scale. Since observations are scarce, parameterizations of entrainment are more primitive than models of surface exchange, resulting in entrainment being one of the weakest aspects of PBL models (Davis et al., 1997).

The focus of this study is to include and evaluate a parameterization of enhanced entrainment in a coupled ecosystem-atmosphere model. The parameterization is based on a closure assumption for the heat flux at the base of the capping inversion, stating that this heat flux is proportional to the heat flux at the surface. It introduces a downward heat flux at the top of the PBL to simulate the effects of overshooting thermals that are neglected in most mesoscale models. The heat flux also has consequences for the model temperature, water vapor mixing ratio, the surface vegetative response to atmospheric conditions, and CO₂.

In order to evaluate this parameterization, something is needed to compare to the parameterized model results. Standard radiosondes are launched at 0 and 12 UTC (locally early morning and late afternoon) and are therefore unable to capture the midday maximum PBL depth over the continental United States. Even at mid-day, PBL depth estimated from radiosondes can differ from the space/time average by up to 40% (Angevine et al., 1994), depending on things such as whether the balloon passed through a cloud layer or through a small gap. Aircraft and wind profilers are able to determine the PBL depth, but are generally deployed only in field campaigns that are meant to observe special conditions and are limited spatially and temporally.

The Cloud-Aerosol LIDAR and Infrared Pathfinder Satellite Observations (CALIPSO) satellite was launched in April 2006 (Winker et al., 2007; 2009). Its onboard LIDAR is sensitive to aerosols trapped within the PBL and to boundary layer clouds that

can help identify the top of the PBL. An algorithm was developed by Jordan et al. (2010) that can identify the top of a feature in the backscatter that is highly correlated with the top of the PBL. Using this algorithm, an automated estimate of the PBL depth is possible which enables millions of observations. After selecting only the most reliable estimates, a data set of PBL depths to which model results can be compared becomes available.

Chapter 2 discusses an idealized case so that the effects of the enhanced entrainment parameterization can be assessed devoid of outside influences. This analysis uses a coupled ecosystem-atmosphere model with a homogeneous surface, cyclic boundary conditions, and neglects all effects from clouds. Chapter 3 evaluates this parameterization in realistic conditions. In addition to the overall influence of the parameterization, the impact of enhanced entrainment on the PBL depth is compared to observations from a wind profiler deployed near the WLEF observation tower in northern Wisconsin. Chapter 4 compares model results using the enhanced entrainment parameterization using varying values for the proportionality constant between the surface and PBL top heat fluxes. Chapter 5 discusses the modifications to the Jordan et al. (2010) algorithm to determine PBL depth from CALIPSO and the results obtained for summertime conditions for 5 years for which there are observations. Chapter 6 provides a summary and conclusions.

Chapter 2

Idealized Case Study

An edited version of this chapter was published by the American Geophysical Union.

McGrath-Spangler, E. L., A. S. Denning, K. D. Corbin, and I. T. Baker (2009), Sensitivity of land-atmosphere exchanges to overshooting PBL thermals in an idealized coupled model, *Journal of Advances in Modeling Earth Systems*, 1(Art. #14), 13 pp.

Summary

The response of atmospheric carbon dioxide to a given amount of surface flux is inversely proportional to the depth of the planetary boundary layer (PBL). Overshooting thermals that entrain free tropospheric air down into the boundary layer modify the characteristics and depth of the mixed layer through the insertion of energy and mass. In addition, entrainment “dilutes” the effects of surface fluxes on scalar quantities (temperature, water vapor, carbon dioxide, etc.) in the PBL. Therefore, incorrect simulation of PBL depth can lead to linear errors in estimates of carbon dioxide fluxes in inverse models. Dilution by entrainment directly alters the surface-air gradients in scalar properties, which serve as the “driving force” for surface fluxes. In addition, changes in near-surface temperature and water vapor affect surface fluxes through physiological processes in plant canopies (e.g. stomatal conductance). Although overshooting thermals are important in the physical world, their effects are unresolved in most regional models. We explore the sensitivity of surface fluxes and PBL scalars to the intensity of PBL top

entrainment by manipulating its strength in an idealized version of the coupled SiB-RAMS model. An entrainment parameterization based on the virtual potential temperature flux at the surface is implemented into SiB-RAMS to produce a warmer and drier mixed layer, to alter the surface fluxes, and to increase the depth of the PBL. These variations produce modified CO₂ concentrations and vary with the strength of the parameterized entrainment.

2.1 Introduction

The planetary boundary layer depth (Z_i) is important for carbon budget studies. Carbon dioxide (CO₂) is released and absorbed by land ecosystems on a daily and seasonal basis. The amount of uptake and release of carbon by plants is diluted through the volume of the boundary layer so that the concentration of carbon dioxide within the boundary layer is dependent upon the PBL height (Denning et al. 1995; Yi et al. 2001, 2004). The PBL to which we refer is also described as the mixed layer or the boundary layer. We will refer to the PBL and the boundary layer interchangeably.

Atmospheric inversions are a useful method for estimating surface sources and sinks of CO₂ (e.g. Gurney et al. 2002; Gerbig et al. 2003a; Zupanski et al. 2007). Downstream tracer concentrations are compared to observations and used to optimize prior upstream sources and sinks (Gerbig et al. 2003b; Zupanski et al. 2007). In this manner, model fluxes of CO₂ are corrected with observations. The sensitivity of tracer concentrations to surface fluxes is inversely proportional to the depth of the boundary layer, so errors in Z_i translate linearly to errors in retrieved fluxes (Denning et al. 1995,

1996b, 1999, 2008; Zhang 2002; Gerbig et al. 2003a, 2008). These errors can lead to the inaccurate estimation of carbon sources and sinks.

During the daytime, in the clear atmosphere, the surface heats up through absorption of solar radiation producing a statically unstable temperature profile. This warm surface air is positively buoyant and rises through the mixed layer in warm air plumes or thermals. Due to their momentum, rising thermals overshoot their neutral level and continue into the overlying inversion layer, becoming negatively buoyant. These thermals fall back down into the mixed layer, bringing with them warm, dry free tropospheric air that is then entrained into the boundary layer by turbulent eddies (Stull 1976, 1988; Sullivan et al. 1998).

The boundary layer is the volume through which surface CO₂ exchange occurs. As this layer deepens, the effect of carbon assimilation is diluted through a greater volume. This means that for equal rates of assimilation, a deeper boundary layer exhibits a smaller decrease in the concentration of carbon (Denning et al. 1995; Yi et al. 2001, 2004; Gerbig et al. 2008). The temperature and humidity conditions of the boundary layer not only affect the energy budget of the layer, but also the physiological state of the vegetation. As temperatures increase and humidity decreases, the plants can begin to show signs of stress (Davis et al. 1997). This decreases the assimilation of carbon and higher soil temperatures increase heterotrophic respiration. All of these effects combine to modify CO₂ concentrations near the surface. The importance of including the effects of overshooting thermals in modeling studies thus becomes apparent if the concentration of carbon in the boundary layer or the behavior of the surface vegetation is vital to the study.

Mesoscale meteorological modeling usually uses a resolution too coarse to resolve even the largest overshooting thermals and thus does not capture the entrainment process at the top of the boundary layer (Ayotte et al. 1996; Gerbig et al. 2003a); consequently, these models must include a parameterization of entrainment (André et al. 1978). The horizontal scale of boundary layer thermals is about $1.5 \cdot Z_i$ or on the scale of 100 meters to two kilometers (Stull 1988). According to Pielke (1991), at least four grid increments are required to represent an atmospheric feature reasonably. This means that, at best, the horizontal grid increment of the mesoscale model would need to be 500 meters and sometimes as fine as twenty-five meters. Even finer grid increments would be needed in order to resolve the mixing across the inversion. Currently, model simulations with this resolution are too computationally expensive for large model domains and over long periods of time and cannot be done to fully resolve boundary layer thermals.

Since one of the most important roles of any model is to represent boundary layer top entrainment (Ayotte et al. 1996), several attempts have been made to understand entrainment better through large eddy simulations (LES) (Sullivan et al. 1998; Stevens and Bretherton 1999) and through laboratory experiments (Sayler and Breidenthal 1998). These studies conclude that overshooting thermals play a crucial role in entrainment mechanics and that the strength of entrainment varies with atmospheric conditions. Unfortunately, atmospheric observations of entrainment rates are difficult because of mesoscale variations and coupling between physical processes (Davis et al. 1997; Sullivan et al. 1998; Cohn and Angevine 2000).

Beljaars and Betts (1992) used the European Centre for Medium-Range Weather Forecasts (ECMWF) model in their simulations of the boundary layer. They found in their August simulations over the Konza prairie during the First ISLSCP (International Satellite Land Surface Climatology Project) Field Experiment (FIFE) that the model produced boundary layer conditions that were too cool and too moist and that this boundary layer grew too slowly. They suggested that this was due to the lack of entrainment in their model. The ECMWF model, like SiB-RAMS, grew the PBL through encroachment as the surface warmed, rather than through explicit PBL top entrainment. After including an entrainment parameterization, their results improved.

In the current formulation of the Brazilian version of the Regional Atmospheric Modeling System (BRAMS) version 2.0, boundary layer top entrainment is implicitly included as layer by layer mixing and is not adequate to represent the mixing associated with overshooting thermals (Freitas et al. 2006). The boundary layer depth is diagnosed from the virtual potential temperature profile by finding the lowest layer where the virtual potential temperature profile increases by a specified amount (0.5 K in these simulations), indicating the capping inversion.

In RAMS, the vertical eddy diffusivities for momentum, heat, and TKE are inversely proportional to the vertical gradient of potential temperature through an equation for the turbulent length scale for stable conditions by André et al. (1978). They admit that this parameterization is crude and not elaborate enough to describe the turbulence in a strongly thermally stratified environment. As the stratification increases, the turbulent length scale and the vertical eddy diffusivities decrease, increasing the TKE eddy dissipation term, and can do so enough to prevent vertical mixing. The temperature

inversion at the top of the boundary layer can then act similar to a material surface and retard the exchange of energy and mass that occurs in the physical world. The PBL in RAMS grows by encroachment as the surface warms, but there is no explicit representation of PBL top entrainment. If the simulated boundary layer is too cold, too moist, and too shallow when compared to observations, such as was found by Beljaars and Betts (1992), an entrainment parameterization can produce better results by improving the interactions between entrainment and the surface fluxes.

This paper discusses the sensitivity of the response of the land surface to enhanced entrainment at the top of the PBL that warms, dries, and increases the depth of the boundary layer. The parameterization includes a tunable coefficient that is allowed to vary in the different simulations, and comparisons are presented that show the effects of changing this coefficient. This parameterization has been studied by numerous authors including Betts (1973), Carson (1973), Deardorff (1974), Rayment and Readings (1974), Willis and Deardorff (1974), Stull (1976), Davis et al. (1997), Sullivan et al. (1998), and Yi et al. (2001) and this paper seeks to understand the interaction with the surface and the subsequent effects on the mixed layer. Section 2.2 is a description of the model setup. Section 2.3 discusses the parameterization itself and its implementation into RAMS. Results of idealized model simulations using the parameterization are given in section 2.4. A conclusion and direction for future work is presented in section 2.5.

2.2 Model setup

The parameterization has been implemented in a modified form of RAMS version 5.04 called BRAMS version 2.0. The major differences between RAMS and BRAMS are the implementation of the Grell convection scheme and the shallow convection scheme (Walko et al. 2002). The surface model used is the third version of the Simple Biosphere Model (SiB3), initially developed by Sellers et al. (1986). The coupling of the surface model and atmospheric model is called SiB-RAMS (Denning et al. 2003; Nicholls et al. 2004; Wang et al. 2007; Corbin et al. 2008).

RAMS was initially developed at Colorado State University as a non-hydrostatic three-dimensional model in order to study mesoscale and cloud-scale phenomena (Pielke 1974; Tripoli and Cotton 1982; Pielke et al. 1992; Cotton et al. 2003). It includes time-dependent equations for velocity, ice-liquid water potential temperature, total water mixing ratio and diagnostic formulations of potential temperature and vapor mixing ratio (Denning et al. 2003) on either a terrain-following σ_z coordinate system or the Adaptive Aperture (ADAP) coordinate system. The ADAP coordinate is a fully Cartesian grid in which the grid cells are allowed to intersect the topography and allows partial grid cells along the topography (Walko et al. 2002). The terrain-following coordinate system is used in the simulations discussed in this paper, but the implemented parameterization accommodates both systems.

Plant and plant photosynthesis are parameterized in the SiB model in an attempt to mimic the real world. SiB is a land-surface parameterization used to compute biophysical exchanges in climate models (Sellers et al. 1986), but also includes

ecosystem metabolism (Sellers et al. 1996; Denning et al. 1996a). Farquhar et al. (1980) originally developed the photosynthesis parameterization. SiB is an interactive dynamic land surface model that determines the surface boundary condition to RAMS.

A single grid was used on a domain of 200 km x 200 km with 25 individual grid cells (5x5) with a size of 40 km x 40 km each, centered at 45°N and 90°W. This grid spacing allows the resolution of mesoscale features, but is much too coarse to resolve the individual thermals that entrain free atmospheric air into the boundary layer. Sixty-five vertical grid levels were used with the lowest level at about 30 m and extending up to a domain top of 12.8 km with a vertical grid stretch ratio of roughly 1.1. Increased vertical resolution was included near common boundary layer depth in order to resolve variations in the effects of the parameterization due to variations in the strength of the entrainment flux.

Cyclic boundary conditions were used to isolate local processes that control PBL depth. Since the domain was periodic, large-scale advective influences were not included. The domain characteristics were horizontally homogeneous so that there were no influences from surface heterogeneity and no weather systems were allowed to advect into the domain. The only acting forces were those associated with the diurnal cycle and the parameterization itself. This setup also allowed the runs to be computationally inexpensive and quick to run. The simulation was allowed to run for 72 hours, in addition to a one week spin up. The emphasis of this setup was to produce a simplified and idealized case in order to isolate the effects of the entrainment parameterization. It therefore does not resemble any particular event and model responses should be considered in this context.

The vertical profiles of pressure, temperature, humidity, and wind velocity were initialized horizontally homogeneously from a relatively cool August sounding, typical of Green Bay, Wisconsin at 44.48°N and 88.13°W with winds predominately out of the west and northwest. The topography was defined as flat and at sea level everywhere in the domain, removing any effects of terrain on boundary layer depth or growth. Similarly, the vegetation, soil textural class, fraction of photosynthetically active radiation (FPAR), and leaf area index (LAI) were all prescribed as horizontally homogeneous. The vegetation type was C3 tall broadleaf and needleleaf trees while the soil type was loam. The default FPAR and LAI used were 0.93 and 6.2, respectively. In order to isolate the effects of dry convection, all water present in the model had to remain as water vapor, even if supersaturation occurred, in order to prevent the formation of clouds and precipitation in order to simplify the problem. The turbulence closure option used during these simulations was the Mellor and Yamada (1982) scheme for vertical diffusion. Mellor and Yamada is a local option that employs a prognostic turbulent kinetic energy.

2.3 Entrainment parameterization and implementation

During the growing season, at the inversion interface, overshooting thermals inject cool, moist, CO₂-depleted turbulent boundary layer air into the overlying inversion and entrain warm, CO₂-rich free tropospheric air downward creating negative heat and carbon fluxes in the region of overshoot. The profile of heat flux throughout the well-mixed, quasi-steady boundary layer is often approximated as linear (Stull 1976). Above

the inversion, the perturbation vertical velocity is assumed zero, implying the heat flux is also zero.

This implies that the negative heat flux at the base of the capping inversion ($\overline{w'\theta_v'}|_{z_i}$) is linearly proportional to the heat flux at the surface, leading to the closure assumption for the heat flux at the top of the boundary layer:

$$\overline{w'\theta_v'}|_{z_i} = -\alpha \overline{w'\theta_v'}|_s \quad (2.1)$$

where α is the proportionality constant (Stull 1988). Estimates of α from experimentation and theory range anywhere from zero to one with most published values being between 0.1 and 0.3 (e.g. Betts 1973; Carson 1973; Deardorff 1974; Rayment and Readings 1974; Willis and Deardorff 1974; Stull 1976; Davis et al. 1997; Sullivan et al. 1998; Yi et al. 2001).

The assumption that the heat flux at the top of the boundary layer is negatively proportional to the surface heat flux was used to include fluxes of multiple variables from overshooting thermals to alter the temperature, water vapor mixing ratio, winds, and CO₂ mixing ratios of the boundary layer and the lowest layer of the inversion. The heat flux can be used to define a time rate of change of potential temperature:

$$\frac{\partial \theta}{\partial t} = \frac{\alpha \overline{w'\theta_v'}|_s}{\Delta z} \quad (2.2)$$

where Δz is the thickness of the layer. The heat flux across the capping inversion can be used to define a mass flux representative of the amount of mixing between the layers surrounding the interface between the boundary layer and the capping inversion required to produce these temperature changes. This mass flux is given by:

$$M = \frac{\rho \alpha \overline{w'\theta_v'}|_s}{\Delta \theta_v} \quad (2.3)$$

where ρ is the density of the air and is computed from the total Exner function and ice-liquid potential temperature prognosed by RAMS (Medvigy et al. 2005). This gives the mass flux the units of $\text{kg m}^{-2} \text{s}^{-1}$. When multiplied by the specific humidity of the layer, r_v , this becomes a mass flux of water vapor. This can be used to find a time rate of change of the mixing ratio:

$$\frac{\partial r_v}{\partial t} = \frac{\Delta r_v M}{\rho \Delta z} \quad (2.4)$$

This induces a drying of the whole boundary layer through turbulent mixing and a moistening of the capping inversion.

This same mass flux can be used to define time rates of change of the different components of the wind vector, TKE, and CO_2 concentration given in the equations below.

$$\frac{\partial u_i}{\partial t} = \frac{\Delta u_i M}{\rho \Delta z} \quad (2.5)$$

$$\frac{\partial w}{\partial t} = \frac{\Delta w M}{\rho \Delta z} \quad (2.6)$$

$$\frac{\partial TKE}{\partial t} = \frac{\Delta TKE * M}{\rho \Delta z} \quad (2.7)$$

$$\frac{\partial C}{\partial t} = \frac{\Delta C * M}{\rho \Delta z} \quad (2.8)$$

In these equations, u_i represents the two components of the horizontal wind vector. These equations represent the mixing across the overlying capping inversion and introduce negative fluxes of horizontal momentum and CO_2 concentration and positive vertical fluxes of vertical velocity and TKE.

The simulated boundary layer height is diagnosed from the virtual potential temperature profile as the height where the temperature increases by 0.5 K, defining the capping inversion. After the PBL height is determined by this method, the temperature, mixing ratio, wind velocity, TKE, and carbon dioxide concentration tendencies for the layers above and below Z_i are altered by the above equations. Before the end of the timestep, the seven variables are updated by their respective tendency arrays.

2.4 Results

a. Physical effects

Inclusion of a parameterization for boundary layer entrainment due to overshooting thermals results in a deeper boundary layer as is evident in Figure 2.1. It is important to note that the simulated boundary layer is about two times deeper than that typically observed due to the idealized and simplified nature of the model in this case. A residual layer that retains its well-mixed properties throughout the night develops during the evening transition. In the morning, when the sun heats the surface and the nocturnal inversion is broken, the boundary layer quickly grows to the depth of the residual layer. While the morning growth is very rapid once the convective boundary layer reaches the base of the residual layer (Stull 1988) this transition is more rapid in the simplified case than what is typically observed due to little adjustment of the residual layer. The entraining case is the one for which α in the parameterization is given a value of 0.2. The control case does not include the PBL top entrainment parameterization. The greater depth is a product of the input of heat energy from the overlying inversion and the

upward transport of turbulent kinetic energy, physically incorporating the lowest levels of the inversion into the boundary layer. The modeled boundary layer is allowed to grow as long as the surface sensible heat flux is positive. Once it becomes negative, an inversion is formed and the boundary layer collapses. The discretized nature of the model does not allow the boundary layer to grow in a smooth way as it would in the physical world. Z_i is limited by the predetermined model levels and can only change when enough energy is present to move from one level to the next.

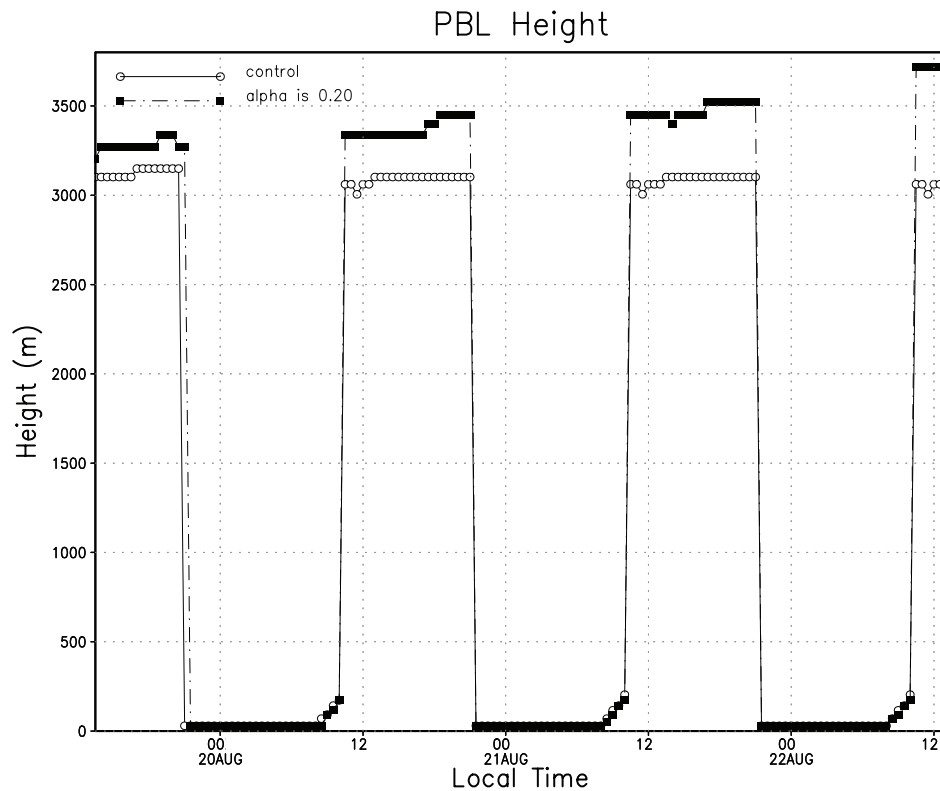


Figure 2.1 Temporal evolution of the boundary layer height for the enhanced entrainment and control cases.

Figure 2.2 shows a vertical profile of potential temperature. Throughout the depth of the boundary layer, the entraining case is warmer than the control case by about a degree. However, the inversion is slightly cooler in the entraining case. The combination of a warmer mixed layer and a weaker capping inversion means that it is

easier for overshooting thermals to break through the inversion and grow the boundary layer through entrainment. In addition, since the boundary layer is warmer, less surface heating is required to erode the inversion and grow the boundary layer. Turbulent mixing within the boundary layer distributes this warming throughout its depth.

The water vapor mixing ratio profile is also modified by the parameterization (Figure 2.3a). The upward transport of moisture, carried by the overshooting thermals, results in a drier boundary layer and a moister inversion layer in the entraining case.

The effects of the parameterization on the potential temperature and the water vapor mixing ratio act in opposite directions, since increased water vapor decreases the density of an air mass. Virtual potential temperature (Figure 2.3b) can be related to potential temperature and water vapor mixing ratio through the equation:

$$\theta_v = \theta(1 + 0.61r_v) \tag{2.9}$$

and so demonstrates the combined effect of the parameterization.

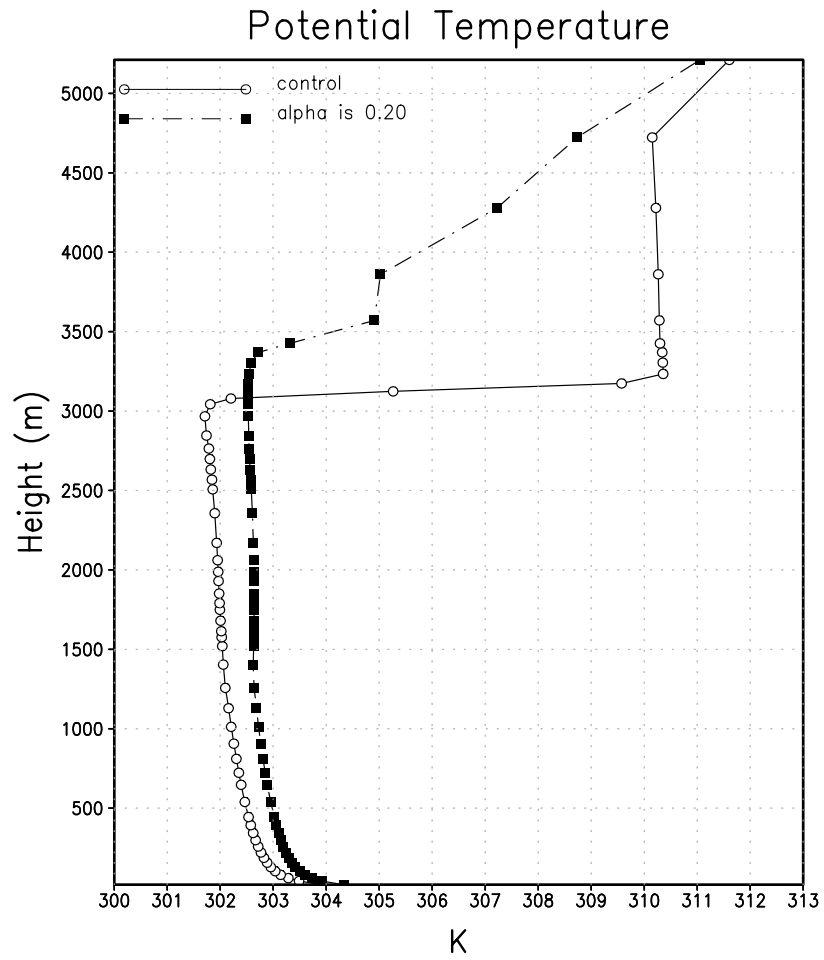


Figure 2.2 Vertical profile of potential temperature for both the enhanced entrainment and control cases at 13:00 LST on 21 August.

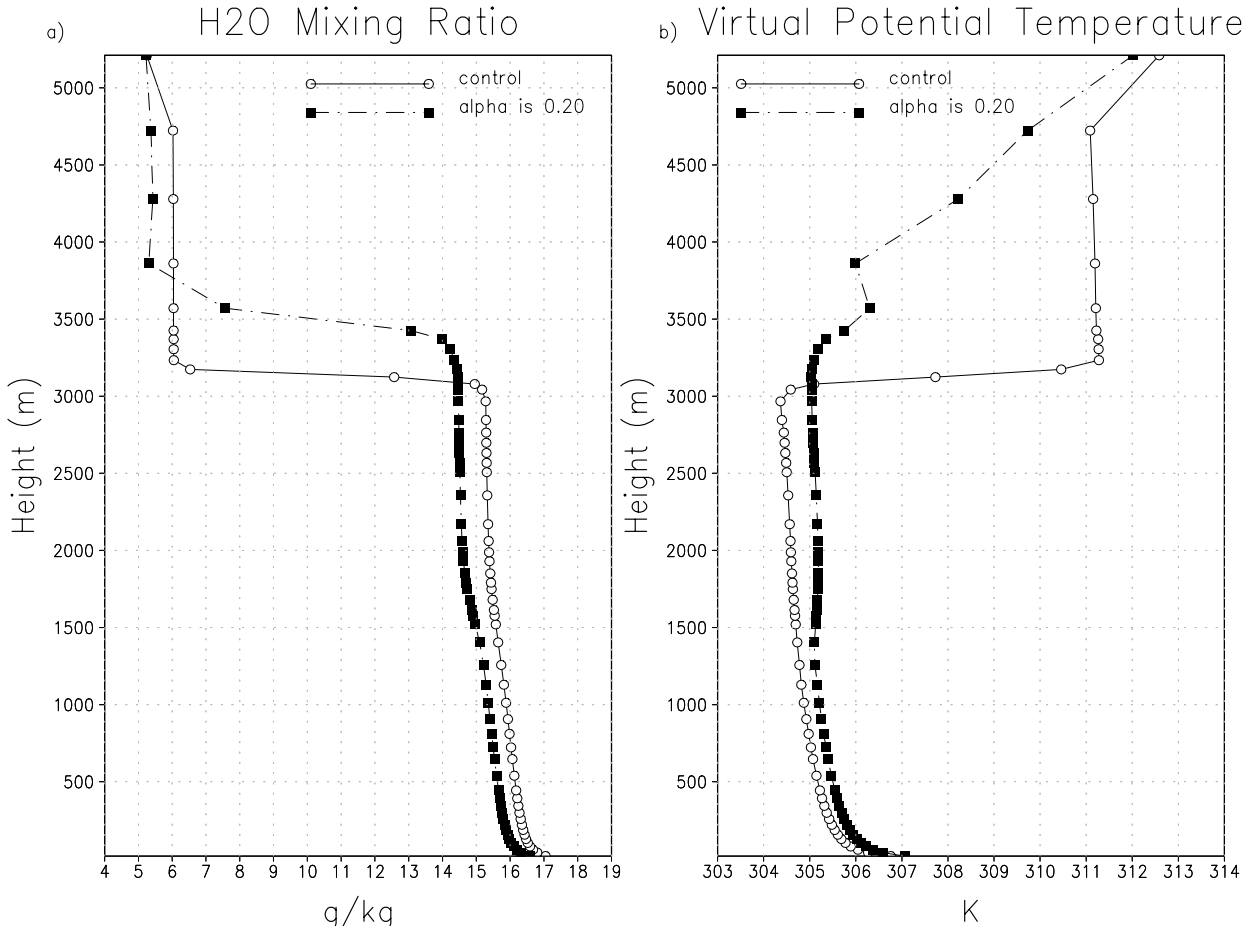


Figure 2.3 Profile of water vapor mixing ratio (a) and virtual potential temperature (b) for both the enhanced entrainment and control cases at 13:00 LST on 21 August.

The temporal evolution of latent and sensible heat fluxes from the canopy air space (CAS) into the boundary layer is shown in Figures 2.4a and 2.4b respectively. The enhanced entrainment case minus the control case is shown in Figure 2.4c for both sensible and latent heat fluxes. The daytime sensible heat flux is smaller in the entraining case due to the altered conditions that result from the enhanced PBL top entrainment. Since the parameterization is proportional to the surface heat flux, reducing this flux reduces the effects of the thermals.

As was the case for potential temperature and water vapor mixing ratio, the response of PBL top entrainment has opposite impacts on the sensible and latent heat fluxes. The drier boundary layer means that the gradient in water vapor mixing ratio between the boundary layer and the CAS is stronger in the entraining case. The impact of increasing latent heat flux to the total virtual potential temperature flux is to increase it. The larger heat flux then contributes to a larger impact of the parameterization on the heat flux at the top of the boundary layer. The additional moisture from the surface source is then mixed upward by turbulent eddies to moisten the depth of the boundary layer.

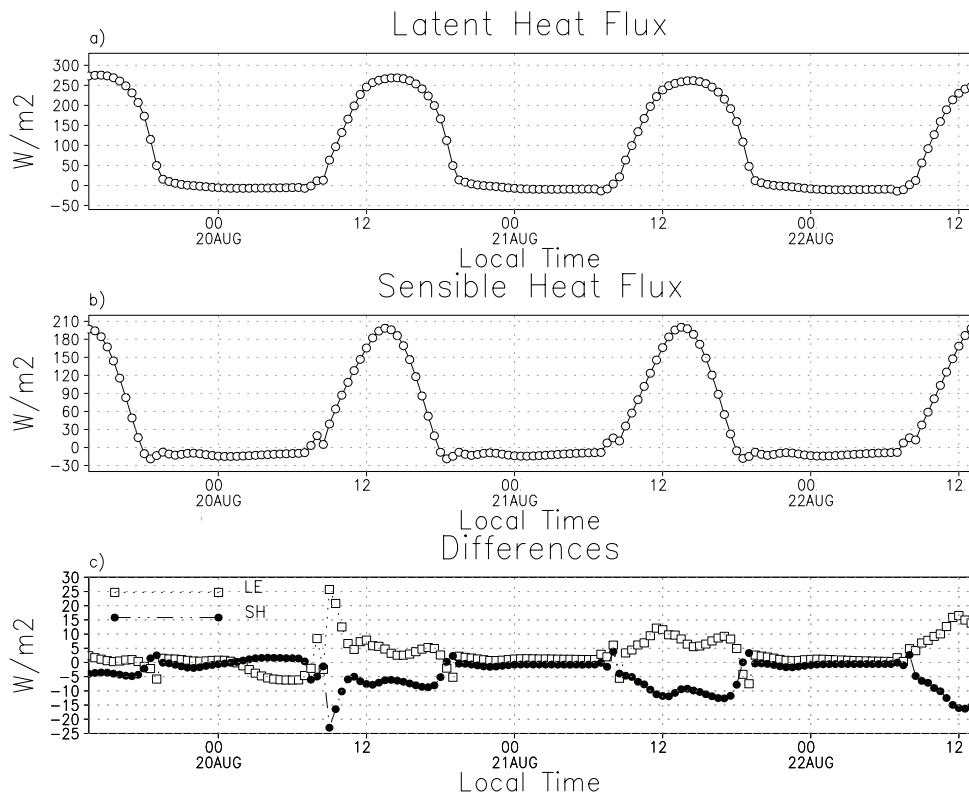


Figure 2.4 Temporal evolution of the latent (a) and sensible (b) heat fluxes in the lowest atmospheric model level for the control case and the difference (c) given by the enhanced entrainment case minus the control case.

b. Physiological effects

The physical modifications to the boundary layer directly impact the vegetation at the surface. The energy budget of the vegetated land surface partitions net downward radiation into turbulent fluxes of heat and moisture that warm and moisten the atmosphere, plus a smaller heat flux into the soil. The Bowen ratio of sensible to latent heat fluxes is determined by the conductance of plant stomata, which is actively controlled as an evolved response by plants to maximize CO₂ uptake by photosynthesis while minimizing water loss (Ball et al. 1987; Collatz et al. 1991; Bonan et al. 2002). Stomatal conductance (and hence transpiration) is generally greatest when photosynthetic carbon uptake is greatest, the air is nearly saturated with respect to water vapor, and the temperature moderate. The drying influence of entrainment can produce a humidity stress on the plants so that they close their stomata, causing a response in transpiration, the surface energy budget, and photosynthetic rates (Davis et al. 1997).

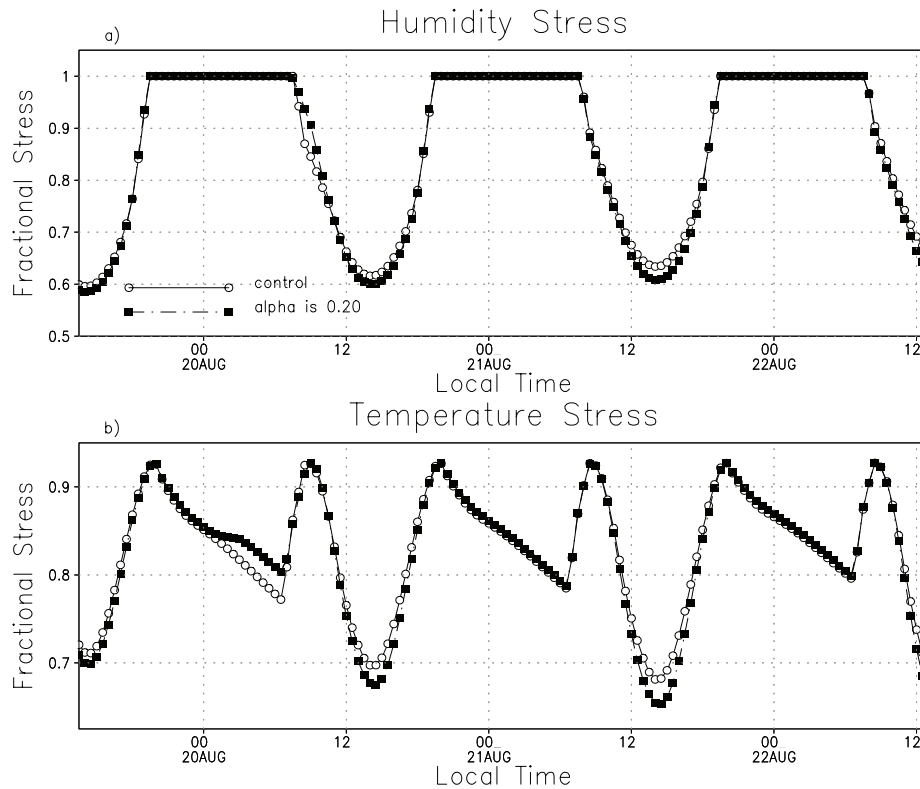


Figure 2.5 Temporal evolution of vegetative stress factors for the enhanced entrainment and control cases. (a) Humidity stress (b) Temperature stress.

Stomatal conductance and photosynthesis were calculated iteratively according to enzyme kinetics, diffusion of CO_2 and water vapor, and the Ball-Berry equation (Collatz et al, 1991). Stomatal conductance is directly proportional to the relative humidity at the leaf surface (inside the laminar boundary layer surrounding the leaf), and is adjusted downward by multiplying by nondimensional “stress factors” to account for non-optimal temperatures or insufficient soil moisture (Sellers et al, 1996) (Figure 2.5).

Simulated stomatal conductance (Figure 2.6) was reduced during the hottest part of each day due to a combination of slightly reduced humidity and high-temperature stress. Entrainment of dry air into the boundary layer by overshooting thermals is communicated through turbulent mixing, leading to a slightly warmer and drier stomatal microenvironment, and therefore reduced stomatal conductance. Note that despite the

slight reduction in stomatal conductance, the simulated sensible heat flux was suppressed and latent heat flux was enhanced in the entraining case due to stronger gradients in the surface layer (Figure 2.4).

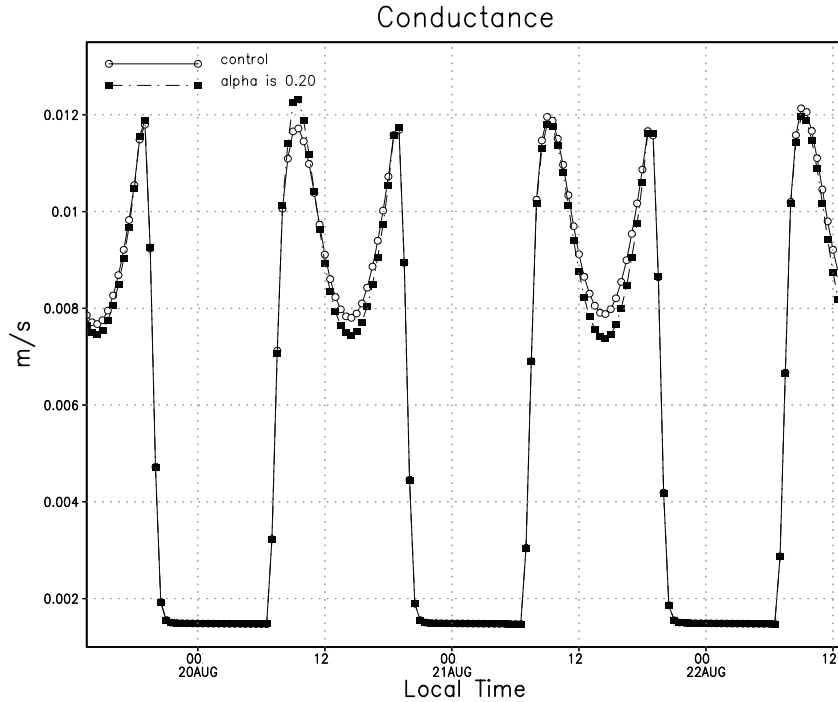


Figure 2.6 Temporal evolution of conductance for both the enhanced entrainment and control cases.

Figure 2.7 shows the impact of the vegetative stress on the net ecosystem exchange (NEE) of CO₂ (Figures 2.7a and 2.7b) and its components. In the morning, warmer temperatures cause the entraining case to have very slightly enhanced uptake of carbon. High-temperature stress and low humidity at mid-day produce less uptake. The NEE at night is very similar between the entraining and control cases with slightly greater respiration in the entraining case due to the warmer surface temperature. Ground respiration is a function of the surface soil temperature and varies with the diurnal cycle of temperature (Figures 2.7c and 2.7d). Since the entraining case is warmer throughout

the simulation, the ground respiration is larger and more carbon is released into the atmosphere from soil decomposition. Warmer and drier air at mid-day suppresses photosynthetic assimilation (Figures 2.7e and 2.7f). The entraining thermals in the simulation thus act indirectly on both components of the net CO₂ exchange to suppress the drawdown of CO₂ from the PBL through their effects on temperature and moisture.

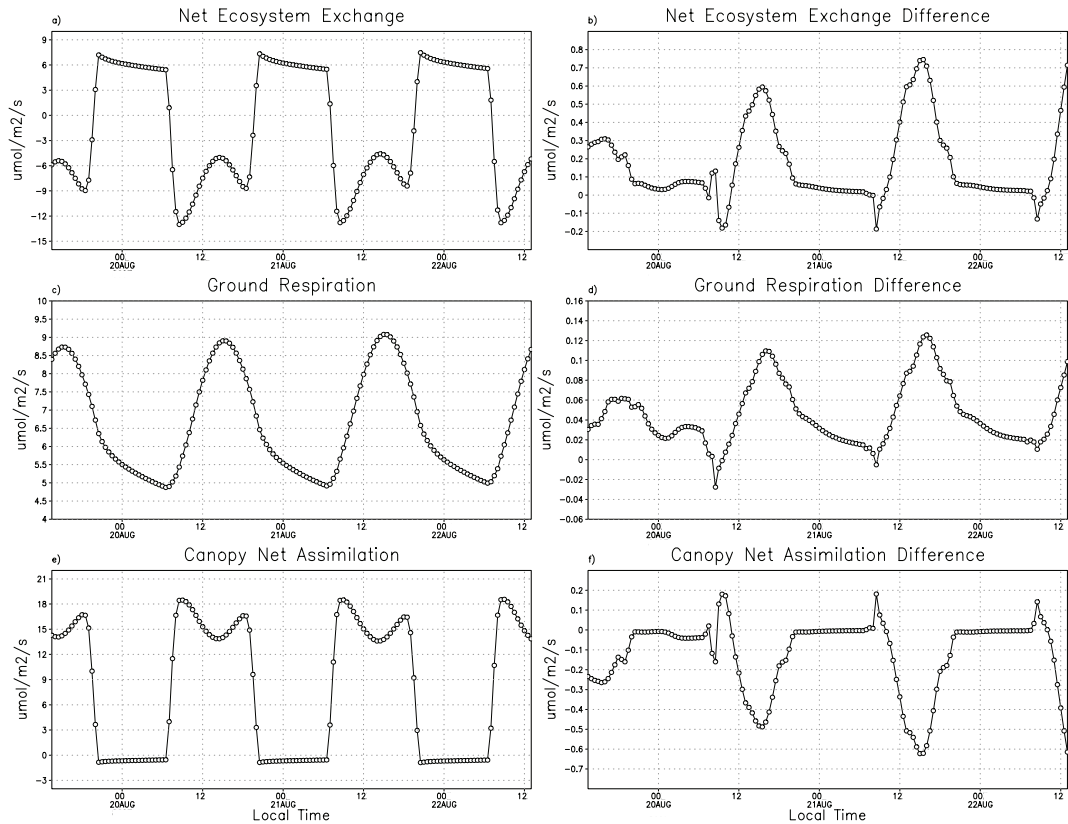


Figure 2.7 Temporal evolution of NEE (a), ground respiration (c), and canopy net assimilation (e) for the control case and the enhanced entrainment case minus the control case for NEE (b), ground respiration (d), and net assimilation (f).

The overall impact of simulated entrainment on CO₂ in the PBL reflects the modified NEE as well as dilution through the deeper mixed layer and enhanced mixing through the PBL top. Figure 2.8 shows only the daytime concentration of CO₂ since this study is not concerned with nighttime values. During the day, negative NEE draws down

the CO₂ concentration. The daily minimum in CO₂ concentration occurs near sunset, just as the vegetation stops removing carbon from the atmosphere.

CO₂ concentrations in the entraining case are higher than the control due to both the reduced assimilation and the depth of the boundary layer. The dilution effect dominates the increased CO₂ concentrations. As the boundary layer grows, a greater volume of the atmosphere is in contact with the surface and the removal of a given amount of carbon through photosynthesis reduces the CO₂ concentration less.

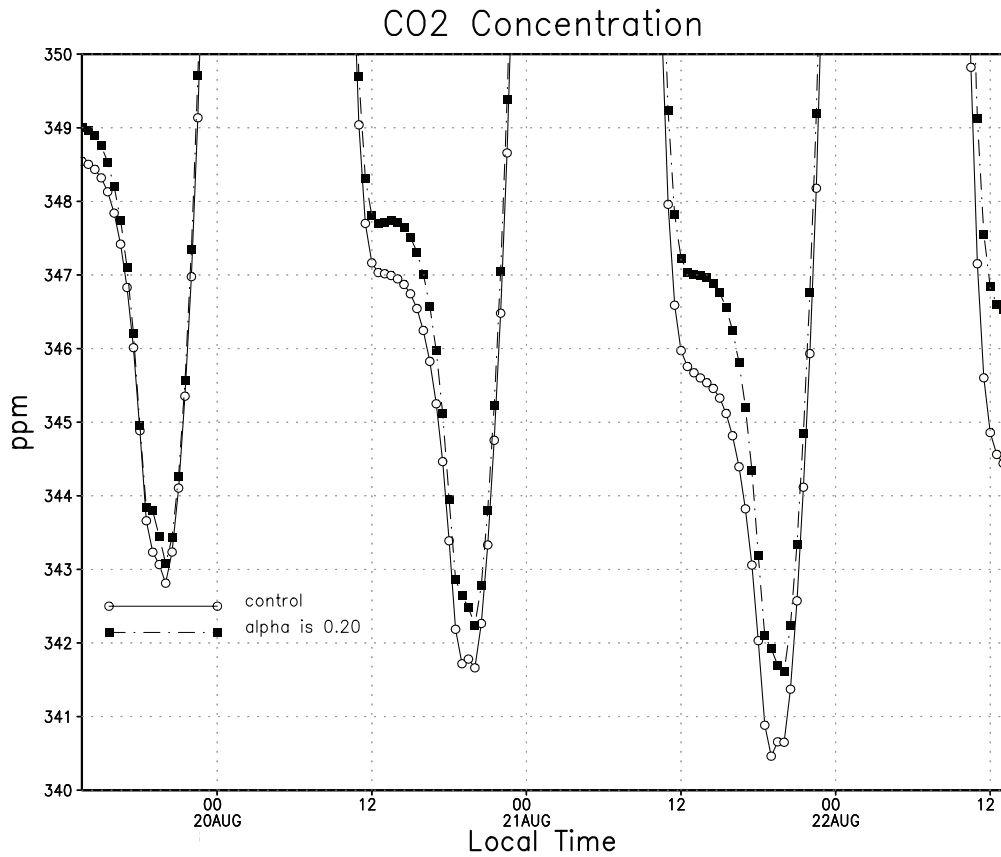


Figure 2.8 Temporal evolution of carbon dioxide concentration in the lowest atmospheric model level for the enhanced entrainment and control cases.

c. Parameterization magnitude effects

The previous results were obtained by setting the tunable parameter, α , to 0.20, indicating that the entrainment heat flux at the top of the boundary layer was assumed to be 20% of the surface heat flux. The following discussion determines the sensitivity of the system to varying strengths of the parameterization by using values of α between 0.0 and 0.5.

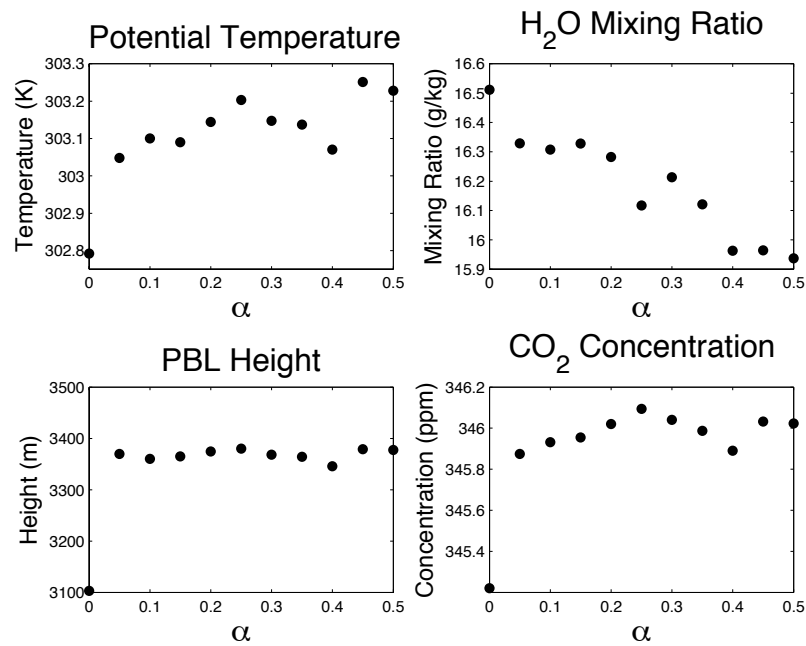


Figure 2.9 Sensitivity of potential temperature (a), water vapor mixing ratio (b), PBL depth (c), and CO₂ concentration (d) in the lowest model level to α . Values are averaged over an 8 hour period centered on 4 pm for 20-22 August.

Figure 2.9 illustrates how potential temperature (Figure 2.9a), water vapor mixing ratio (Figure 2.9b), Z_i (Figure 2.9c), and CO₂ concentration (Figure 2.9d) in the lowest atmospheric model level vary as functions of α . The values are averaged over 8 hour periods centered on 4 pm (from 12 pm - 8 pm) for the 3 days of 20 – 22 August. The potential temperature nearly linearly increases with α . Neglecting entrainment can result

in boundary layer temperature errors that can also affect the assimilation of carbon by plants.

The water vapor mixing ratio generally declines for increasing α . As α increases, overshooting thermals remove water from the boundary layer and transfer it to the overlying inversion. As the boundary layer dries, the moisture gradient between the CAS and the boundary layer increases, producing a greater latent heat flux. The latent heat flux moistens the boundary layer, acting contrary to the overshooting thermals.

The boundary layer height is dependent upon the vertical grid spacing. Energy is needed for Z_i to jump from one level to the next, and greater vertical resolution requires less energy to make a jump, but each jump is smaller.

Figure 2.9d shows how CO_2 concentration varies as a function of α . As α increases, so also does the concentration of CO_2 . This can be attributed to deeper boundary layers diluting the effect of photosynthetic uptake and increased vegetative stress associated with the warmer and drier conditions of an entrainment heat flux. The dependency of CO_2 concentration with the strength of this entrainment process is important for understanding carbon inversion study results.

2.5 Conclusions

The effects of PBL top entrainment are important to studies of the carbon budget using modeling. This study examines the impacts of overshooting thermals in an idealized experiment in an attempt to understand the complex interactions between PBL top entrainment, boundary layer processes, and the surface vegetation. Surface fluxes of

NEE, sensible and latent heat and CO₂ concentration are sensitive to the magnitude of the entrainment rate through a coupling between these fluxes and those at the PBL top.

Increased PBL depth means that uptake of carbon is diluted through a deeper layer, increasing carbon concentrations while the mass and heat fluxes associated with entrainment affect the atmospheric conditions to which the underlying vegetation respond. The altered response, in turn, affects the photosynthetic uptake of carbon thereby increasing the daytime CO₂ concentration even further. Since most observations of CO₂ are performed within the boundary layer, neglect of this process in models such as SiB-RAMS produces a model-observation mismatch and introduces errors into the assumed distribution of sources and sinks.

With this end in mind, the parameterization added to SiB-RAMS introduces a negative sensible heat flux and a positive water vapor flux at the top of the boundary layer and the sensitivity of the surface response was examined. The parameterization does induce a warmer, drier boundary layer that affects such characteristics as sensible and latent heat fluxes, wind velocity, and carbon dioxide concentration.

Chapter 3

1999 Case Study

An edited version of this chapter was published by John Wiley and Sons, Inc.

McGrath-Spangler, E. L., and A. S. Denning (2010), Impact of entrainment from overshooting thermals on land-atmosphere interactions during summer 1999, *Tellus B*, 62(5), 441-454.

Summary

The depth of the planetary boundary layer (PBL) or mixed layer is important for carbon dioxide source/sink estimation because the response of atmospheric carbon dioxide concentration to a given amount of surface flux is inversely proportional to this depth. The PBL depth is affected by entrainment from overshooting thermals that is often underestimated in mesoscale meteorological models. An experiment was performed for the late summer of 1999 that includes a parameterization of PBL top entrainment that is based on a downward buoyancy flux at the top of the PBL. Simulations with this parameterization produce a warmer, drier, and deeper boundary layer than a control simulation. The monthly mean diurnal cycle of PBL depth at a location in northern Wisconsin is better simulated with this enhanced entrainment when compared to observations. The altered atmospheric conditions cause the vegetation's stomata to respond and possibly close in an evolved response to limit water loss, thus reducing transpiration and shifting the Bowen ratio. The stomatal closing also reduces

carbon assimilation, consequently altering horizontal and vertical carbon gradients. The overall effect of enhanced PBL entrainment is to alter time-mean regional gradients in CO₂ mixing ratio by as much as 7 ppmv over 1000 km.

3.1 Introduction

The response of carbon dioxide (CO₂) concentration to the surface fluxes of carbon is inversely proportional to the depth of the planetary boundary layer (PBL) (Denning et al., 1995; Yi et al., 2001; 2004). However, vertical turbulent mixing and PBL depth are not often simulated correctly by models (Denning et al., 1995; 1996a; 2008; Gurney et al., 2003) and an error in the depth of the PBL relates to an error in the modeled concentration of CO₂ in the boundary layer (Denning et al., 1995; 1996b; 1999; 2008; Zhang, 2002; Gerbig et al., 2003). CO₂ inversion studies are negatively impacted by an error in PBL depth because this translates to an error in the estimates of carbon sources and sinks (e.g. Gurney et al., 2002; Gerbig et al., 2003; Baker et al., 2006; Zupanski et al., 2007). For example, in a back of the envelope calculation, assuming a 10% increase in the PBL depth produces a 9% response in the CO₂ concentration. During the summer, this implies a higher daytime CO₂ concentration.

The PBL is a well-mixed layer in turbulent contact with the surface with weak vertical gradients and is capped by a temperature inversion. In order to resolve the PBL in models, high resolution is needed near the inversion, but a high concentration of model levels is excessive over the rest of the PBL. To complicate things further, since the depth of the PBL varies spatially and temporally, the height at which the added resolution is

needed is also variable (Denning et al., 2008). The computational expense associated with including the number of model levels necessary to resolve the capping inversion for all of the different potential heights of the PBL is prohibitive.

PBL growth and development are controlled by small-scale processes that are generally not well resolved by mesoscale models (Ayotte et al., 1996; Gerbig et al., 2003). One such process is entrainment at the top of the boundary layer that is a result of rising thermals from the PBL overshooting their neutral level and pulling free tropospheric air into the PBL on their subsequent descent (Stull, 1988). Using the European Centre for Medium-Range Weather Forecasts (ECMWF) model, Beljaars and Betts (1992) found that the model produced conditions that were too cool and moist in a boundary layer that grew too slowly when simulating August conditions over the Konza prairie. After inclusion of an entrainment parameterization, their results improved indicating the importance of entrainment in numerical simulations. The PBL in the Regional Atmospheric Modeling System (RAMS) grows by encroachment as the surface warms, but does not include an explicit representation of PBL top entrainment, suggesting that important processes are not being represented. This process also alters the canopy air space (CAS) to which the vegetation responds by the incorporation of warmer and drier free tropospheric air into the mixed layer.

An entrainment parameterization (McGrath-Spangler et al., 2009) was introduced to the coupled ecosystem-atmosphere model SiB-RAMS (Denning et al., 2003; Nicholls et al., 2004; Wang et al., 2007; Corbin et al., 2008) based on the assumption that the downward buoyancy flux at the top of the PBL is proportional to the buoyancy flux at the surface (e.g. Betts, 1973; Carson, 1973; Deardorff, 1974; Rayment and Readings, 1974;

Willis and Deardorff, 1974; Stull, 1976; Davis et al., 1997; Sullivan et al., 1998; Yi et al., 2001). It has been shown in idealized simulations that the introduction of this parameterization results in a warmer, drier, and deeper PBL with a higher daytime concentration of CO₂ (McGrath-Spangler et al., 2009).

The primary objective of this study is to evaluate the performance of this parameterization in the summer of 1999 during which observations of PBL depth were being made at the WLEF very tall tower in northern Wisconsin (Angevine et al., 1998; Yi et al., 2001, 2004; Denning et al., 2008). The months of July, August, and September of that year have observations at nearly an hourly timescale and provide a good timeframe for comparison. In addition, micrometeorological, eddy flux, and CO₂ concentration measurements are made at several levels along the tower height providing a vertical profile (Yi et al., 2001, 2004; Davis et al., 2003; Denning et al., 2008). Other authors have examined the impact of subgrid-scale land surface heterogeneity on PBL processes, specifically the partitioning between sensible and latent heat fluxes due to variations in amount of vegetation cover (e.g. Avissar and Pielke 1989; Pielke and Avissar 1990; Avissar 1991; Liu et al., 1999; Weaver and Avissar 2001). This partition is important for determining PBL depth and induced mesoscale circulations. The emphasis of this paper, however, is not on mesoscale circulations, but on the local impact of overshooting thermals on entrainment and PBL growth. It would be interesting in the future to examine the impacts of both of these complex processes together.

Section 3.2 describes the SiB-RAMS model and the entrainment parameterization. Section 3.3 discusses the observations and measurement techniques. Section 3.4 illustrates the results and the final section provides some conclusions.

3.2 Methods

a. Model description

The ecosystem model in the coupled SiB-RAMS model is the third version of the Simple Biosphere (SiB3) model developed by Sellers et al. (1986). SiB3 calculates the transfer of energy, mass, and momentum between the atmosphere and land surface (Sellers et al., 1996a,b; Corbin et al., 2008) and is coupled to the Brazilian version of the Regional Atmospheric Modeling System (BRAMS) (Freitas et al., 2006). Denning et al. (2003), Nicholls et al. (2004), and Wang et al. (2007) describe the coupled model in more detail.

The simulations presented here were performed on a single grid centered on the WLEF tower in northern Wisconsin. The grid used an increment of 40 km and spanned the continental United States and southern Canada. Vegetation data was derived from the 1-km AVHRR land cover classification data set (Hansen et al., 2000) while Normalized Difference Vegetation Index (NDVI) data were derived from 1-km resolution SPOT 10-day composites from the VEGETATION instrument on board the SPOT-4 (Système Probatoire d'Observation de la Terre) polar orbiting satellite. The NDVI data were provided by the United States Department of Agriculture Foreign Agriculture Service (USDA/FAS) through collaboration with the Global Inventory Modeling and Mapping Studies (GIMMS) Group at the National Aeronautics and Space Administration Goddard Space Flight Center (NASA/GSFC). Surface fluxes of carbon from anthropogenic sources are derived from 1995 CO₂ emission estimates from Andres et al. (1996) with a

scale of 1.1055 to adjust for 1999 values (Marland et al., 2005; Wang et al., 2007). Air-sea CO₂ fluxes are the monthly 1995 estimates from Takahashi et al. (2002) and are assumed to adequately represent the conditions present in 1999.

Meteorological fields are initialized by the National Center for Environmental Prediction (NCEP) mesoscale Eta-212 grid reanalysis with 40-km horizontal resolution (AWIPS 40-k). This data set was also used to nudge the lateral boundary conditions every 30 minutes. Soil respiration factors and soil moisture were initialized from an offline SiB3 simulation run for 10 years using NCEP/NCAR (National Center for Atmospheric Research) reanalysis driver data from 1989 to 1999. Initial and hourly lateral boundary CO₂ concentrations were specified by the Parameterized Chemistry Transport Model (PCTM) (Kawa et al., 2004; Parazoo et al., 2008).

b. Entrainment parameterization

The entrainment parameterization was discussed in an idealized case study by McGrath-Spangler et al. (2009) and is based on the idea that the buoyancy flux at the top of the PBL is negatively proportional to the buoyancy flux at the surface (e.g. Betts, 1973; Carson, 1973; Deardorff, 1974; Rayment and Readings, 1974; Willis and Deardorff, 1974; Stull, 1976, 1988; Davis et al., 1997; Sullivan et al., 1998; Yi et al., 2001). The profile of buoyancy flux throughout the well-mixed, quasi-steady boundary layer is often approximated as linear, decreasing from the surface and becoming negative within the entrainment zone (Stull 1976). This implies that the negative buoyancy flux at

the base of the capping inversion is linearly proportional to the buoyancy flux at the surface. This assumption produces the equation:

$$\overline{w'\theta_v'}|_{z_i} = -\alpha \overline{w'\theta_v'}|_s. \quad (3.1)$$

In (3.1), $\overline{w'\theta_v'}$ is the turbulent virtual potential temperature flux at the height of the inversion (Z_i) and at the surface (s) and α is the tunable proportionality constant. Estimates of α range from zero to one, but most published values are between 0.1 and 0.3 with a value of 0.2 being the most appropriate for free convection (Stull, 1988).

Equation (3.1) can be used to derive equations for the time rate of change of potential temperature, wind velocity, water vapor mixing ratio, turbulent kinetic energy (TKE), and CO₂ concentration across the interface separating the PBL from the overlying inversion. These equations mix the properties of the boundary layer with those of the free troposphere as would be done by overshooting thermals in the physical world. The result is warmer, drier, less turbulent conditions being mixed into the top model layer of the PBL to be mixed downward by turbulent eddies and cooler, moister, turbulent air being mixed up into the lowest layer of the overlying inversion.

In idealized simulations, the parameterization resulted in an insertion of heat energy into the PBL and an upward transport of TKE into the lowest layer of the overlying inversion, producing a deeper PBL. The downward advection of heat and upward moisture transport induced a warmer and drier boundary layer and a cooler and moister inversion layer.

The drying and warming caused by entrainment increases physiological stress thereby limiting carbon assimilation by plants. When conditions within the atmosphere in the immediate vicinity of the leaf become less than optimal, the stomata close, limiting

water loss through transpiration and reducing carbon assimilation. This increases the Bowen ratio (the ratio of sensible to latent heat fluxes) as latent heat flux is reduced in favor of sensible heat flux. Increased sensible heat flux raises temperatures and encourages further PBL growth. In addition, changes to cloud cover and precipitation result from the shift in the Bowen ratio and multiple interrelated processes.

3.3 Observations

Evaluation of the entrainment parameterization uses observations from the WLEF television tower located in the Park Falls Ranger District of the Chequamegon National Forest, about 15 km east of Park Falls, Wisconsin, USA at 45.95°N latitude, 90.27°W longitude.

Since 1996, micrometeorological and eddy covariance flux measurements have been made at 30 m, 122 m, and 396 m (Berger et al., 2001; Davis et al., 2003). High precision, high accuracy CO₂ concentrations have been made at six levels (11 m, 30 m, 76 m, 122 m, 244 m, and 396 m) since 1994. The CO₂ measurements are made using LI-COR 6251 infrared gas analyzers (IRGA) (Bakwin et al., 1998; Davis et al. 2003).

During 1999, from July to September, an Integrated Sounding System (ISS) was deployed about 8 km east of the WLEF tower (Angevine et al., 1998; Yi et al., 2001; 2004; Denning et al., 2008). The ISS included a radar profiler, a Radar and Radio-Acoustic Sounding System (RASS), and a radiosonde (Yi et al., 2001). The profiler is a sensitive 915 MHz Doppler radar designed to respond to fluctuations of the refractive index in clear air (Ecklund et al., 1988; White et al., 1991; Angevine et al., 1993;

1994a,b; Yi et al., 2001) and can be used to detect the height of the PBL in conditions without precipitation or heavy clouds (Yi et al., 2001; 2004).

Boundary layers shallower than 400 m, such as those that occur at night and in the early morning, are not well defined from the profiler signal to noise ratio (SNR) measurements (Yi et al., 2001; 2004). In these cases, the strong stratification present in the nocturnal boundary layer produces a gradient in the CO₂ concentration (Yi et al., 2001; 2004; Denning et al., 2008) that is detected by the vertical profile of CO₂ measured along the depth of the tower and can be used to determine the depth of the nocturnal boundary layer.

3.4 Results

a WLEF comparison

Figure 3.1 compares the observed monthly mean diurnal cycle of PBL depth measured near the WLEF tower in northern Wisconsin to the SiB-RAMS model for both the control ($\alpha = 0$) and enhanced entrainment cases ($\alpha = 0.2$). The error bars on the observations (thickest bars), control case (medium thickness) and enhanced entrainment case (thinnest bars) represent the standard deviation of daily values at each hour. Modeled daytime and nighttime PBL depths are determined by the potential temperature and CO₂ concentration gradients respectively. The simulated monthly mean diurnal cycle was found by averaging non-precipitating hours to account for the lack of observations during precipitation events.

In all three months shown in Figure 3.1, the enhanced entrainment case performed better in representing the observations than did the control case. Although the afternoon PBL depths in the control case fell within the error bars in July and August, these values were near the low end, especially in August, and were well below the observations and their associated error bars in September. This was partly due to the model's inadequate representation of the rapid late morning growth of the PBL that is better simulated in the enhanced entrainment case. Since nighttime values of PBL depth are similar for both model simulations, the steeper morning growth of the enhanced entrainment case produces a deeper PBL in the early afternoon that continues into the afternoon when PBL growth begins to slowdown. The enhanced entrainment simulation performed better in the afternoon as well with deeper maximum PBL depths in all three months, falling within the error bars. However, this simulation produced PBL depths that were still too shallow in August and September, indicating a need for further improvements.

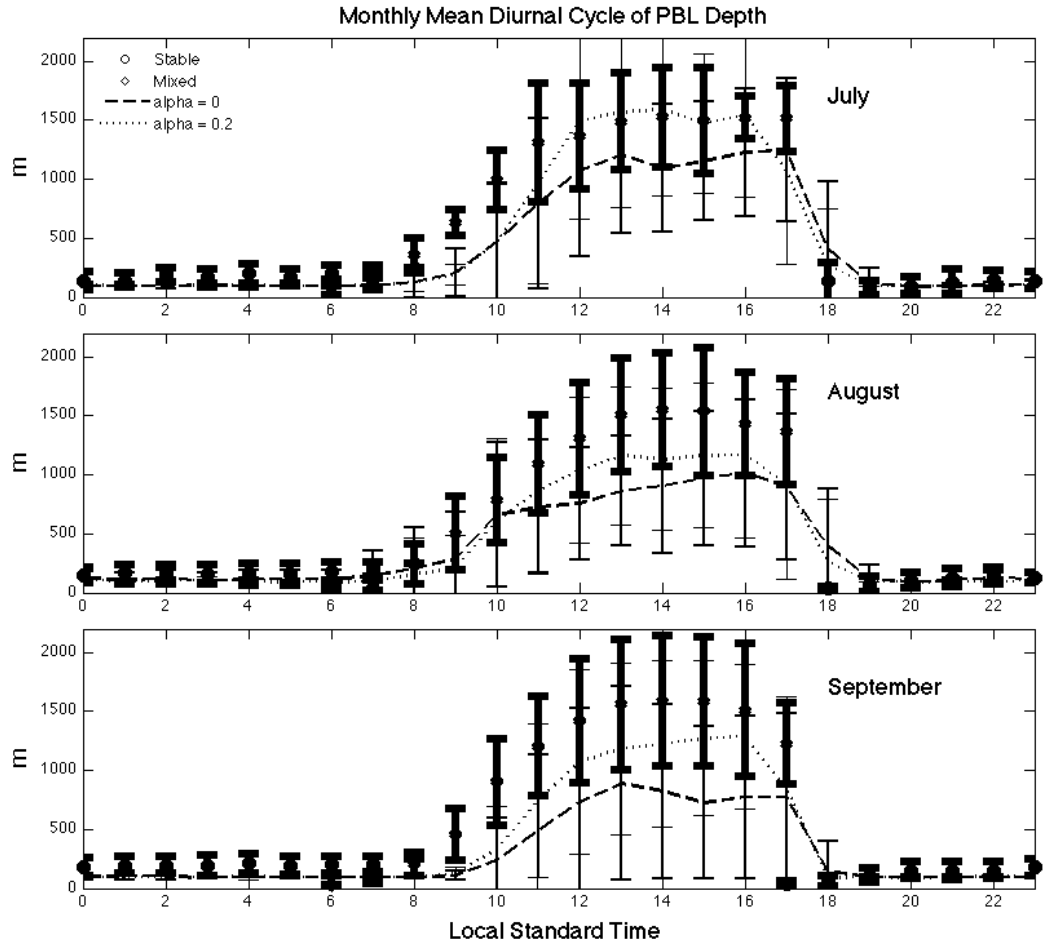


Figure 3.1 Monthly mean diurnal cycle of PBL depth (m) in (a) July, (b) August, and (c) September. Model estimates are averaged over non-precipitating hours only. Error bars are the standard deviation of daily values at each hour. The thickest error bars are for the observations, the next thickest are for the control case and the thinnest error bars are for the enhanced entrainment case.

PBL depth has large implications for CO_2 concentrations and gradients within the boundary layer. Deeper PBL depths dilute the effect of assimilation on carbon concentrations and the warming and drying associated with entrainment alters the stomatal openings of vegetation and therefore the uptake of CO_2 . Accurately simulating CO_2 concentration is important for determining sources and sinks through atmospheric inversions and thus it is important to accurately simulate the PBL depth.

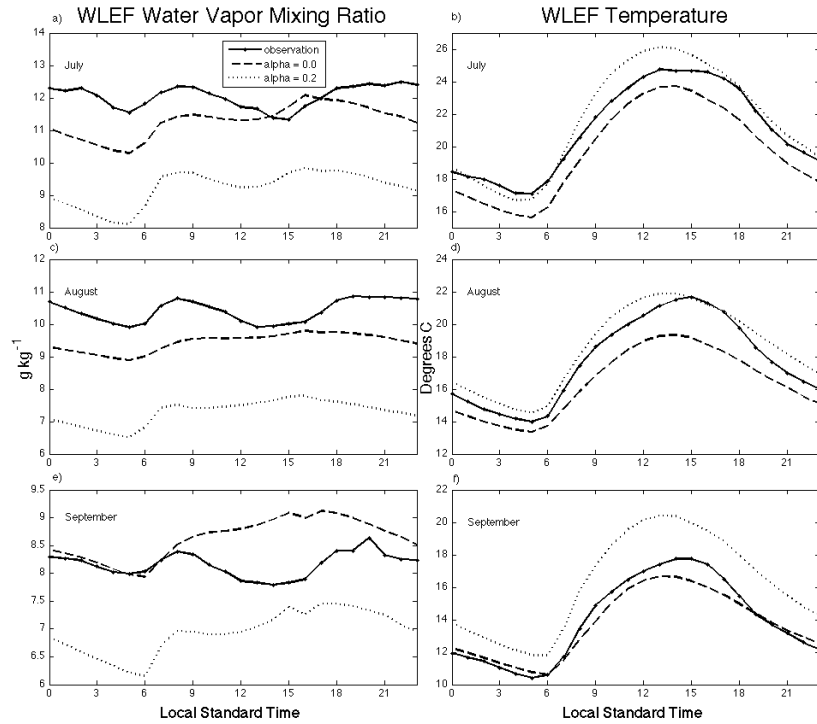


Figure 3.2 Monthly mean diurnal cycle at WLEF of water vapor mixing ratio (g kg^{-1}) in the left column and temperature ($^{\circ}\text{C}$) in the right column for July (a and b), August (c and d), and September (e and f) at 30 m.

Figure 3.2 shows the differences in water vapor mixing ratio and temperature in July (a, b), August (c, d), and September (e, f) produced by the two model simulations compared to the observations. In general, the parameterization of overshooting thermals produced warmer and drier results, with mixed success. Water vapor was better simulated in the control simulations. Only in the mid-afternoon of September was the mixing ratio too moist and a drying improved the results. Although the mixing ratio was poorly simulated by the enhanced entrainment case in July and August, the warming associated with the enhanced entrainment improved the temperature in these months and even warmed a little too much in July. In September, the control simulation better represented the temperature.

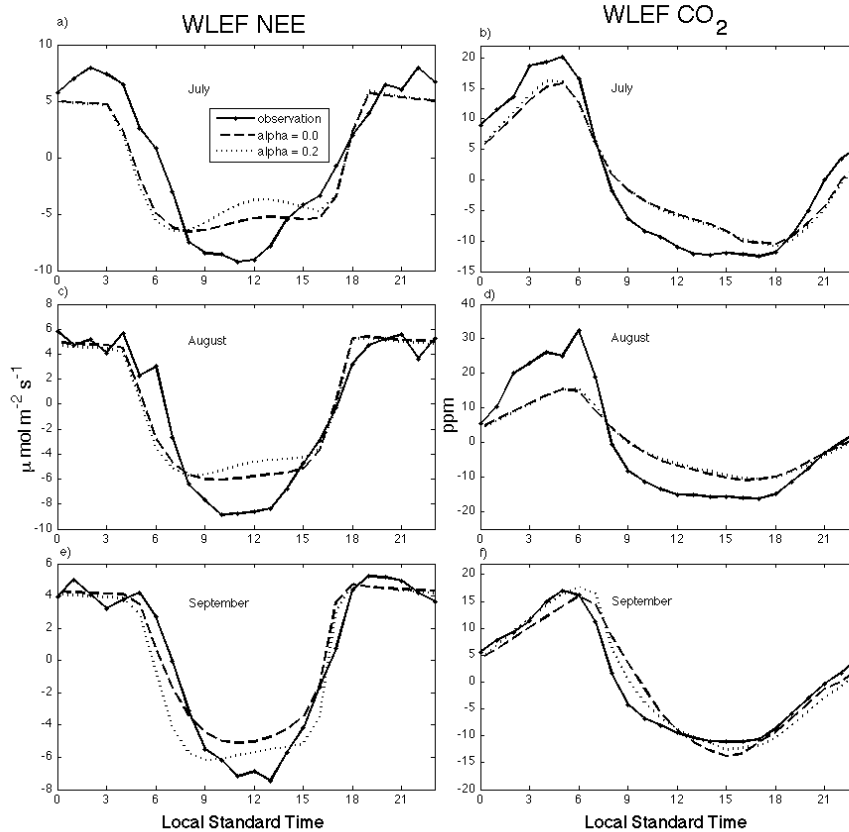


Figure 3.3 Monthly mean diurnal cycles at WLEF of net ecosystem exchange ($\mu\text{mol m}^{-2} \text{s}^{-1}$) in the left column and of CO_2 concentration perturbations (ppmv) in the right column during July (a and b), August (c and d), and September (e and f) at 30 m.

Figure 3.3 presents the modifications of additional entrainment on net ecosystem exchange (NEE; respiration – carbon assimilation) (a, c, e) and CO_2 concentration (b, d, f) at 30 m at the WLEF tower during the summer of 1999. Too much uptake occurred in the morning and late afternoon of both cases, a known issue in SiB at the WLEF tower (Baker et al., 2003). The enhanced entrainment case was warmer in the early morning, allowing plant stomata to open earlier and begin carbon assimilation. The warmer and drier conditions at midday reduced stomatal conductance in the enhanced entrainment case, reducing carbon uptake in order to minimize water loss. In August, the control case

produced a better estimate of NEE summed over the diurnal cycle, but in July and September, the additional entrainment produced better results.

The differences in CO₂ concentration at WLEF between the control and enhanced entrainment cases are small because of the conditions at WLEF during the simulation time frame. During these three months, northern Wisconsin is relatively unstressed and is not experiencing much water limitation. The warmer and drier conditions associated with enhanced PBL top entrainment do not change these overall conditions and the ecophysiological stress is only minimally changed so NEE (Figure 3.10) is not much affected. However, even these small changes accumulate over time and, along with the changes in PBL depth, produce regional changes in CO₂ concentration (Figure 3.11).

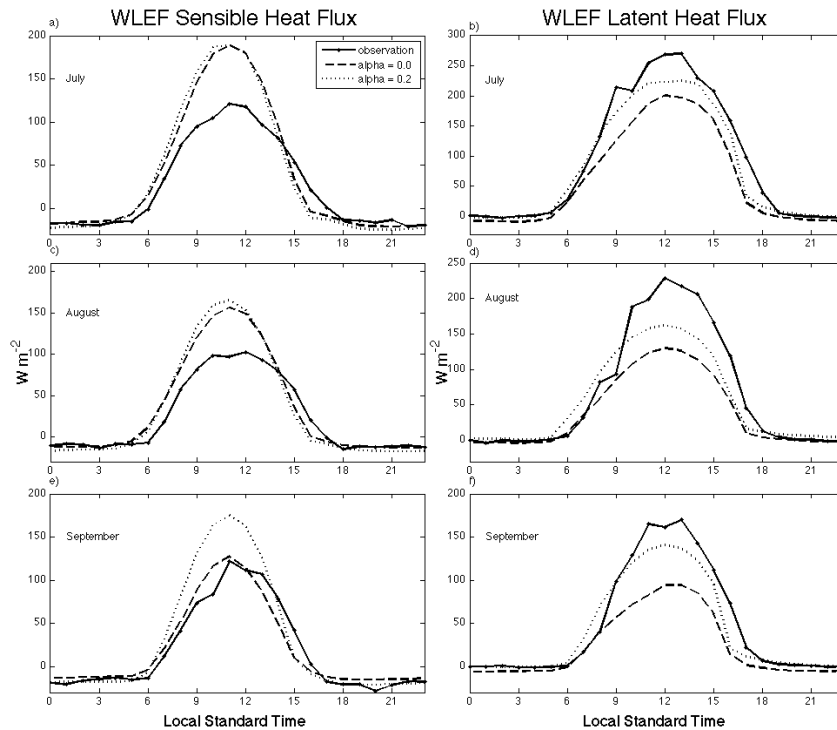


Figure 3.4 Monthly mean diurnal cycle at WLEF of sensible heat flux (W m^{-2}) in the left column and of latent heat flux (W m^{-2}) in the right column during July (a and b), August (c and d), and September (e and f) at 30 m.

Figure 3.4 illustrates the differences in sensible (a, c, e) and latent (b, d, f) heat fluxes. The variations in the heat fluxes between the control and enhanced entrainment cases demonstrate the interactions between the PBL, the physiological responses, and the large-scale weather. As gradients in temperature and water vapor mixing ratio increase between the CAS and the PBL, the sensible and latent heat fluxes increase respectively. The SiB model, in point simulations, has been shown to have a warm bias at WLEF, producing too much sensible heat flux and a high Bowen ratio (Baker et al., 2003) and this bias is also present in the SiB-RAMS coupled model (Denning et al., 2003). Baker et al. (2003) hypothesize that this bias is due to nearby wetlands not being simulated by the model.

The warming and drying of the atmosphere can close or open leaf stomata in an evolved response to limit water loss. Closing the stomata limits transpiration, thus shifting the Bowen ratio in favor of sensible heat flux. In addition, closing the stomata reduces carbon assimilation, increasing NEE and the CO₂ concentration. Cloud cover, radiation, and regional geopotential gradients are tied to PBL temperature and moisture (Stull, 1988) so the large-scale weather is also modified. Reduced cloud cover over the eastern United States and Midwest, associated with a drier PBL, allows more solar radiation to reach the ground, increasing the surface energy budget and amending sensible and latent heat fluxes. In a few small regions where cloud cover was increased and less solar radiation was able to reach the ground, the surface heat budget was decreased. As the surface heat budget changes, so also does the simulated entrainment buoyancy flux at the top of the PBL through the proportionality between them.

The sensible heat flux of the control case was similar to that observed in September and too great in July and August. The additional entrainment produced larger sensible heat fluxes and so was less representative of the observations. However, enhanced entrainment from overshooting thermals improved estimates of latent heat flux during all three months. The latent heat flux of the control case was too little and the additional entrainment increased this flux.

b. NARR comparison

Figure 3.5 compares the model results to the North American Regional Reanalysis (NARR; Mesinger et al., 2006) over the time mean of the months of July, August, and September. The left column shows the results of the control model minus the NARR while the right column shows the differences between the enhanced entrainment case and the reanalysis. When examining this figure, it is important to remember that the lateral boundaries of the SiB-RAMS model are nudged to the NCEP Eta model output and so should not be used for comparison.

The top row shows the model CAS temperature compared to the NARR 2m temperature. This temperature is at the land-atmosphere interface and is impacted by the complex interactions of radiation, advection, and sensible heat flux. It is important for determining the vegetative stress and therefore the NEE and CO₂ concentration. The CAS temperature is prognosed by SiB and is therefore valid only on land. The enhanced entrainment parameterization warmed the air within the PBL everywhere (Figure 3.7b), but the effect on the CAS temperature was not quite as simple. While the temperature increased in much of the domain, the states along the Gulf Coast actually experienced a

cooling. When compared to the NARR, this indicated a weakness of the model. However, in the upper Midwest, including WLEF, the northeastern United States, and southeastern Canada, warmer temperatures indicated an improvement in the simulation results and a closer match to the reanalysis result.

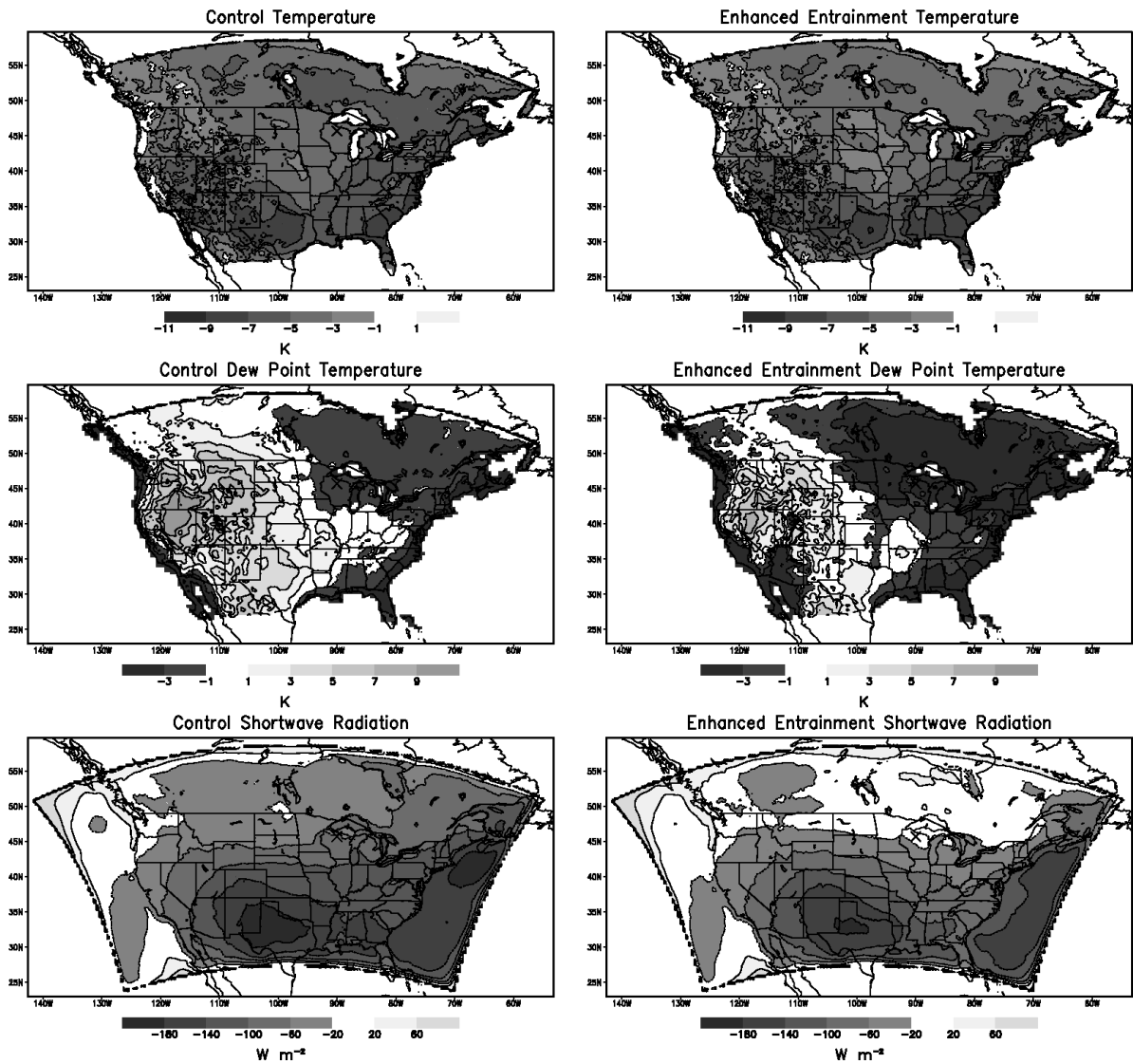


Figure 3.5 Comparison between the North American Regional Reanalysis (NARR) product and the control (left) and enhanced entrainment ($\alpha=0.2$; right) models for 2m temperature (top; K), 2m dew point temperature (middle; K) and downward shortwave radiation (bottom; $W m^{-2}$). The X in this and all subsequent figures marks the WLEF tower.

The middle row compares the CAS dew point temperature, computed from SiB prognostic variables, to the NARR 2m dew point temperature. The dew point temperature is a measure of the amount of water vapor surrounding the vegetation and is important for calculations of vegetative stress. It therefore impacts NEE and CO₂ concentration through its impact on stomatal conductance. The CAS dries under enhanced entrainment, producing a decrease in the dew point temperature. In the Midwest, including the WLEF tower, the control simulation is too dry compared to the NARR and a further drying through enhanced entrainment worsens the problem. The result also degrades in southeastern Canada and in the southeastern United States. In the western states, however, where the control model is too moist, a drying improves the result. This illustrates the spatial variability of the response of the model to the parameterization.

Since more downward shortwave radiation reaches the surface on clear days than on days with heavy cloud cover, the shortwave radiation gives an indication to the amount of cloud cover. Over much of the domain, specifically the northeastern United States and southeastern Canada, the shortwave radiation is increased. This is important for photosynthesis because photosynthetic rates increase with increasing solar radiation up to a saturation amount. This affects the NEE (Figure 3.10) and consequently the CO₂ concentration in addition to the sensible and latent heat fluxes. In general, both models predict less downward solar radiation than the NARR, indicating cloudier conditions, with the enhanced entrainment simulation showing an improvement over the control simulation in areas such as southern Canada and along the Gulf Coast. Although the decreased cloud cover would lead to increased PBL temperatures, idealized simulations

by McGrath-Spangler et al. (2009) show that the qualitative results of this study are independent of changes in cloud cover.

Comparisons to the NARR data highlight the spatial inhomogeneity of the model response to the enhanced entrainment parameterization, the dependence upon the underlying surface conditions, and the complex interactions between the land surface and the atmosphere. The following subsection examines these points in further detail in direct comparisons between the two simulations.

c. Regional comparison

The following figures represent the time mean differences between the enhanced entrainment and control cases averaged over the months of July, August, and September. These difference plots show the impact of overshooting thermals on the model environment.

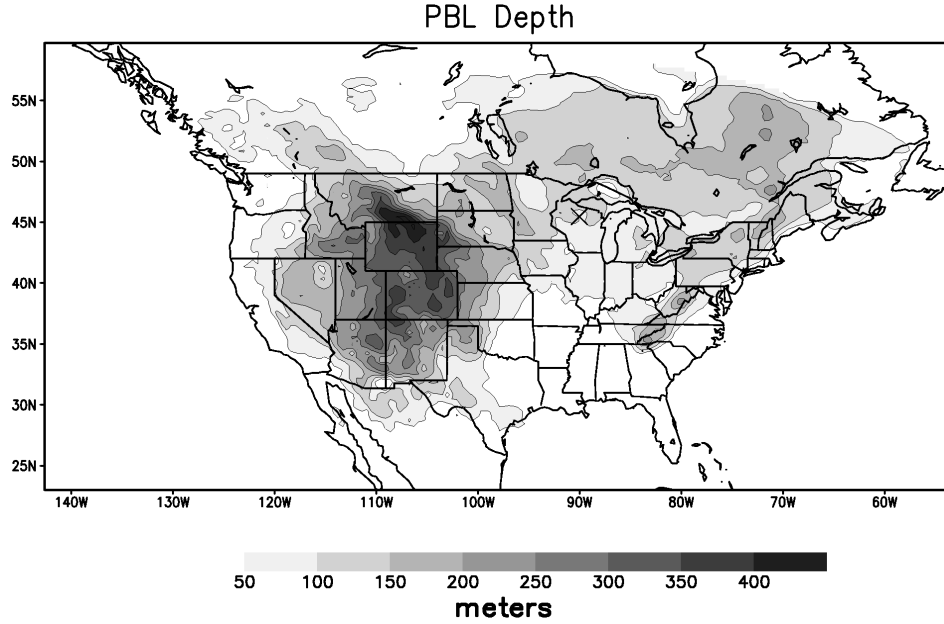


Figure 3.6 Effect of entrainment from overshooting thermals (enhanced entrainment case minus control case) on PBL depth (m) in the time mean from July through September including both daytime and nighttime values.

Figure 3.6 shows the impact of the enhanced entrainment parameterization on the simulated PBL. Enhanced entrainment produced, on average, a 70m (11%) deeper PBL. The largest increases of around 300 to 400 m occurred over the dry Rocky Mountain region where the Bowen ratio was largest. Enhanced entrainment is proportional to the surface buoyancy flux ($H = \overline{\rho c_p w' \theta_v'}$) where

$$H \approx Q_H + \frac{0.61 c_p \theta Q_E}{L}. \quad (3.2)$$

Q_H represents the sensible heat flux, Q_E the latent heat flux, c_p the specific heat at constant pressure, and L the latent heat of vaporization. This equation is derived using Reynolds averaging and a few simplifying assumptions. Therefore, for a given amount of radiation, the larger the Bowen ratio (Q_H large compared to Q_E) the larger the heat flux and by extension the entrainment flux and the influence on the PBL depth.

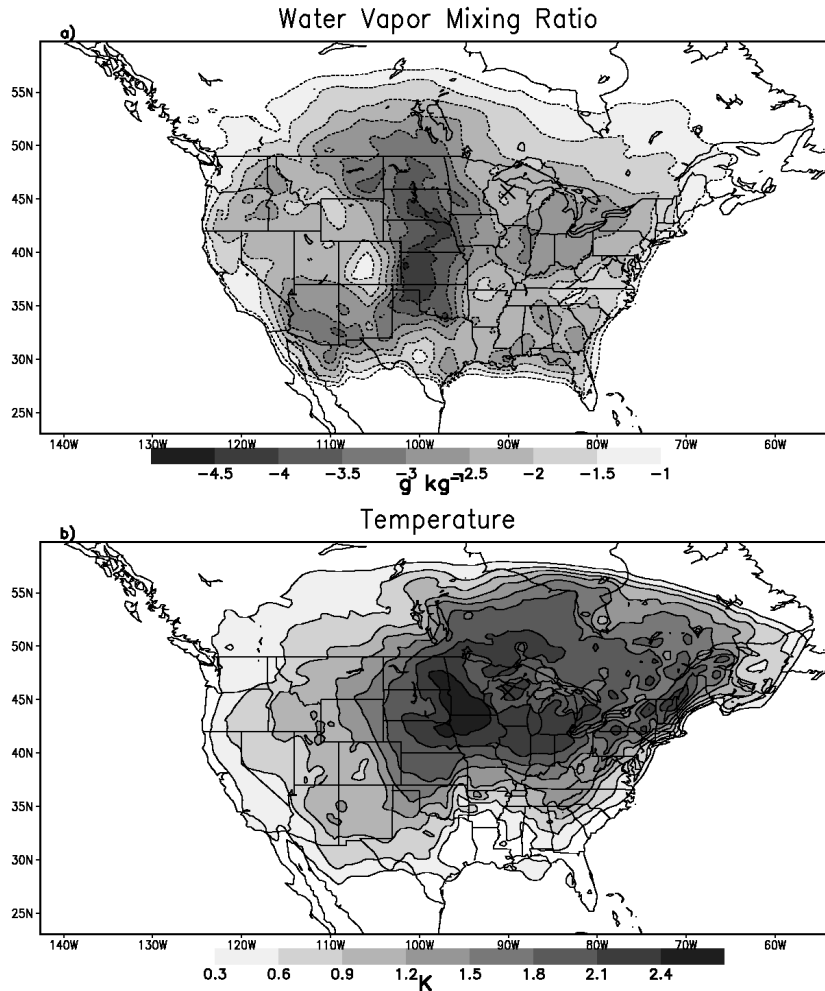


Figure 3.7 Effect of entrainment from overshooting thermals (enhanced entrainment case minus control case) on (a) water vapor mixing ratio (g kg^{-1}) and (b) temperature (K) at 30 m in the time mean from July through September.

Figure 3.7a shows a map of the difference in water vapor mixing ratio between the two cases. The domain-wide decrease in mixing ratio had an average of 18% (1.5 g kg^{-1}). The largest decrease was just downstream of the Rocky Mountains, where PBL depth was most affected, from North Dakota south into northern Texas. When the air left the Rocky Mountain region, it characterized the accumulated effect of the enhanced entrainment. Large decreases in mixing ratio were also present in the Midwest from

Illinois into Ohio and Michigan and along the Mexican border with Arizona and New Mexico. Smaller decreases were present in central Colorado and the Carolinas.

Figure 3.7b shows the map of average change in temperature due to the enhanced entrainment. Temperature increased everywhere with an average increase of 4.3% (0.7°C). The greatest increases occurred in the eastern sections of the Dakotas, Nebraska, and Minnesota down into Iowa. Since the lateral boundaries were nudged to the same values in both cases, temperature changes were weakest there.

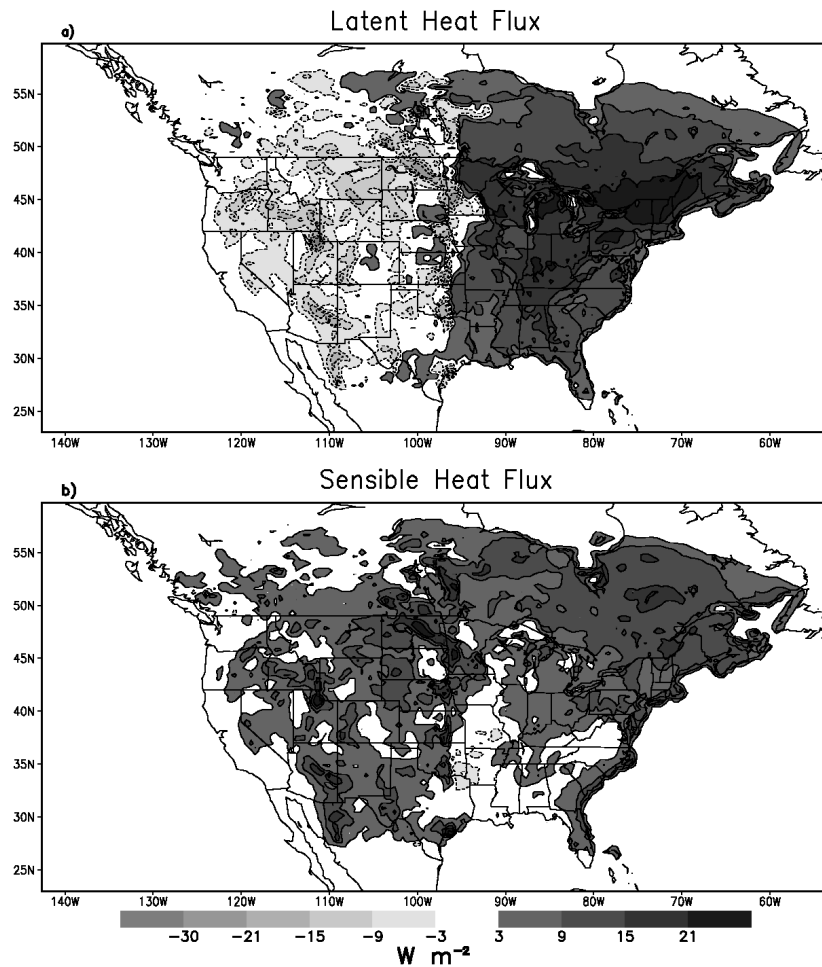


Figure 3.8 Effect of entrainment from overshooting thermals (enhanced entrainment case minus control case) on (a) latent heat flux ($W m^{-2}$) and (b) sensible heat flux ($W m^{-2}$) in the time mean from July through September.

Figure 3.8a is a map of the time mean difference in latent heat flux from the CAS to the boundary layer. On average, the latent heat flux was increased by just over 12% (12.7 W), mostly in the eastern half of the United States. The sharp transition between a decrease in latent heat flux in the west and an increase in the east is a result of a coupled surface-atmosphere response to the modifications to the PBL top entrainment. The surface response to the warmer and drier PBL is dependent upon several factors including vegetation type and prevailing surface conditions. In the west, increased solar radiation imposes an ecophysiological stress that the vegetation responds to by closing their stomates, limiting transpiration and decreasing the latent heat flux. The eastern United States is not as water limited as in the west and although overall stress is increased, the additional radiation benefit compensates for the drier conditions, allowing plant stomates to open further in order to permit more carbon assimilation. More water is lost through transpiration and the latent heat flux is increased.

Figure 3.8b is a map of the differences in sensible heat flux between the CAS and the boundary layer for the enhanced entrainment and control cases. Sensible heat flux, on average, increased by almost 4 W in the time period of July through September. A drier, deeper PBL resulted in fewer clouds and more solar radiation reaching the ground. This allowed both the sensible and latent heat fluxes to increase. For this study, the addition of the enhanced entrainment parameterization produced a nearly 1% decrease in cloud cover over a large portion of the domain. This decrease extended southeastwards from Montana to Florida and the Gulf of Mexico, up along the United States eastern coast and then up into Canada and the northern boundary of the domain. Portions of southeastern Montana and Idaho as well as parts of the Gulf Coast and Atlantic experienced an

increase in the amount of cloud cover, however, on the average, the parameterization produced a 0.3% decrease in the amount of cloud cover (not shown). This effect is only relevant when there are variations in cloud cover between the control and enhanced entrainment cases.

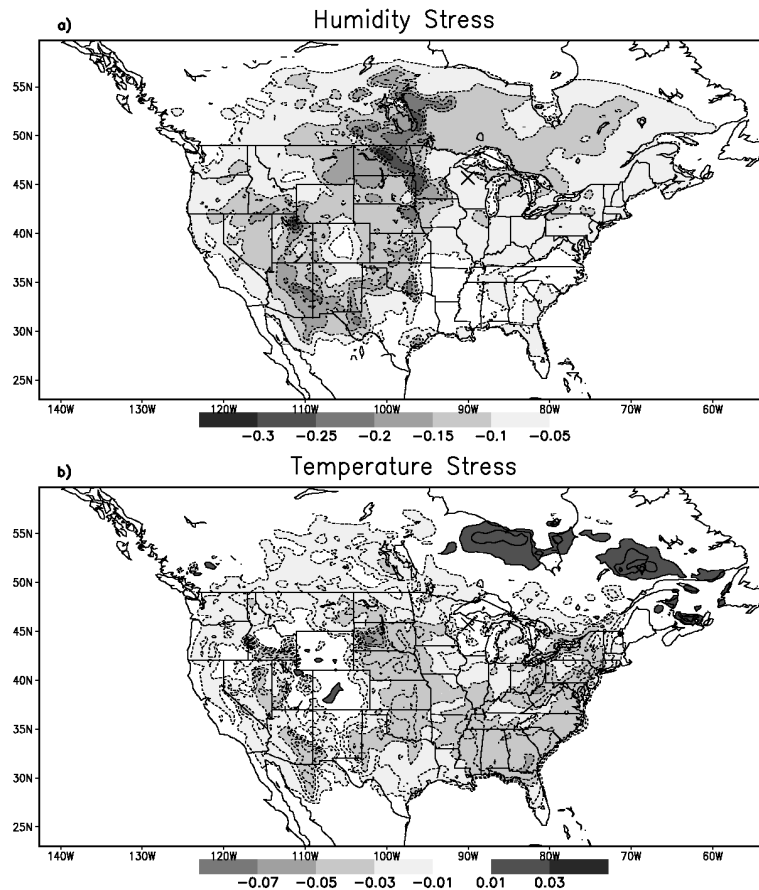


Figure 3.9 Effect of entrainment from overshooting thermals (enhanced entrainment case minus control case) on (a) humidity stress and (b) temperature stress in the time mean from July through September.

Figure 3.9a shows the physiological stress on vegetation due to low humidity. Stomata close to restrict water vapor loss when the leaf surface dries (Bonan et al., 2002; Ball et al., 1987; Collatz et al., 1991). This is expressed in the model as a decreased stress parameter. The stress parameters are dimensionless multiplicative factors that modify the stomatal conductance. They are scaled between 1 for optimal conditions

(resulting in unstressed conductance and fully open stomates) to 0 (severely stressed conductance) when environmental conditions decrease the stomatal opening (Sellers et al., 1997). Stomatal closing results in decreased transpiration, reduced latent heat flux, and increased sensible heat flux. This acts to reduce the boundary layer humidity and increase its temperature. Since a smaller stomatal opening produces decreased carbon assimilation, this parameter also indicates CO₂ concentration changes. The drying associated with entrainment from overshooting thermals produced a 10% change in the humidity stress parameter, indicating diminished stomatal conductance.

The effect of entraining thermals on physiological stress due to departures from a moderate temperature is illustrated in Figure 3.9b. This parameter has the same effect on stomatal conductance as the humidity parameter. Although warmer temperatures were present everywhere as was shown in Figure 3.7b, the temperature stress is not as straightforward. In regions where the summer temperature was already on the warm end of optimal vegetative temperatures, warmer temperatures due to enhanced entrainment produced smaller stomatal conductance. However, in relatively cool locations, such as northern latitudes and at high altitude, warmer temperatures were more moderate for the plants and stomatal conductance increased. In regions of Canada and along the Rocky Mountains, warmer temperatures were actually beneficial to the plants.

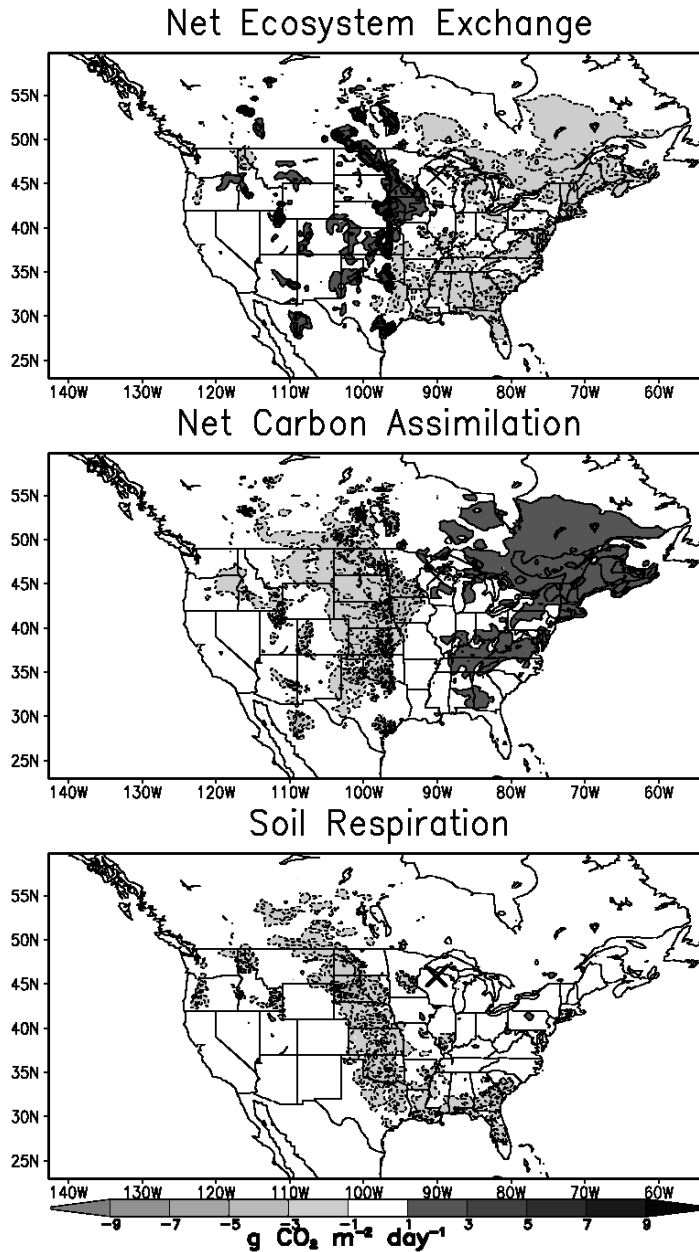


Figure 3.10 Effect of entrainment from overshooting thermals (enhanced entrainment case minus control case) on (a) net ecosystem exchange ($\text{g m}^{-2} \text{ day}^{-1}$), (b) carbon assimilation ($\text{g m}^{-2} \text{ day}^{-1}$), and (c) soil respiration ($\text{g m}^{-2} \text{ day}^{-1}$) in the time mean from July through September.

Stomatal conductance controls the amount of carbon that the vegetation is able to assimilate and therefore the NEE (Figure 3.10). NEE (Figure 3.10a) is decreased from

the Mississippi River eastwards to the Atlantic Ocean while, in the western United States, NEE is increased. Most of these changes are due to changes in carbon assimilation (Figure 3.10b). Assimilation was increased in the eastern half of the domain, mostly due to decreased cloud cover. Fewer clouds permit more solar radiation to penetrate to the surface, allowing more photosynthesis by the surface vegetation. The strongest increase in solar radiation (about 20 W m^{-2} in the average) occurred primarily in the eastern United States and southeastern Canada (not shown). Decreased carbon assimilation along the Great Plains was a result of warmer and drier conditions producing a closing of plant stomata. Reduced soil respiration (Figure 3.10c) through the Great Plains and along the Gulf of Mexico was a result of slightly reduced soil moisture. Enhanced soil respiration in the Ohio valley and New England was a result of warmer soil temperatures.

Figure 3.11 illustrates the CO_2 concentration effects at 500 m caused by the parameterized PBL top entrainment. Lower concentrations are present in southeastern Canada and New England because lower temperature stress (Figure 3.9b) and greater solar radiation allowed greater carbon assimilation (Figure 3.10b) through increased stomatal conductance in this region. Higher CO_2 concentrations centered on the upper Midwest are a result of reduced assimilation (Figure 3.10b) from the increased stress due to warmer and drier conditions (Figure 3.9) and a deeper PBL (Figure 3.6). The dilution of the carbon assimilation impact by the deeper PBL in addition to the weaker uptake of CO_2 produced higher CO_2 concentrations. The combination of a weak PBL depth response (Figure 3.6), greater carbon assimilation (Figure 3.10b) from increased solar radiation, and weaker soil respiration (Figure 3.10c) due to decreased soil moisture led to lower CO_2 concentrations over the states along the Gulf of Mexico, including Louisiana,

Alabama, and Florida. On average, there was no change in CO₂ concentration, but the gradients of CO₂ were largely impacted by entrainment. Enhanced entrainment produces a 7 ppmv gradient in CO₂ at 500 m above ground level from the eastern Minnesota/Iowa border to the border of New York and Canada, relative to the control case. These simulated differences in spatial patterns of atmospheric CO₂ suggest that the degree of entrainment at the PBL top could be an important influence on source/sink estimation by transport inversion.

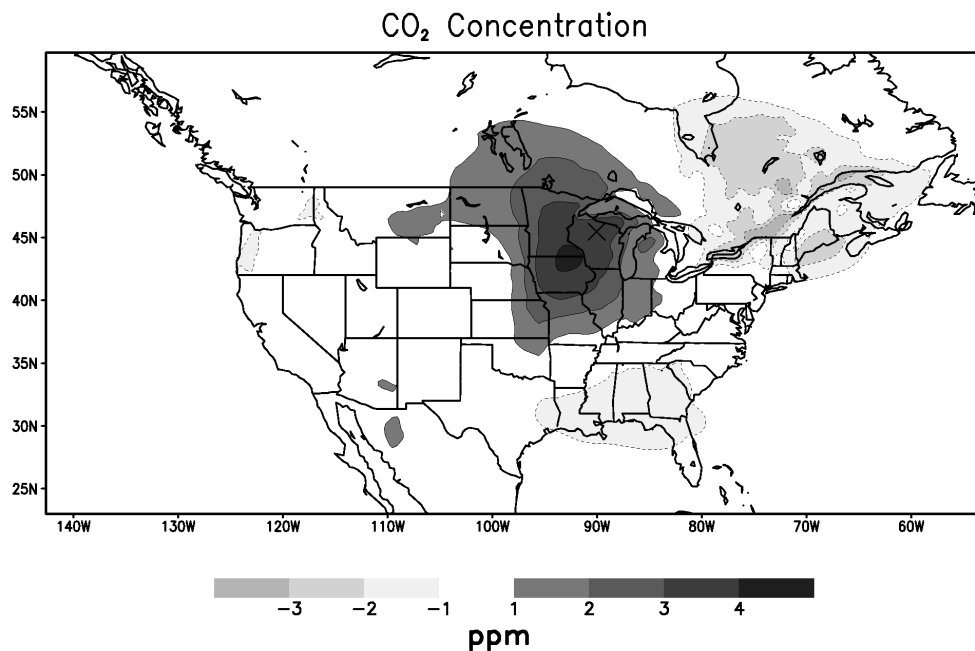


Figure 3.11 Effect of entrainment from overshooting thermals (enhanced entrainment case minus control case) on CO₂ concentration at 500 m in the time mean from July through September.

3.5. Conclusions

An entrainment parameterization was added to SiB-RAMS to include the effects of overshooting thermals. The parameterization warms and dries the boundary layer while cooling and moistening the inversion layer through a downward buoyancy flux at

the PBL top. The enhancement of entrainment effects increased the model estimate of the PBL depth in a simulation representing the weather conditions of late summer 1999.

The monthly mean diurnal cycle of PBL depth in July, August, and September at the WLEF tower in northern Wisconsin was simulated better when the enhanced entrainment was included. This depth is important for CO₂ studies as an error in PBL depth relates linearly to errors in CO₂ concentration. It was seen in Figure 3.11 that this could impact horizontal gradients of CO₂ and produce a model-observation mismatch even when the simulated fluxes are correct. Since most CO₂ concentration measurements are made near the surface and depend on the depth of the PBL and source/sink estimates of carbon from inversion studies depend on the CO₂ concentrations, correcting the PBL depth should also improve the source/sink estimates.

Overshooting thermals produce a complex interaction of PBL processes. In addition to increasing the PBL depth and modifying CO₂ concentration gradients, overshooting thermals and their associated entrainment impact temperature and water vapor mixing ratios which, in turn, impact sensible and latent heat fluxes and vegetative response. The warmer and drier conditions at the leaf surface alter stomatal conductance, modifying the Bowen ratio and cloud cover. Closing of the stomata produces decreased carbon assimilation which, when combined with the dilution effect of a deeper PBL, produces higher CO₂ concentrations. Decreased cloud cover results in greater net radiation at the surface and a greater surface heat flux. Given that the buoyancy flux at the top of the PBL is proportional to that at the surface, this produces a positive feedback and a large impact on the PBL and the land surface. Overshooting thermals, although small, can interact to produce large-scale changes in the land-atmosphere interaction.

Chapter 4

Sensitivity of Coupled Simulations to the Magnitude of Entrainment Fluxes

Summary

It has been shown that the concentration of carbon dioxide (CO_2) often measured is sensitive to the depth of the planetary boundary layer (PBL) or mixed layer. Unfortunately, due to the small-scale nature of many boundary layer processes, the PBL is often not well simulated and this leads directly to an error in the model CO_2 . One option is to parameterize the effects of these small-scale processes. An entrainment parameterization is added to a coupled land-atmosphere model and the sensitivity to the strength of the entrainment flux is evaluated. The results are subtle differences in the spatial patterns of meteorological and ecological variables. These small variations ease the gradient between the warm, dry southwestern United States and cooler, moister locations. The Bermuda High, off the east coast of the United States, is also weakened, changing advection patterns. These changes combine to form a CO_2 difference of up to 4.5 ppm over 280 km during midday and a change of about 3.5 ppm over the same distance in the diurnal mean.

4.1 Introduction

The planetary boundary layer (PBL) or mixed layer is the turbulent layer closest to the Earth's surface with a depth of about 1-2 km at midday and is crucial to many aspects of weather and climate. The PBL mediates exchanges of energy, moisture, momentum, carbon, and pollutants between the surface and the atmosphere and is important to the large-scale weather and climate. Unfortunately, no observation-based global PBL climatology exists (Seidel et al., 2010) and there are many problems with simulating the processes involved (Martins et al., 2010).

The sensitivity of tracer concentrations to surface fluxes is inversely proportional to the depth of the boundary layer, so errors in the PBL depth translate linearly to errors in the retrieved fluxes in inversion studies (Denning et al., 1995, 1996b, 1999, 2008; Zhang 2002; Gerbig et al., 2003a, 2008). The amount of uptake and release of carbon by plants is diluted through the volume of the boundary layer so that the concentration of carbon dioxide within the boundary layer is dependent upon the PBL depth (Denning et al., 1995; Yi et al., 2001; 2004). This means that errors in vertical mixing lead to inaccurate estimations of carbon sources and sinks.

Overshooting thermals modify the characteristics and depth of the PBL through the insertion of energy and mass through a process called entrainment. Entrainment “dilutes” the effects of surface fluxes in the PBL and is one of the most important processes models must represent (Ayotte et al., 1996). Overshooting thermal effects are, however, unresolved in most regional models. Mesoscale meteorological modeling usually uses a resolution too coarse to resolve even the largest overshooting thermals and

thus does not capture the entrainment process at the top of the boundary layer (Ayotte et al., 1996; Gerbig et al., 2003a).

Previous work used an idealized version of an ecosystem-atmosphere model called SiB-RAMS to study the effects of entrainment (McGrath-Spangler et al., 2009). The authors ran an enhanced entrainment parameterization to simulate the impacts of overshooting thermals and found that to produce a warmer, drier mixed layer, altered surface fluxes, increased PBL depths, and modified carbon dioxide (CO₂) concentrations. The parameterization is based on the assumption that the heat flux at the top of the boundary layer is negatively proportional to the heat flux at the surface. From experimentation and theory, estimates of this tunable proportionality constant range anywhere from zero to one with most published values between 0.1 and 0.3 (e.g. Betts, 1973; Carson, 1973; Deardorff, 1974; Rayment and Readings, 1974; Willis and Deardorff, 1974; Stull, 1976; Davis et al., 1997; Sullivan et al., 1998; Yi et al., 2001). This parameterization alters the temperature, water vapor mixing ratio, winds, and CO₂ mixing ratios of the boundary layer and the lowest layer of the capping inversion at the top of the PBL. In addition to these direct impacts, there are multiple complex interactions with the land surface.

Changes in the near-surface temperature and water vapor affect the surface fluxes through physiological processes in plant canopies (e.g. stomatal conductance). When conditions within the atmosphere in the immediate vicinity of leaves, the stomata close, limiting water loss through transpiration and reducing carbon assimilation. This increases the Bowen ratio (the ratio of sensible to latent heat fluxes) as latent heat flux is reduced in favor of sensible heat flux. This can modify the carbon fluxes directly.

McGrath-Spangler et al. (2009) found that in the morning, warmer temperatures from enhanced entrainment produced more optimal conditions and uptake of carbon was enhanced. In the midafternoon, high-temperature stress and low humidity produced a decrease in carbon assimilation. The overall impact of simulated entrainment on carbon dioxide concentrations in the PBL reflects the modified NEE as well as dilution through a deeper mixed layer. This idealized study demonstrated the complex interactions between PBL top entrainment, boundary layer processes and surface vegetation.

An additional experiment was performed using realistic conditions for the late summer of 1999 (McGrath-Spangler and Denning, 2010). This experiment was performed in order to evaluate the performance of this parameterization against observations of PBL depth made at the WLEF very tall tower in northern Wisconsin (Angevine et al., 1998; Yi et al., 2001, 2004; Denning et al., 2008). The monthly mean diurnal cycle of PBL depth using this parameterization was better simulated when compared to observations than the control case due to steeper morning growth producing deeper PBL depths in the early afternoon. In the time-domain average, the PBL depth was increased by 11%, the temperature by 4.3%, and the water vapor mixing ratio was decreased by 18% (McGrath-Spangler and Denning, 2010). Although the addition of the parameterization improved the representation of PBL depths at WLEF, the midday PBL depth was still too shallow. This suggests that the strength of the entrainment flux could be improved and motivates a discussion on the sensitivity of the model to this parameterization.

The overall effect of enhanced entrainment in this experiment on CO₂ concentrations was to alter the time-mean regional gradients by as much as 7 ppm over

1000 km. These changes were due to modified assimilation from changes in stress, deeper PBL dilution of surface fluxes, and greater assimilation from increased solar radiation from changes in cloud cover. This work reinforces the importance of the complex interactions of boundary layer processes and the feedbacks between the atmosphere and land surface.

The next step is to evaluate the sensitivity of these previous results to the strength of the entrainment flux using a realistic simulation. Using a data assimilation framework, the magnitude of the PBL-top entrainment could be optimized against well-observed measurements of temperature and dewpoint and even PBL depth where available. This improvement in one model process would eventually improve simulations of weather and climate and diagnoses of the carbon budget. This chapter evaluates the sensitivity of the model climate to PBL-top entrainment in order to establish a basis for future data assimilation work.

The following section is a description of the model and methods used. Section 4.3 describes the results from simulations varying the strength of the entrainment flux. The final section offers brief conclusions.

4.2 Methods

The enhanced entrainment parameterization has been implemented in a modified form of the Regional Atmospheric Modeling System (RAMS) version 5.04 also known as BRAMS version 2.0. The land surface model used is the third version of the Simple Biosphere Model (SiB3) initially developed by Sellers et al. (1986). The coupling of the

two models is called SiB-RAMS (Denning et al. 2003; Nicholls et al. 2004; Wang et al. 2007; Corbin et al. 2008). The SiB-RAMS version used here differs from the one used by McGrath-Spangler et al. (2009) and McGrath-Spangler and Denning (2010) in several significant ways. Since the previous work, tiles and crops (Lokupitiya et al., 2009; Corbin et al., 2010) have been incorporated into the SiB model. In addition, several errors in the radiation, large-scale precipitation and model coupling have been fixed (A. Schuh, personal communication, September 2011). These changes have modified the model output in significant ways.

RAMS was initially developed at Colorado State University as a non-hydrostatic three-dimensional model in order to study mesoscale and cloud-scale phenomena (Pielke 1974; Tripoli and Cotton 1982; Pielke et al. 1992; Cotton et al. 2003). SiB is a land-surface parameterization used to compute biophysical exchanges in climate models (Sellers et al., 1986), but also includes ecosystem metabolism (Sellers et al., 1996; Denning et al., 1996a). Farquhar et al. (1980) originally developed the photosynthesis parameterization in SiB. SiB is an interactive dynamic land surface model that determines the surface boundary conditions for and receives its upper boundary from RAMS.

The grid domain spans the continental United States and Southern Canada with a grid increment of 40 km. This grid increment allows the resolution of mesoscale and synoptic features, but is much too coarse to resolve the individual thermals that entrain free tropospheric air into the boundary layer. The vegetation data comes from the 1-km AVHRR land cover classification data set (Hansen et al., 2000). Anthropogenic surface fluxes of carbon are derived from the high resolution Vulcan fossil fuel inventory fields

(Gurney et al., 2009). This data set has 10 km horizontal resolution and hourly temporal resolution and includes mobile emission sources and power plants away from densely populated areas. Meteorological fields are initialized by the North American Regional Reanalysis (NARR) and this data is also used to nudge the lateral boundaries. Soil respiration factors and soil moisture were initialized from offline SiB simulations run for 10 years. Initial and lateral boundary CO₂ concentrations were specified by the Parameterized Chemistry Transport Model (PCTM) (Kawa et al., 2004; Parazoo et al., 2008).

The entrainment parameterization was discussed in an idealized case study by McGrath-Spangler et al. (2009) and in a realistic simulation by McGrath-Spangler and Denning (2010) and is based on the idea that the buoyancy flux at the top of the PBL is negatively proportional to the buoyancy flux at the surface (e.g. Betts, 1973; Carson, 1973; Deardorff, 1974; Rayment and Readings, 1974; Willis and Deardorff, 1974; Stull, 1976, 1988; Davis et al., 1997; Sullivan et al., 1998; Yi et al., 2001). The profile of buoyancy flux throughout the well-mixed, quasi-steady boundary layer is often approximated as linear, decreasing from the surface and becoming negative within the entrainment zone (Stull 1976). This implies that the negative buoyancy flux at the base of the capping inversion is linearly proportional to the buoyancy flux at the surface.

This assumption produces the equation:

$$\overline{w'\theta_v'}|_{z_i} = -\alpha \overline{w'\theta_v'}|_s. \quad (4.1)$$

In Equation (4.1), $\overline{w'\theta_v'}$ is the turbulent virtual potential temperature flux at the height of the inversion (Z_i) and at the surface (s) and α is the tunable proportionality constant. Equation (4.1) can be used to derive equations for the time rate of change of potential

temperature, wind velocity, water vapor mixing ratio, turbulent kinetic energy (TKE), and CO₂ concentration across the interface separating the PBL from the overlying inversion. These equations mix the properties of the boundary layer with those of the free troposphere as would be done by overshooting thermals in the physical world. Estimates of α range from zero to one, but most published values are between 0.1 and 0.3 with a value of 0.2 being the most appropriate for free convection (Stull, 1988).

This study uses six simulations, a control run without the enhanced entrainment parameterization ($\alpha = 0$) and five enhanced entrainment simulations with values of α ranging from 0.05 to 0.4. After a five-month spin-up, the month of June 2007 is analyzed.

4.3 Results

Figure 4.1 shows the midday (17 – 21 UTC) PBL depth averaged over June 2007. The upper left panel in this and in all subsequent figures shows the control ($\alpha = 0$) simulation and does not include the enhanced entrainment parameterization. The remaining plots show the difference between the enhanced entrainment parameterization (α value given) and the control simulation again averaged over June. The PBL is deepest in the southwestern United States and the depth is shallower in the eastern United States and over the oceans. Differing from previous results, the model response to enhanced entrainment is subtle and there is not a uniform deepening of the PBL. Variations in cloud cover and therefore incoming shortwave radiation (not shown) contribute to this more complex response. The enhanced entrainment produces shallower depths over the

southwestern United States and a deepening in the southeast and along the southern border of Hudson Bay. These changes reduce the PBL gradient and act to homogenize the continent.

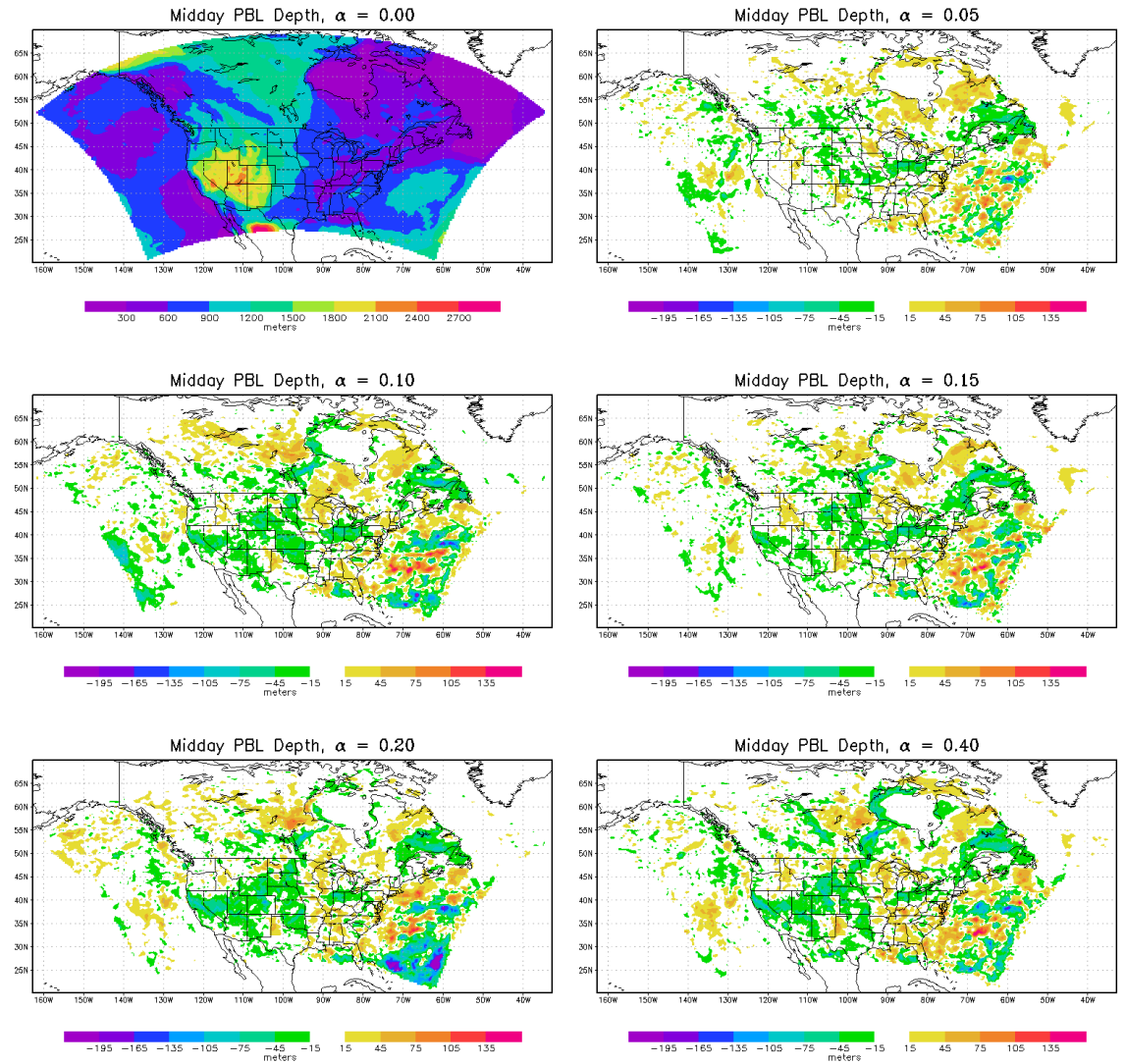


Figure 4.1 MIDDAY PBL depth averaged over June 2007 in the control run (upper left) and the difference between the given enhanced entrainment case and the control run.

The canopy air space (CAS) temperature (Figure 4.2) is the temperature of the air within the plant canopy and is defined only over land. In the control, warmer temperatures are present in lower latitudes and altitudes, as would be expected. The effect of topography is evident by cooler temperatures along the Rocky Mountain range in Colorado. However, unexpectedly cool temperatures are present in New England and the higher latitudes. Unrealistically persistent cloud cover in this region prevented incoming shortwave radiation and resulted in much cooler temperatures than would be expected for June.

The CAS temperature in the enhanced entrainment simulations is generally cooler in the southwestern United States and along a line from eastern Texas along the eastern border of the Dakotas and into Canada, associated with a line of enhanced cloud cover reducing shortwave radiation. Warmer temperatures are present in southwestern Canada and the Pacific Northwest. This is similar to the PBL depth pattern with warmer CAS temperatures in the same locations as deeper boundary layers. This pattern also reduces the north-south temperature gradient in the west.

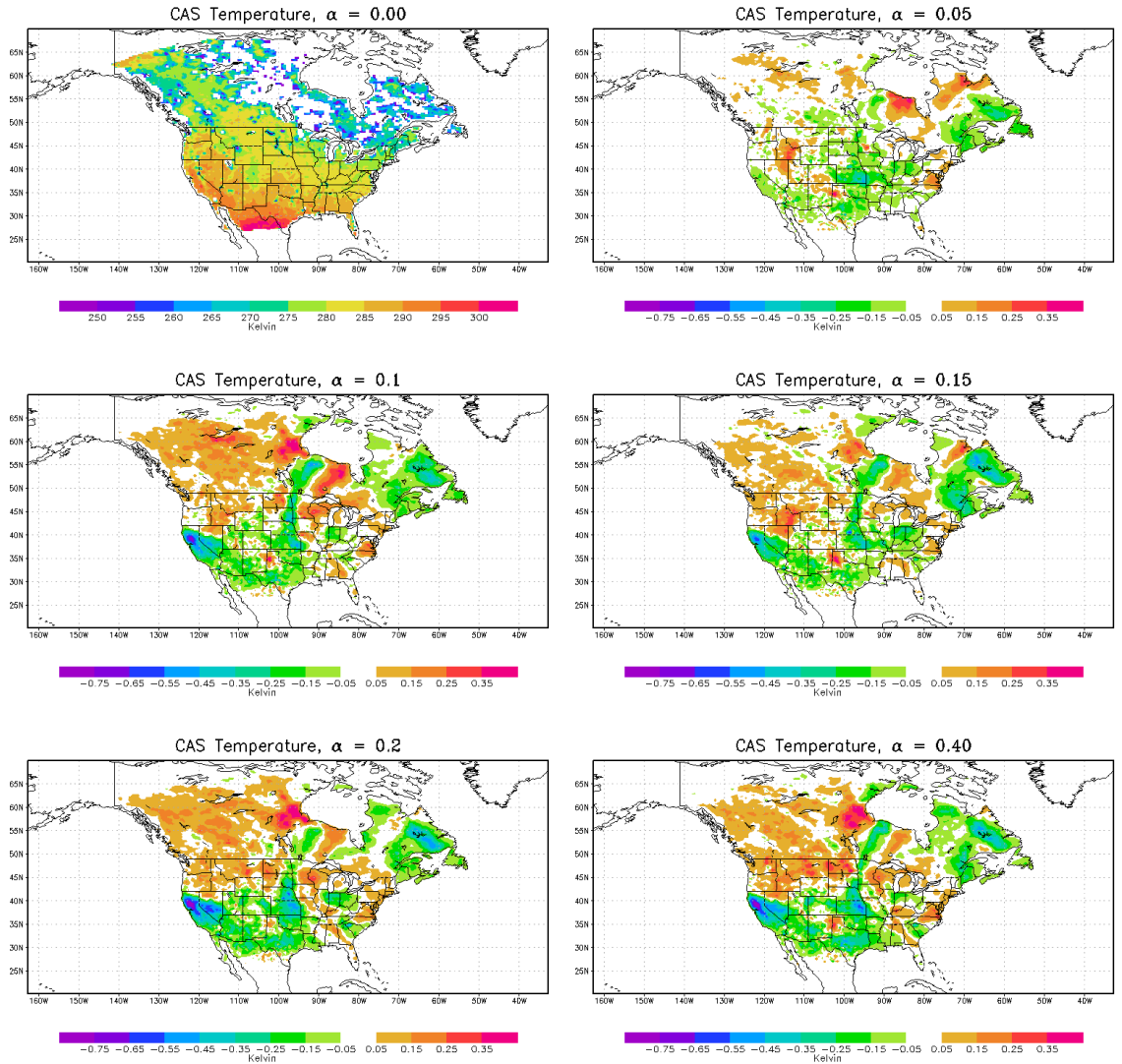


Figure 4.2 Canopy air space temperature averaged over June 2007 in the control run (upper left) and the difference between the given enhanced entrainment case and the control run.

The CAS water vapor pressure (Figure 4.3) is a measure of the water vapor present in the air surrounding the vegetation and is also defined only over land. In the control, the greatest moisture content is along the Gulf Coast from Texas into Florida. The driest locations are the southwestern United States and the colder high latitudes.

Adding the entrainment parameterization dries the Gulf Coast and moistens the southwestern United States, reducing the east-west moisture gradient.

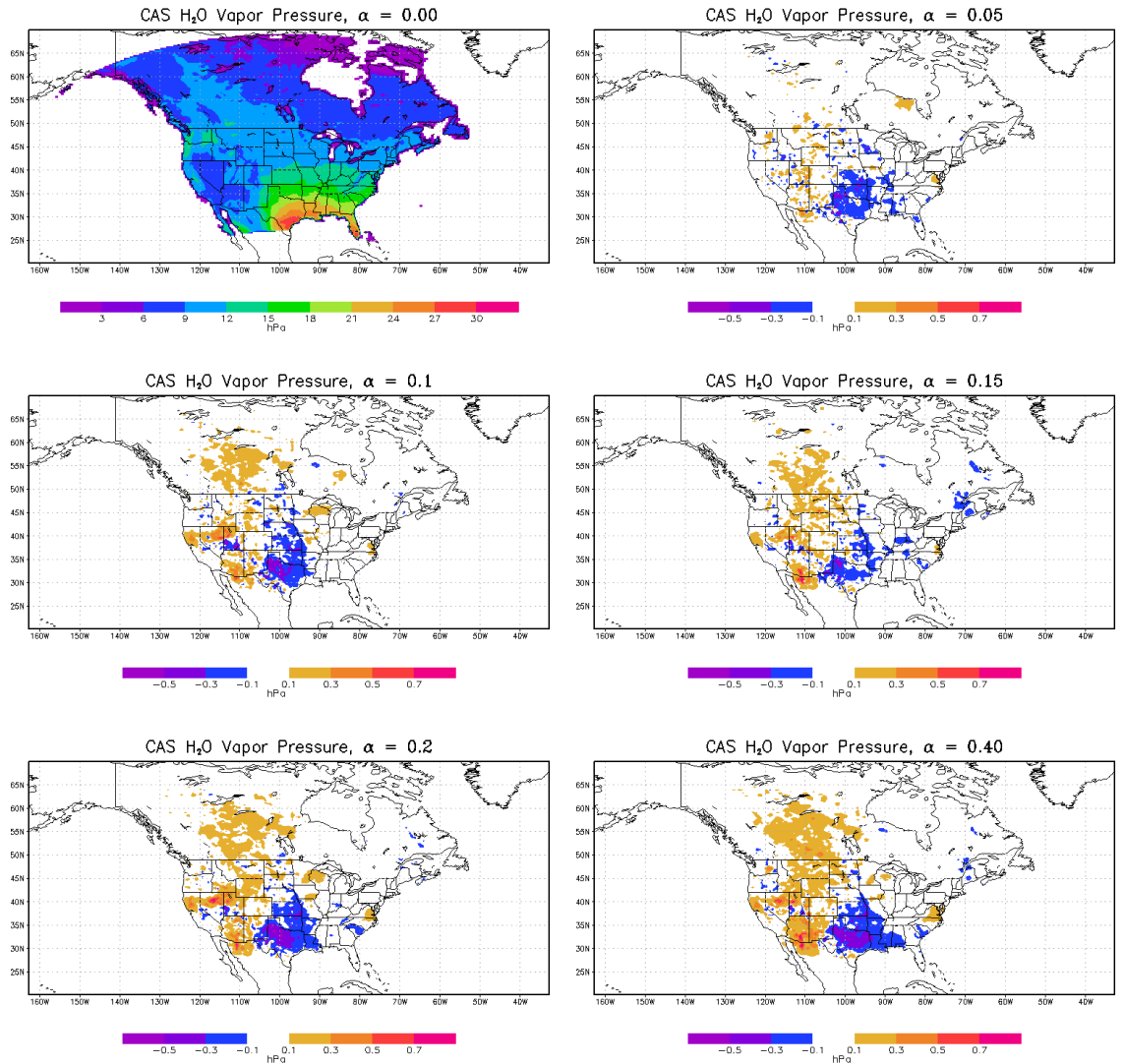


Figure 4.3 Canopy air space water vapor pressure averaged over June 2007 in the control run (upper left) and the difference between the given enhanced entrainment case and the control run.

Figure 4.4 shows the humidity stress factor. Stomatal conductance is adjusted downward by multiplying the by the nondimensional humidity stress factor to account for

insufficient humidity. A value of one indicates that the leaf-surface relative humidity (RH) is high enough for the vegetation. Warmer or drier conditions, which reduce the RH, decrease the stress factor. This then limits transpiration and carbon assimilation by the plants. The control shows the most stressed vegetation exists in the warm, dry southwestern United States and northern Mexico. Less stress is present in the eastern United States. Adding the enhanced entrainment parameterization reduces the humidity stress in the SW United States, reducing the humidity stress factor gradient.

Net carbon assimilation (Figure 4.5) is the net drawdown of carbon by plants. In the control, the strongest assimilation occurs in the southeastern United States, along the Gulf Coast. Unusually low assimilation occurs in New England due to a buildup of clouds in that region reducing radiation necessary for photosynthesis. With enhanced entrainment, assimilation in the southeastern United States is increased due to increased shortwave radiation and decreased in the southern Midwest. This pattern actually increases the carbon assimilation spatial gradient.

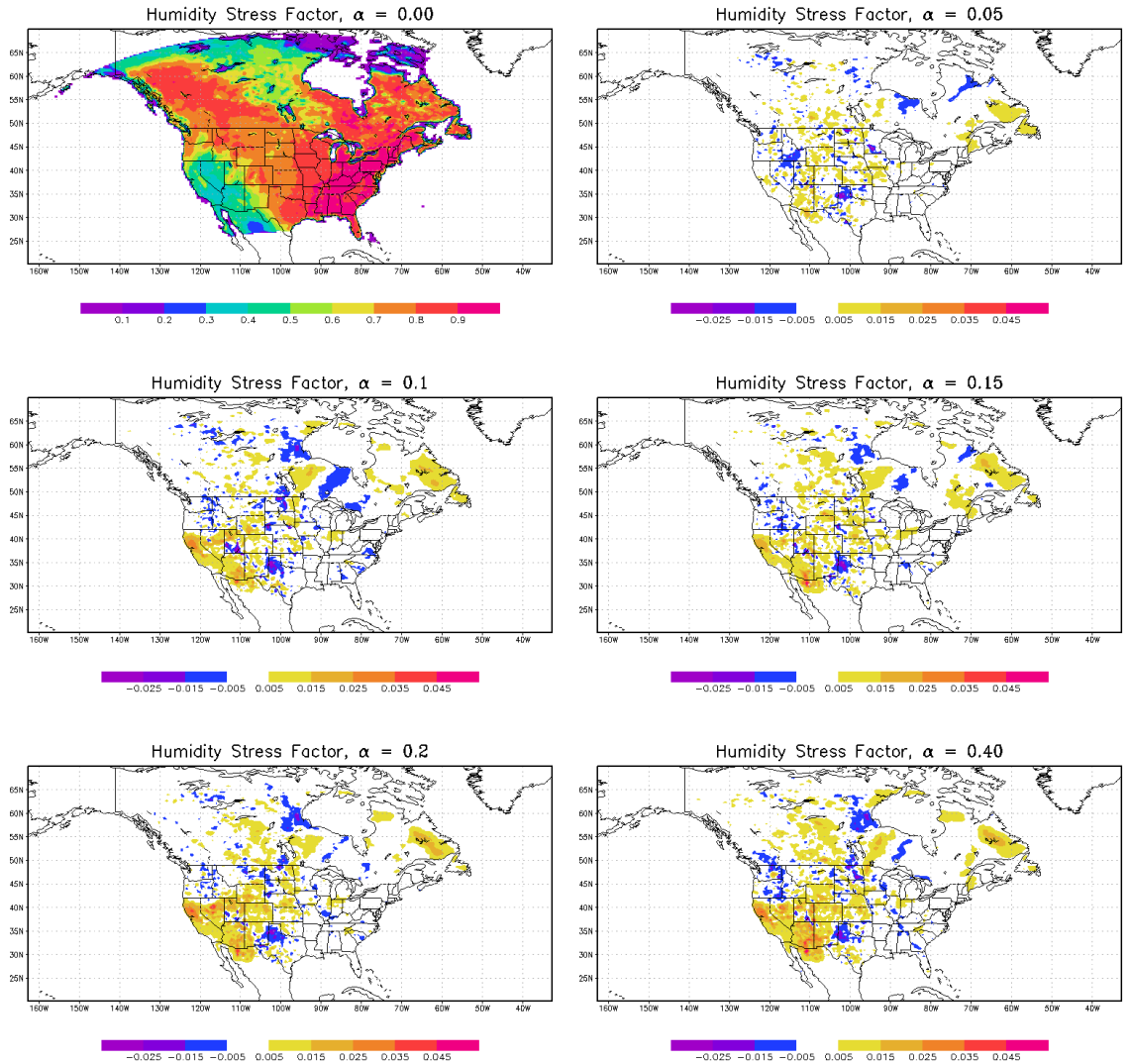


Figure 4.4 Humidity stress factor averaged over June 2007 in the control run (upper left) and the difference between the given enhanced entrainment case and the control run.

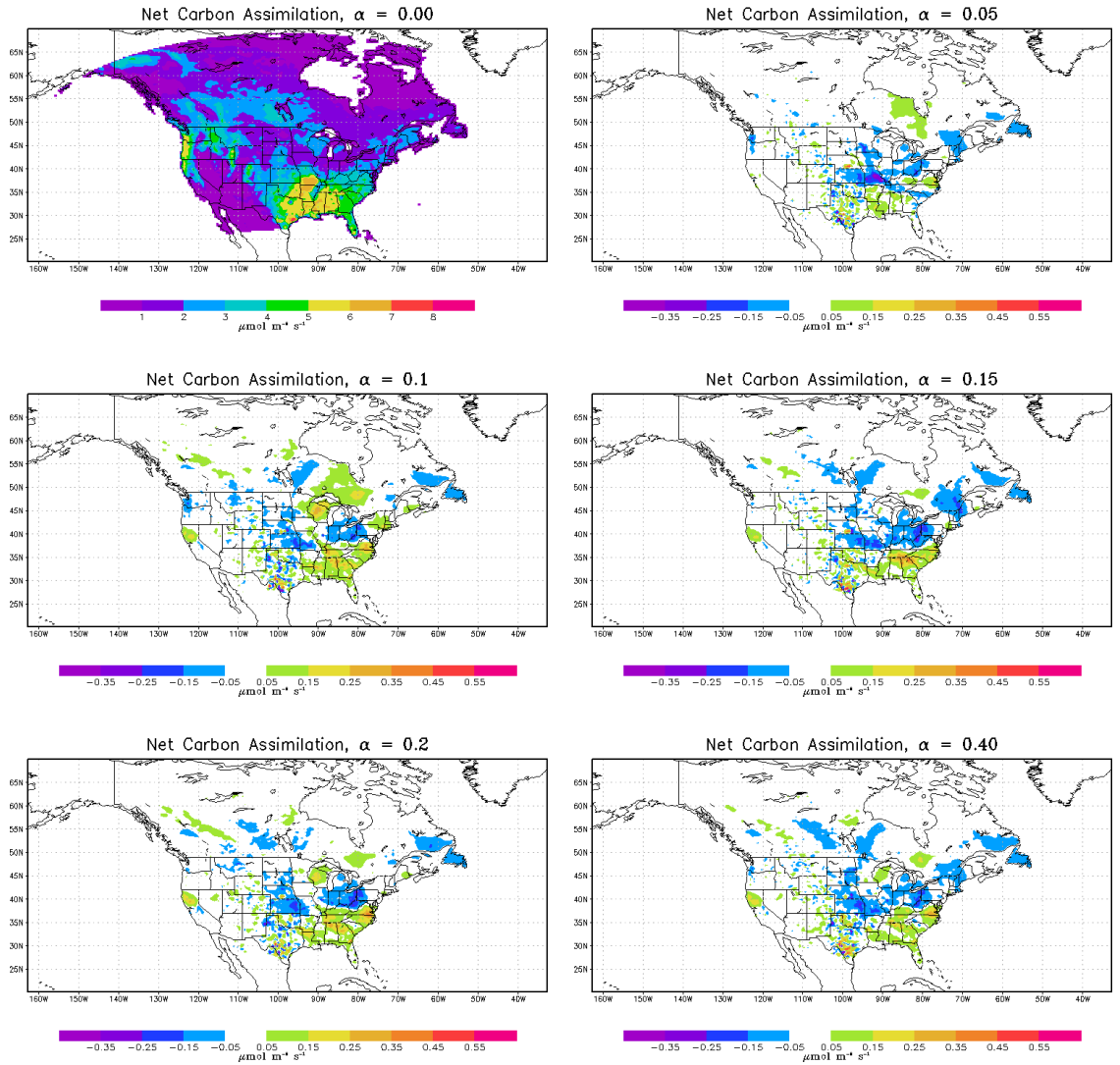


Figure 4.5 Net carbon assimilation averaged over June 2007 in the control run (upper left) and the difference between the given enhanced entrainment case and the control run.

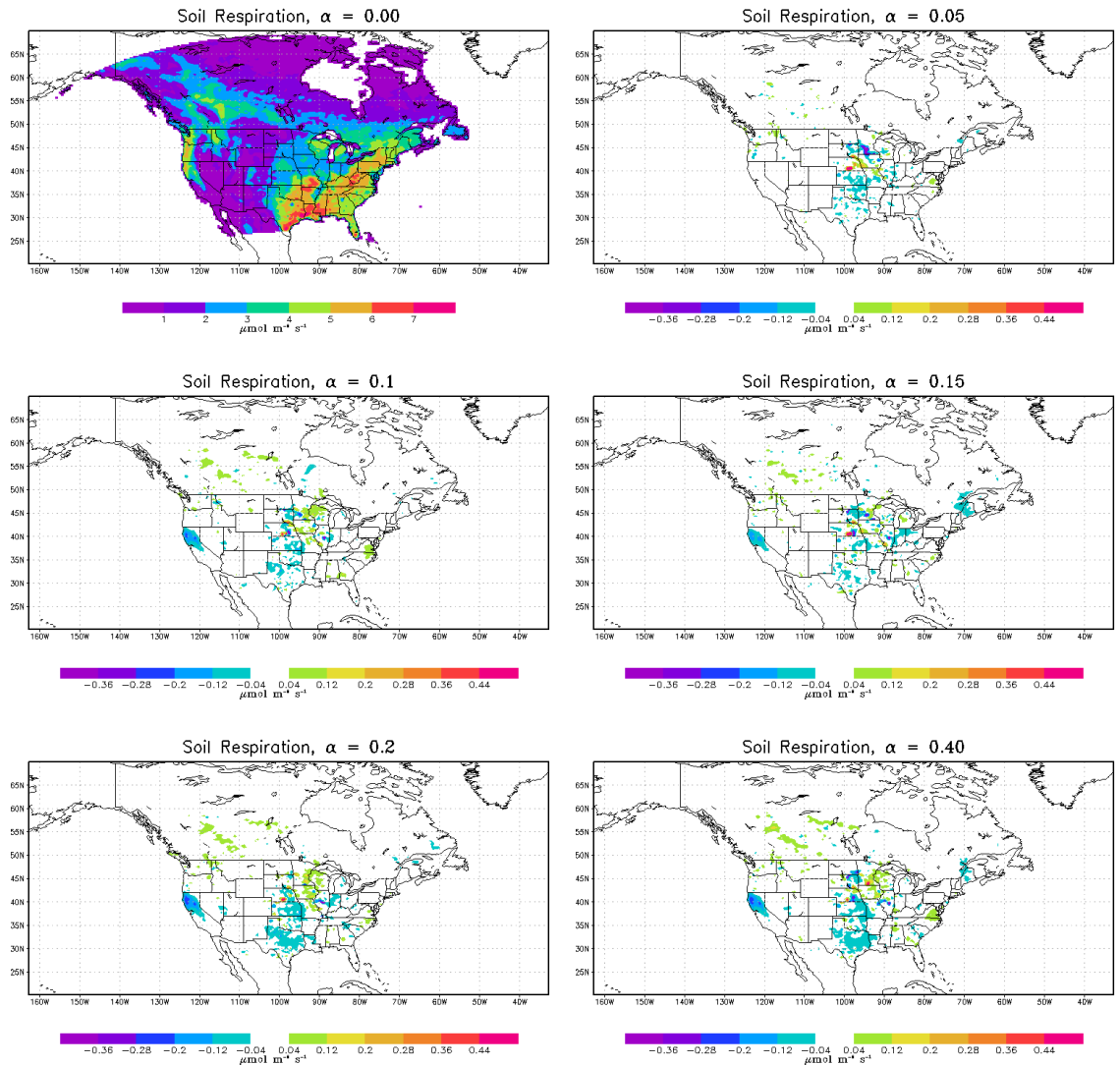


Figure 4.6 Soil respiration averaged over June 2007 in the control run (upper left) and the difference between the given enhanced entrainment case and the control run.

Soil respiration (Figure 4.6) is the flux of carbon into the atmosphere from decomposition in the soil. It is greatest when the temperatures are warm and an optimal amount of soil moisture is present. In these simulations, soil respiration is greatest in the eastern United States and lower in the dry southwestern United States and cooler Canada. The change due to enhanced entrainment is subtle. The largest coherent change is a decrease in respiration in northern California and in Texas and the Great Plains.

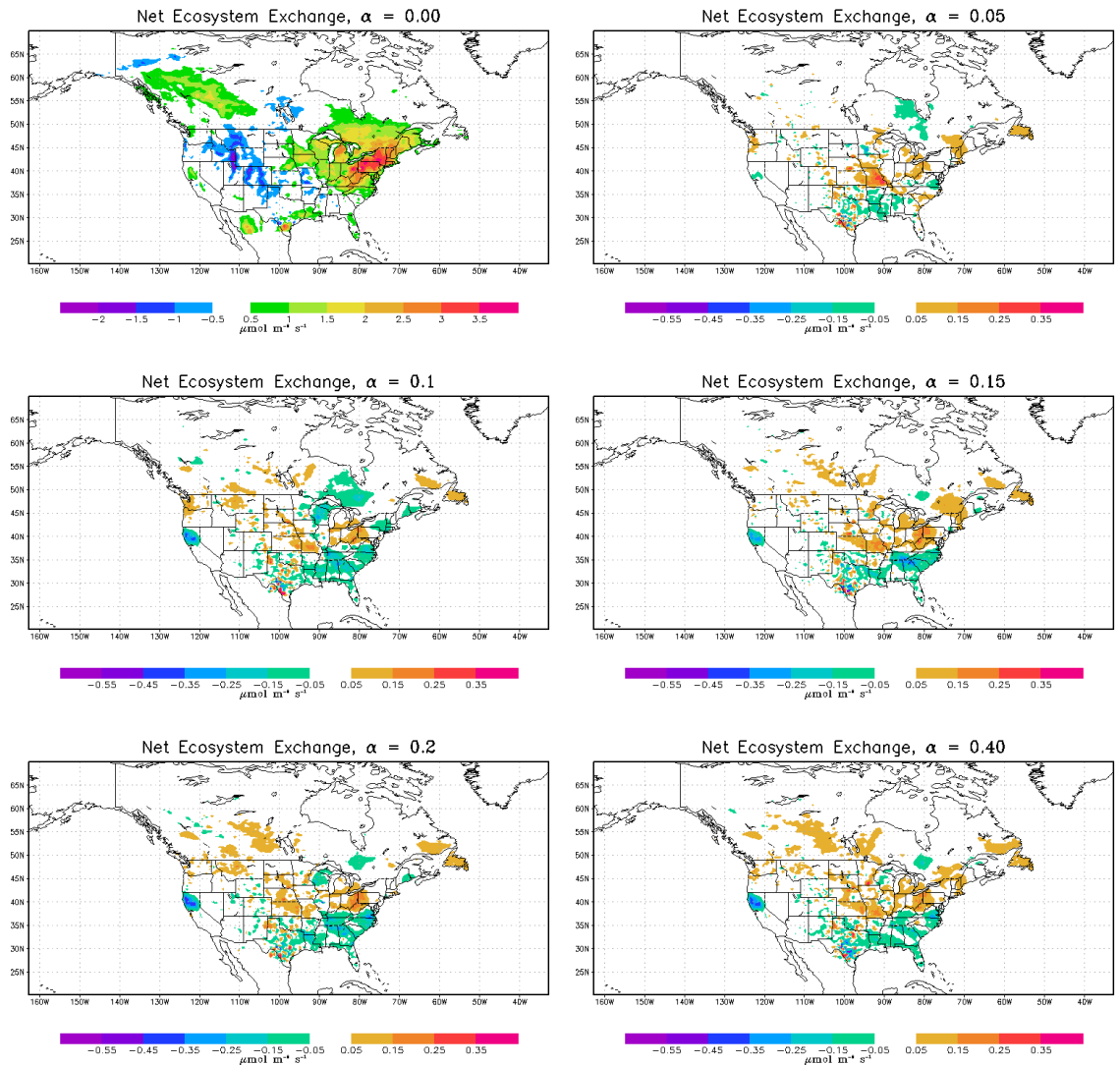


Figure 4.7 Net ecosystem exchange averaged over June 2007 in the control run (upper left) and the difference between the given enhanced entrainment case and the control run.

Net ecosystem exchange (NEE, Figure 4.7) is the net carbon flux. Positive values indicate a flux of carbon into the atmosphere while negative values indicate a net flux into the land surface. It is the difference between the soil respiration (Figure 4.6) and the assimilation (Figure 4.5). In the control, positive NEE is present in the northeastern United States associated with low solar radiation inhibiting carbon assimilation. This is

very unexpected for June and is a result of the unrealistic simulation of clouds. Persistent cloud cover in this region produced much darker conditions than would be expected for June and prevented more realistic photosynthesis from occurring. Because of this, it is the respiration that dominates. A net drawdown of CO₂ is present in the intermountain west. Enhanced entrainment acts to produce a greater carbon drawdown along the Gulf Coast and more carbon is released into the atmosphere over the Midwest, following the pattern of assimilation.

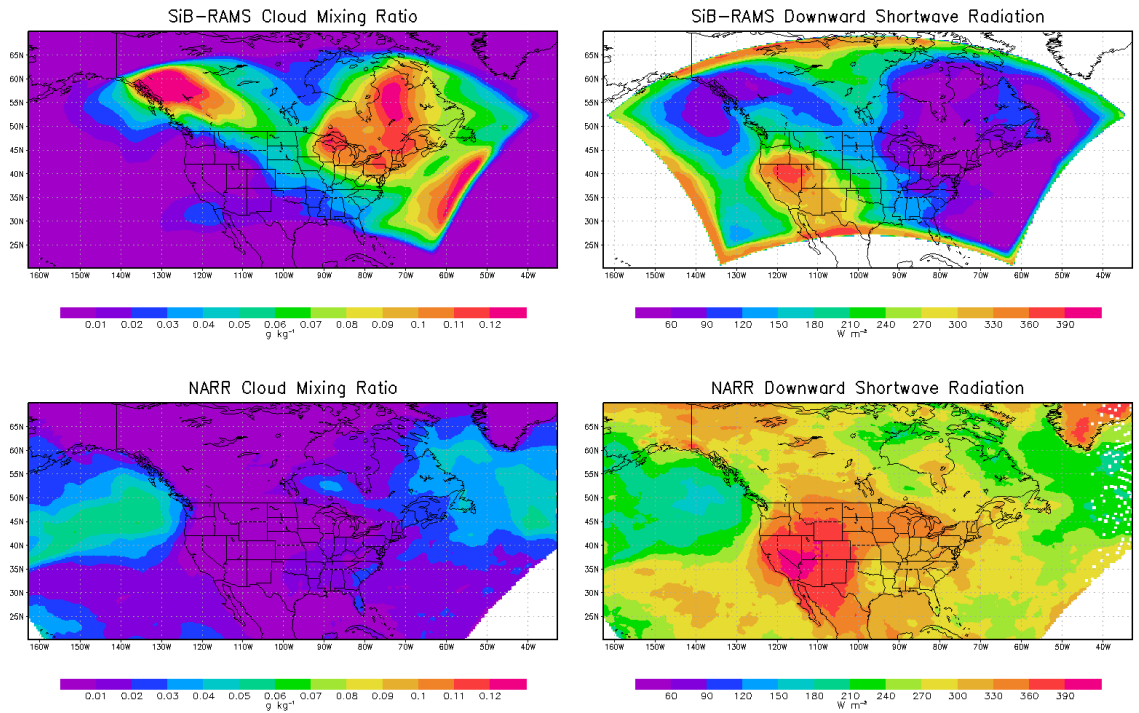


Figure 4.8 Vertically and temporally averaged cloud mixing ratio (left) and downward shortwave radiation (right) from SiB-RAMS and the NARR for June 2007.

Figure 4.8 compares the average (vertical and temporal) control ($\alpha = 0.0$) cloud mixing ratio and that from the NARR as well as the associated downward shortwave radiation. The amount of cloud cover in SiB-RAMS is four times greater than in the

NARR in New England and higher latitudes. This contributes to very little downward shortwave radiation and relatively cold, dark conditions at the surface. This limits photosynthesis and leads to unrealistically positive NEE. This then affects the sensitivity of the model to the enhanced entrainment in these locations and it is hypothesized that this produces more subtle variations than previously shown.

Figure 4.9 shows the horizontal wind. In the control, the average June 2007 circulation is shown with edges of the Bermuda and Pacific highs visible. Enhanced entrainment acts to weaken the Bermuda high leading to more onshore flow near Virginia bringing in more marine air lower in CO₂.

The near surface carbon dioxide mixing ratio is shown in Figure 4.10. The control run plot shows the highest CO₂ in the industrial eastern United States with lower concentrations over the oceans and away from the industrial regions. Enhanced entrainment produces new spatial patterns. Higher CO₂ concentrations are present in Ohio due to decreased carbon assimilation which itself is a result of decreased shortwave radiation and increased temperature stress. Lower CO₂ is present in Virginia due to increased assimilation and onshore flow advecting lower CO₂ air from over the oceans into a region with a large anthropogenic CO₂ concentration. In addition, more shortwave radiation and a reduction in the temperature stress contributed to more assimilation. In Maine, higher CO₂ concentrations are due to cloud cover reducing the shortwave radiation making this region a net source of CO₂ to the atmosphere. The shallower PBL depths amplify this effect. In southeastern Canada, more shortwave radiation lead to increased carbon assimilation and lower CO₂ concentrations.

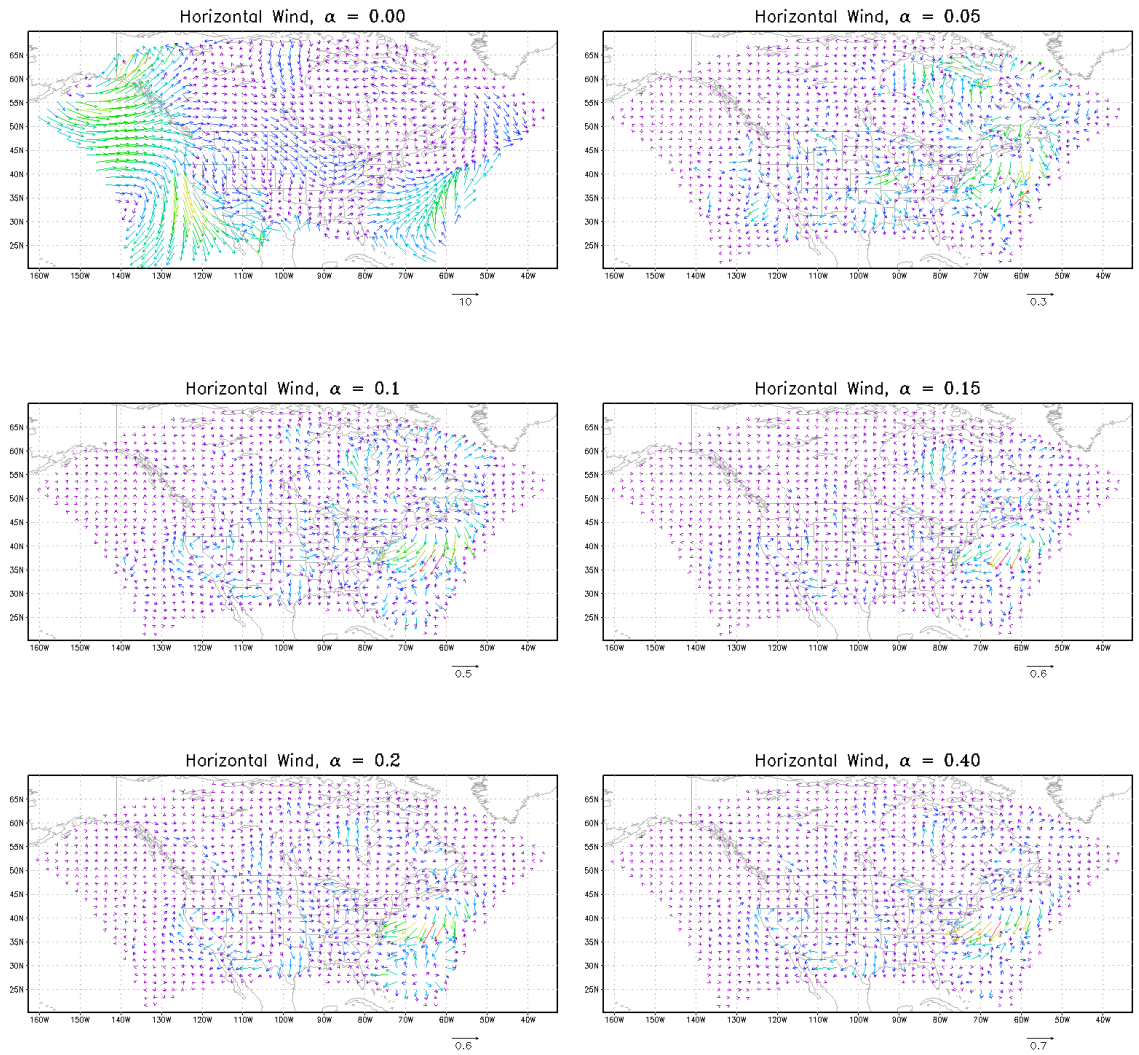


Figure 4.9 Horizontal wind averaged over June 2007 in the control run (upper left) and the difference between the given enhanced entrainment case and the control run.

These new spatial patterns combine to form a 3.5 ppm CO₂ change over about 280 km from southeastern Ohio to Virginia in the $\alpha = 0.4$ case. This gradient is increased to a 4.5 ppm change over the same distance if the analysis is restricted to midday (17-21 UTC) only. Although most atmospheric and ecological variables experienced only subtle changes, the combined impact on CO₂ was quite large.

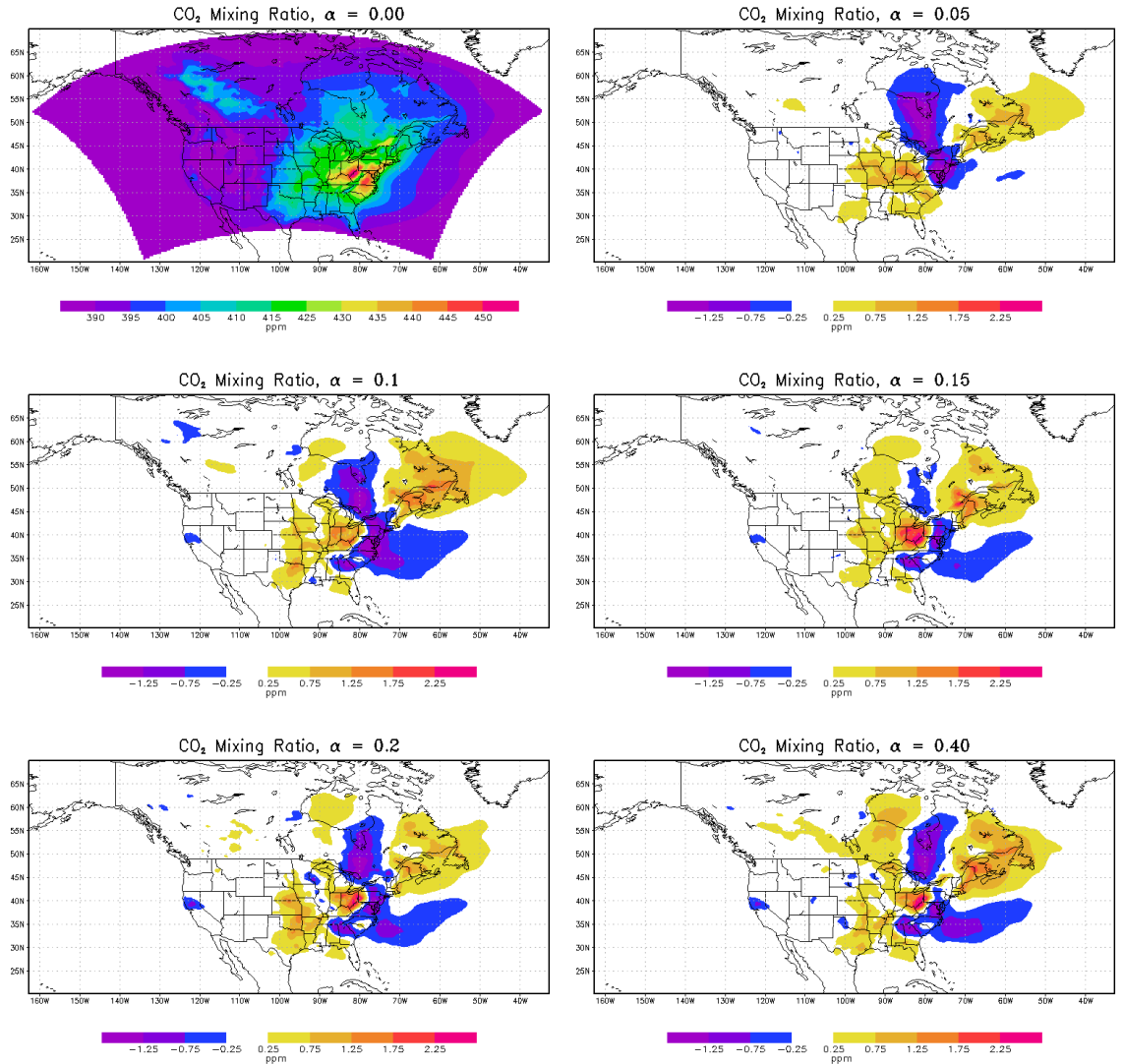


Figure 4.10 CO₂ mixing ratio averaged over June 2007 in the control run (upper left) and the difference between the given enhanced entrainment case and the control run.

4.4 Conclusions

The depth of the planetary boundary layer is important for land-atmosphere interactions and the large-scale weather and climate. Surface fluxes are “diluted” by the depth of the boundary layer and this is important for not only carbon budget studies, but also studies of aerosols and pollutants. In addition, multiple complex and interesting

interactions exist between the boundary layer processes and the land surface that feed back on each other.

A parameterization that takes into account the impact of the small-scale process of overshooting thermals was developed and implemented into the coupled land-atmosphere model SiB-RAMS. The sensitivity of SiB-RAMS to the magnitude of the PBL top entrainment was then evaluated for the month of June 2007. This was performed in order to evaluate the sensitivity of well-observed variables to the entrainment flux in order to enable optimization of the enhanced entrainment parameterization for future data assimilation experiments.

The results showed subtle differences in the spatial patterns of atmospheric and ecological variables. These variations eased the gradient between the warm, dry southwestern United States and cooler, moister areas in the United States and Canada. The strength of the Bermuda high was also weakened, changing advection patterns and bringing lower CO₂ concentration air into the state of Virginia. These processes and interactions combined to produce a 3.5 ppm CO₂ change over 280 km in the monthly mean, a significant gradient. However, the sensitivity of the model to the parameterization was weaker than expected. It is assumed that this is a result of greater than expected persistent cloud cover that then limits downward shortwave radiation and constrains photosynthesis.

Chapter 5

PBL Depth from Space

Summary

The planetary boundary layer (PBL) mediates exchanges of energy, moisture, momentum, carbon, and pollutants between the surface and the atmosphere. In clear sky conditions, space-borne LIDAR backscatter is frequently affected by atmospheric properties near the PBL top. Spatial patterns of 5-year mean mid-day summertime PBL depths over North America were estimated from the CALIPSO LIDAR backscatter and are generally consistent with model reanalyses. The success of the retrieval is greatest over the subtropical oceans where overlying subsidence limits optically thick clouds from growing and attenuating the LIDAR signal. The general success over land is around 50% with decreased success over the Southwestern United States and regions with high rates of convection. The LIDAR-based estimates of PBL depth are somewhat deeper than reanalysis products over the oceans and areas of the boreal forest and shallower over the arid and semiarid regions of North America.

5.1 Introduction

The planetary boundary layer (PBL) is the turbulent layer closest to the Earth's surface with a depth of about 1-2 km at midday and is crucial to many aspects of weather

and climate. The PBL mediates exchanges of energy, moisture, momentum, carbon, and pollutants between the surface and the overlying atmosphere. PBL processes also influence the production of clouds, which modify the radiation budget through their effects on short and longwave radiation (Stull, 1988). The top of the PBL acts as a barrier to surface-emitted pollutants, leading to high concentrations within the PBL (Stull, 1988), so diagnosing the depth of the PBL is critical to air quality studies as well as weather prediction and climate.

Although PBL depth is important, no observation-based global PBL climatology exists (Seidel et al., 2010) and there are many problems with simulating the processes involved (Martins et al., 2010). Extremely high vertical resolution is needed for proper representation of surface layer ventilation and turbulent entrainment at the top of the PBL, but is only required over very thin spatially and temporally changing portions of the atmospheric column in the surface and entrainment layers. Adding hundreds of vertical levels to a model in anticipation of the need to resolve strong gradients in temperature and turbulence at the (unknown) inversion height would be excessive and computationally expensive over the rest of the boundary layer and free troposphere. Therefore, small-scale processes that control PBL development are unresolved by many models (Ayotte et al., 1996; Gerbig et al., 2003; McGrath-Spangler and Denning, 2010). It is difficult to observe PBL depth at large scales (Randall et al., 1998) and to observe fluxes and processes at the top of the PBL because of its height and variable location. As a result, turbulent entrainment at the PBL top is among the weakest aspects of PBL models (Ayotte et al., 1996; Davis et al., 1997).

Multiple methods are used to determine PBL depth and often give different results (Seidel et al., 2010). Model products, such as those from the Modern Era Retrospective-analysis for Research and Applications (MERRA) and North American Regional Reanalysis (NARR), are sensitive to empirical parameters in addition to the diagnostic method chosen and verification by direct observations of PBL depth are sparse (Seibert et al., 2000; Jordan et al., 2010). In addition, radiosondes that could be used to validate PBL depth are launched in the morning and evening over North America (0 and 12 UTC), insufficient times for evaluating daytime maximum PBL depth and estimates made from radiosondes may differ from the space/time average by up to 40% (Angevine 1994).

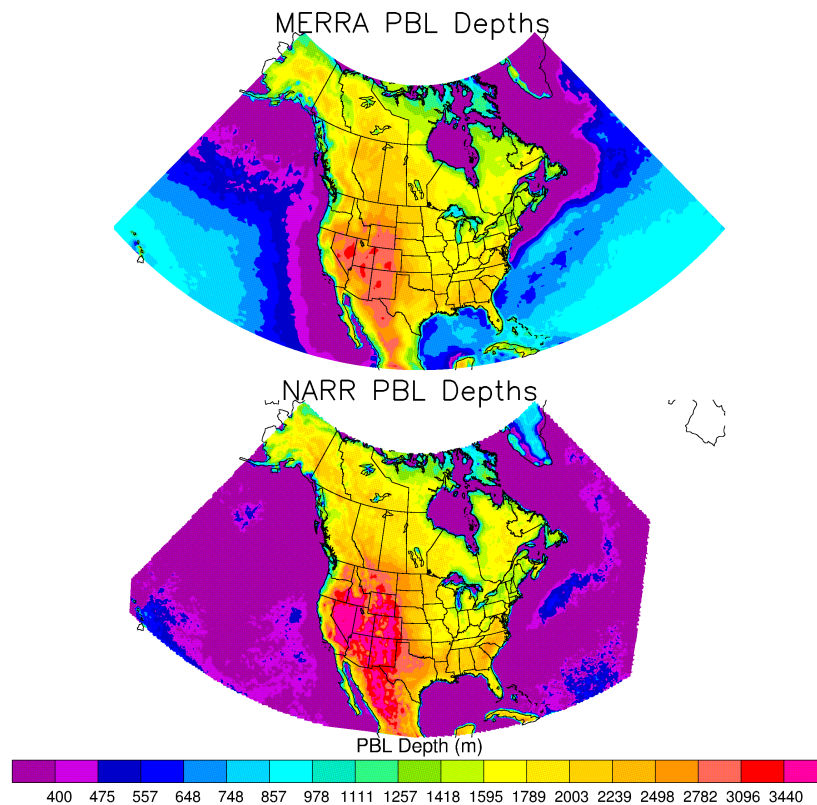


Figure 5.1 2006-2010 JJA estimates of sunny, midday PBL depth above ground level for MERRA (top) and NARR (bottom).

Comparisons between PBL depths diagnosed from MERRA and NARR (Figure 5.1) show qualitatively similar results. In summer, midday the deepest PBL depths in both products occur over the drier western United States, a relatively deep PBL is found over the coast of the Gulf of Mexico, and shallow PBL depths are present over the US Midwest. Quantitatively, the analyzed PBL depths are very different. For instance, over the western United States, the NARR dataset commonly finds a PBL over 3 km while the value for MERRA is closer to 2.5 km.

There have been few, limited scale studies that have examined PBL processes using remote sensing in the past (Martins et al., 2010). The LIDAR-In-space Technology Experiment (LITE) flew for 9 days in September 1994, identifying the PBL top by locating a sharp aerosol gradient (Randall et al., 1998). The Geoscience Laser Altimeter System (GLAS) had limited success making observations of PBL depth as well (Palm et al., 2005). Palm et al. (2005) examined PBL depth over the oceans for October 2003 and found the derived depth from GLAS to be 200-500m deeper than that from the European Centre for Medium-Range Weather Forecasts.

In addition, multiple studies have examined ground-based and airborne LIDAR to determine PBL depth with good results. Davis et al. (1997, 2000) and Brooks (2003) used airborne LIDARs to develop automated methods to derive PBL depth for specific field campaigns and surface/atmosphere conditions. Wiegner et al. (2006) used ground-based LIDAR as the reference for the depth of the mixing layer using the mixing layer definition of an “abundance” of aerosols. Mattis et al. (2008) used a network of ground-based LIDAR to identify the PBL top in order to identify free-tropospheric aerosols. Cohn and Angevine (2000) found good comparisons between two ground-based LIDARs

and a wind profiler deployed during the Flatland96 Lidars in Flat Terrain experiment. Comparisons of these measurements to radiosondes and other remote sensing methods depend upon the definition of the PBL depth used and the instrument used to retrieve it (Seibert et al., 2000; Wiegner et al., 2006; Mattis et al., 2008; Seidel et al., 2010). Furthermore, PBL depth measurements from LIDAR are generally slightly deeper than those derived from temperature profiles since convective plumes transport aerosols above the base of the inversion (Beyrich, 1997).

The Cloud-Aerosol LIDAR and Infrared Pathfinder Satellite Observations (CALIPSO) satellite has the potential to expand the available data tremendously. Such a dataset will provide data to which modelers can compare PBL depth estimates to improve simulations of PBL processes. This paper is a first step in producing such a dataset using space-based LIDAR. The advantage of orbital LIDAR is its ability to provide near global coverage, irrespective of political and land/water boundaries and is important for model validation and data assimilation (Palm et al., 2005). The following section provides a description of a method to determine PBL depth from the CALIPSO satellite. Section 5.3 describes the results using this method during the summer over North America and the final section offers a brief conclusion.

5.2 Methods

The Cloud-Aerosol LIDAR with Orthogonal Polarization (CALIOP) aboard the CALIPSO satellite is the first space-based LIDAR optimized for aerosol and cloud measurements and the first polarization LIDAR in space (Winker et al., 2007).

CALIPSO is part of NASA's Afternoon constellation (A-train) of satellites and is in a 705 km sun-synchronous polar orbit with an equator crossing time of about 1:30 pm local solar time and a 16-day repeat cycle (Winker et al., 2007, 2009). The products used in this analysis are the Version 3.01 Level 1B data available online (http://eosweb.larc.nasa.gov/PRO-DOCS/calipso/table_calipso.html). The atmospheric backscatter retrieved by the LIDAR is available at 30 m vertical and 0.33 km horizontal grid intervals from 0 – 8 km and at reduced resolution above 8 km.

The maximum variance technique developed by Jordan et al. (2010), and used to evaluate PBL depth during two months in 2006, is used here to derive estimates of PBL depth from the CALIOP LIDAR 532 nm backscatter. This technique is based on an idea by Melfi et al. (1985) that at the top of the PBL there exists a maximum in the vertical variance of LIDAR backscatter. This maximum in the variance exists because within the entrainment zone in clear conditions, free tropospheric eddies mix with aerosol laden eddies from within the PBL. This mixture of clear and dirty air produces a large variance in the backscatter (Jordan et al., 2010). In conditions with boundary layer clouds, a maximum in the variance occurs either within or just above the cloud, depending on the specific conditions. The Jordan et al. (2010) technique examines the vertical profile of retrieved backscatter beginning at the surface, and searches for the first occurrence of a maximum in the variance (calculated as the standard deviation of four vertically consecutive layers) collocated with a maximum in the magnitude of the backscatter itself, often identifying the mid level or top of boundary layer clouds. The level of the maximum in the variance and backscatter is well correlated with the top of the PBL because the conditions that affect LIDAR backscatter (e.g. jumps in temperature, relative

humidity, aerosol concentration, etc.) are frequently associated with the PBL top. Since this technique would identify the residual layer at night and not the nocturnal boundary layer, it is applied only to daytime satellite passes. Jordan et al. (2010) found that this technique compared favorably to ground-based LIDAR and radiosonde data at the University of Maryland Baltimore County

Jordan et al. (2010) used visual inspection to evaluate their CALIPSO-based PBL retrieval. We have automated the algorithm in order to process a larger subset of the available data. In order to do this, we made several modifications. We restricted the retrieved depths to between 0.25 and 5 km above the ground surface and added a check for surface backscatter to eliminate surface noise and profiles without a clear aerosol signature within a reasonable height range for the midday PBL. Profiles containing large signal attenuation due to clouds were not analyzed and were instead assigned a missing value. These missing values were defined by the occurrence of three vertically consecutive layers with a 1064 nm backscatter value exceeding $10^{-2.25} \text{ km}^{-1} \text{ sr}^{-1}$ (Okamoto et al., 2007). Cloud-topped boundary layers were of interest, so the feature top was first determined and then the search for attenuating clouds began 750 m above the feature and continued to the top of the profile. This allows us to estimate the depths of both aerosol-topped and cloud-topped PBL as long as deep clouds do not interfere with the retrieval.

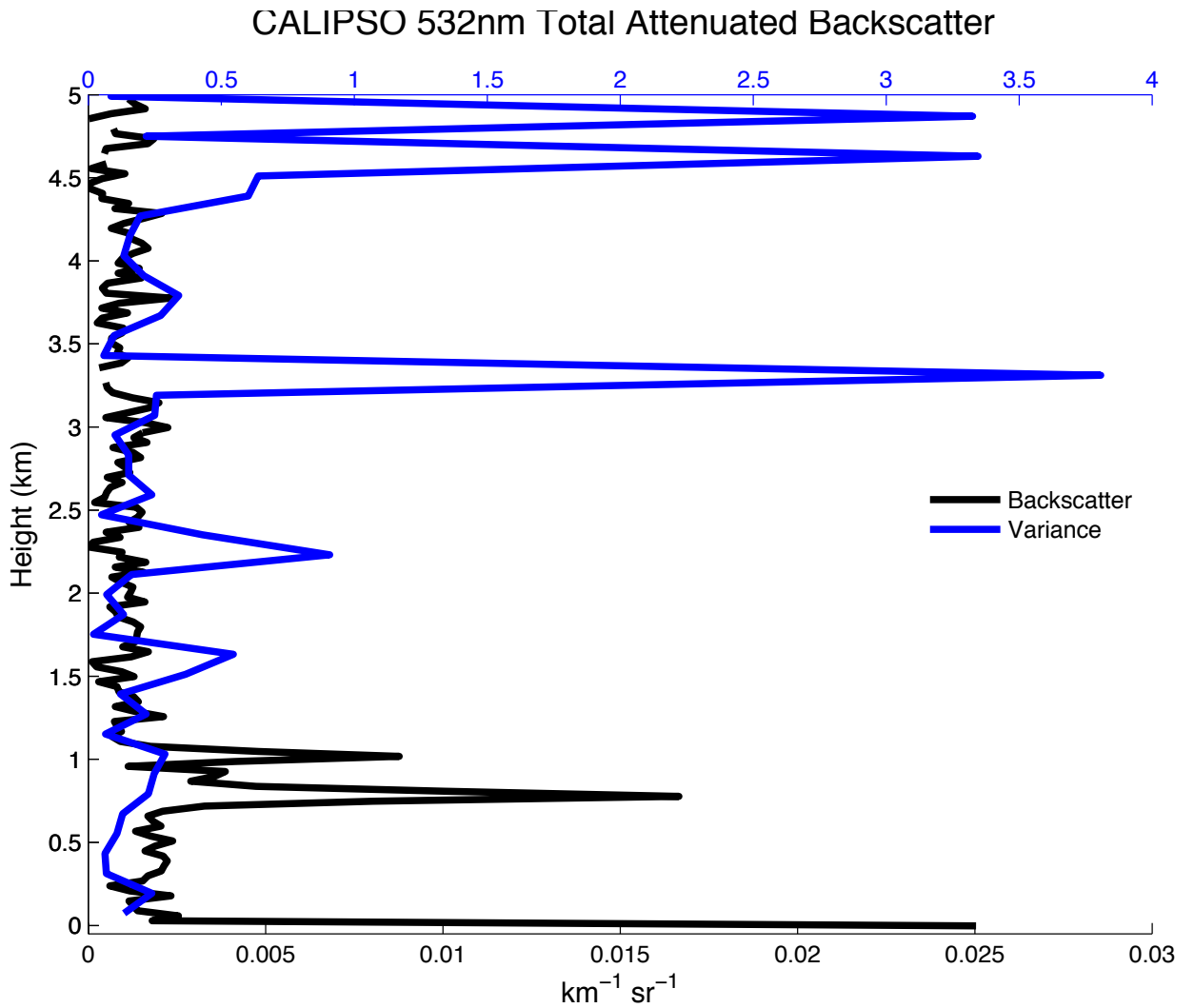


Figure 5.2 Vertical profile of CALIPSO 532 nm total attenuated backscatter (black) and the vertical variance (blue) of the backscatter.

Figure 5.2 shows an example profile that can be analyzed using the above method. This profile has been horizontally averaged using a running mean to increase the signal to noise ratio. At 0 km, there is a large backscatter signal from the surface return. Starting at this point, two peaks are identifiable in the backscatter at 0.8 and 1 km. The lowest peak (at 0.8 km) does not have a corresponding local maximum in the variance and so is rejected. The second peak (1 km), however, is coincident with a local maximum in the variance and so is identified as the top of the backscatter feature.

There are several weaknesses of this method that limit its ability to estimate PBL depth. First, profiles containing deep, optically thick clouds or aerosol layers attenuate the signal making it impossible to detect backscatter features near the surface in convective or otherwise cloudy conditions. Second, the potential exists for the algorithm to detect the aerosol gradient from a previous day and miss a current, shallower feature. Third, a very shallow backscatter feature cannot be resolved due to noise in the backscatter very near to the surface. However, during the afternoon overpass, especially in the summer over land, the PBL should be well developed and deep enough to exceed the minimum depth assigned here except under very unusual circumstances.

5.3 Results and Discussion

Figure 5.3 shows an example of the estimated PBL depths using the above method for a July 2007 overpass of the satellite over the Midwestern United States. The gray line near the bottom of the figure indicates the surface elevation available in the Level 1B product. There is a strong backscatter signal at this level where the LIDAR beam reaches the solid ground. The vertical regions of dark blue are results of attenuation (LIDAR shadows) from overlying clouds for which we do not retrieve a value. The black line indicates the PBL depth estimated by the algorithm and in general does a good job of locating the maximum backscatter signal indicating the PBL top. There are a few regions in which the backscatter feature is not obvious to visual inspection, but is found by the automated algorithm. The profile from Figure 5.2 was taken from this plot at about (29°N, 90°W).

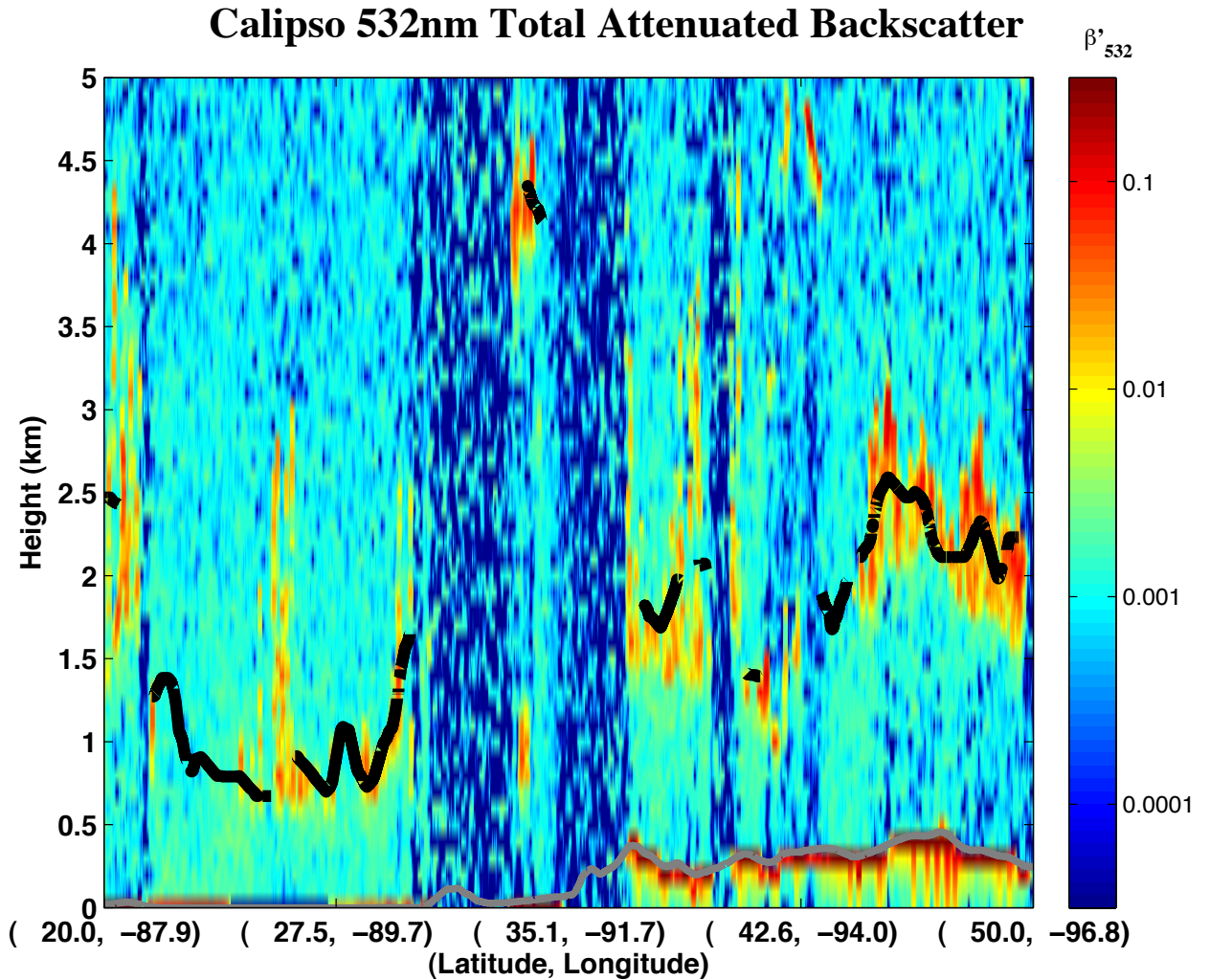


Figure 5.3 Attenuated backscatter plot from CALIPSO on 9 July 2007 over the Midwestern United States. The black line indicates the derived PBL depth and the gray line represents the surface.

The percentage of retrieved backscatter heights to the total available CALIPSO profiles in each $1.25^\circ \times 1.25^\circ$ grid cell during June, July, and August from 2006 to 2010 is shown in the “success” map in Figure 5.4. Here, success refers to whether a height feature was derived and not to whether it is accurate as compared to other observations. The algorithm can fail due to the LIDAR not functioning properly, thick cloud cover above the boundary layer, and/or unclear aerosol profiles: this figure only considers the last two conditions. From this figure it is evident that the algorithm has its greatest

success over the subtropical oceans due to the sparsity of overlying clouds. Reduced success occurs in regions with high frequency of mid-day convection such as Florida, the Gulf Coast region, the US Rocky Mountains, and the Mexican Plateau. In general, the success ranges from a low of 15% near Lake Okeechobee in Florida and southern New Mexico to near 100% in the Pacific Ocean off the coast of California and Mexico.

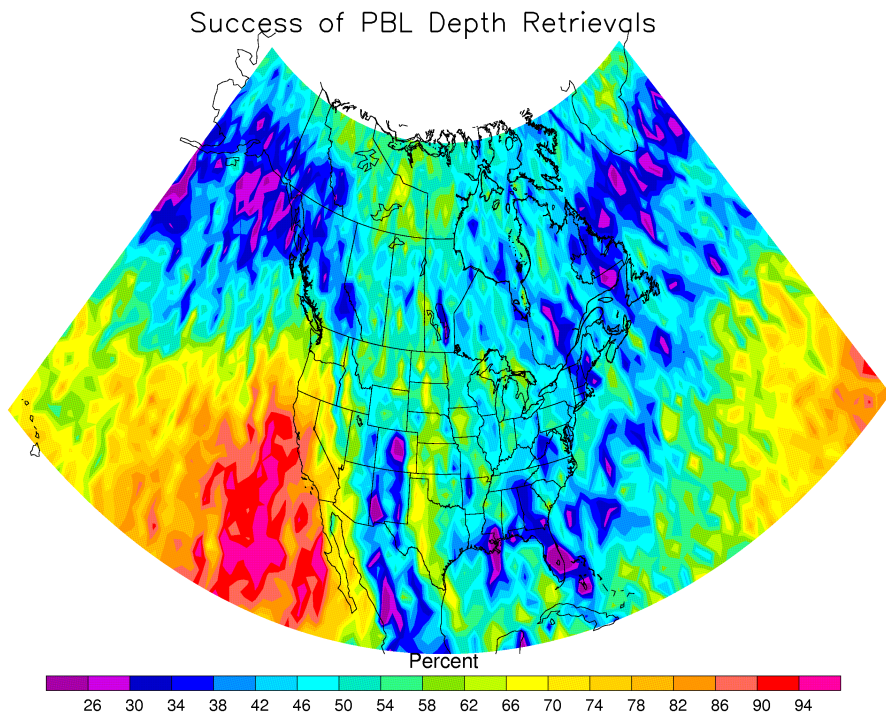


Figure 5.4 Ratio of the number of successfully derived PBL depths to the total number of satellite profiles available times 100%.

Figure 5.5 shows the standard error of the mean of the estimation of PBL depths from the CALIPSO satellite. The standard error of the mean provides a simple measure of sampling error of the estimated depth of the backscatter features. This figure shows that there is an increased sampling error in the gaps between the satellite orbits due to

decreased sampling in those locations. In general, the sampling error is greater over land than over water, as would be expected due to the more heterogeneous nature of PBL processes over land. In addition, the greatest sampling error occurs where the success is smallest and the region experiences convection during the summer months.

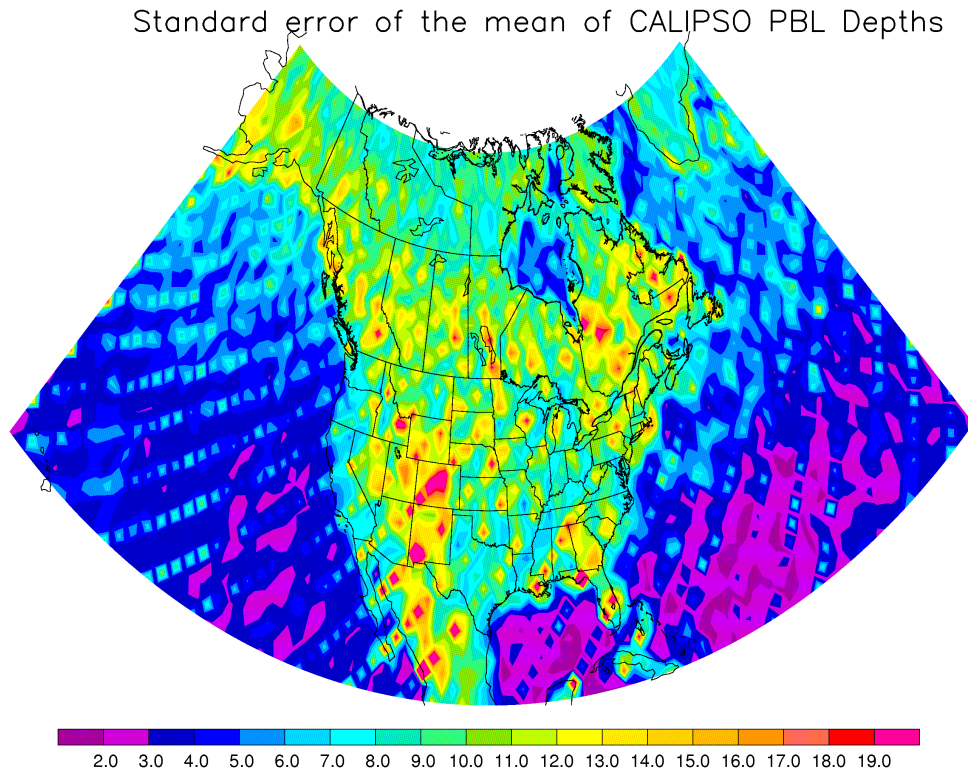


Figure 5.5 2006 – 2010 standard error of the mean of PBL depths estimated from CALIPSO averaged to a 1.25° grid.

The advantage of automating the Jordan et al. (2010) algorithm is the ability to process large quantities of data that can then be combined to form maps of PBL depth estimates. The top figure in Figure 5.6 shows the mean mid-day clear sky PBL depth over North America for June, July, and August (JJA) on a 1.25°x1.25° grid. One can identify deeper PBL depths over land than over water and such features as the Florida

and Yucatán peninsulas and the island of Cuba can be recognized. Shallower boundary layers off the coast of California can be seen associated with cold, upwelling water, stratocumulus clouds, and overlying subsidence. Another prominent feature is the relatively shallow boundary layers over the farmland of the US Midwest. High moisture availability means that a large portion of net radiation in this region is used to evaporate water and less energy is available to grow the PBL. This regional minimum in PBL depth roughly follows the valley of the Mississippi River.

The deepest backscatter features occur along the semiarid Rocky Mountains in the southwestern United States and the Mexican Plateau. Relatively deep boundary layers are present over Canada. A possible explanation for this is that in the boreal ecosystem, low soil temperatures and nutrient availability reduce stomatal conductance and lead to a high ratio of sensible to latent heat flux (Margolis and Ryan 1997). Additionally, during summertime at high latitudes, the longer day length results in higher amounts of incoming solar radiation, leading to more available energy. The higher Bowen ratio and amount of solar radiation create a situation in which deeper than expected (over 2 km) PBL depths have occurred in June during the Boreal Ecosystem-Atmosphere Study (BOREAS) field experiment (e.g. Betts et al., 1996; Margolis and Ryan, 1997).

The bottom plot in Figure 5.6 shows the ratio of MERRA reanalysis PBL depths to the PBL-associated backscatter heights derived from CALIPSO. Over much of the United States and portions of the subtropical oceans, the MERRA PBL depths are within 25% of the estimates derived from CALIPSO. This LIDAR-based backscatter feature is deeper and more variable over the oceans and boreal forest than the PBL depth estimated in the reanalysis product. The MERRA PBL in boreal Canada has not fully developed by

the time of satellite overpass and therefore is an underestimate of the mid-day conditions seen by the satellite. This is the source of the apparent line in the ratio at about 55°N. CALIPSO also records shallower features over the dry, complex terrain of the American Southwest.

From 20 June to 6 July 2008, rawinsondes were launched in the morning and afternoon from West Branch, Iowa in support of the North American Carbon Program's Mid-Continent Intensive Program. CALIPSO's closest approach during this time period occurred on 20 June at a distance of about 175 km. Using the potential temperature method of Seidel et al. (2010), the derived PBL depth is 3.71 km. The depth found from the CALIPSO backscatter is 3.69 km, a difference of less than 1%.

Figure 5.7 shows histograms of the backscatter feature depths over land (top) and over water (bottom). Over land, the probability distribution function (PDF) has a mode at 1.5 – 2 km. Over water, the features are biased more toward shallow depths. Due to surface noise, it is forbidden to obtain very shallow depths (less than 250 m). The mode of the water-based PDF is around 500 m and there is near exponential decay at greater depths.

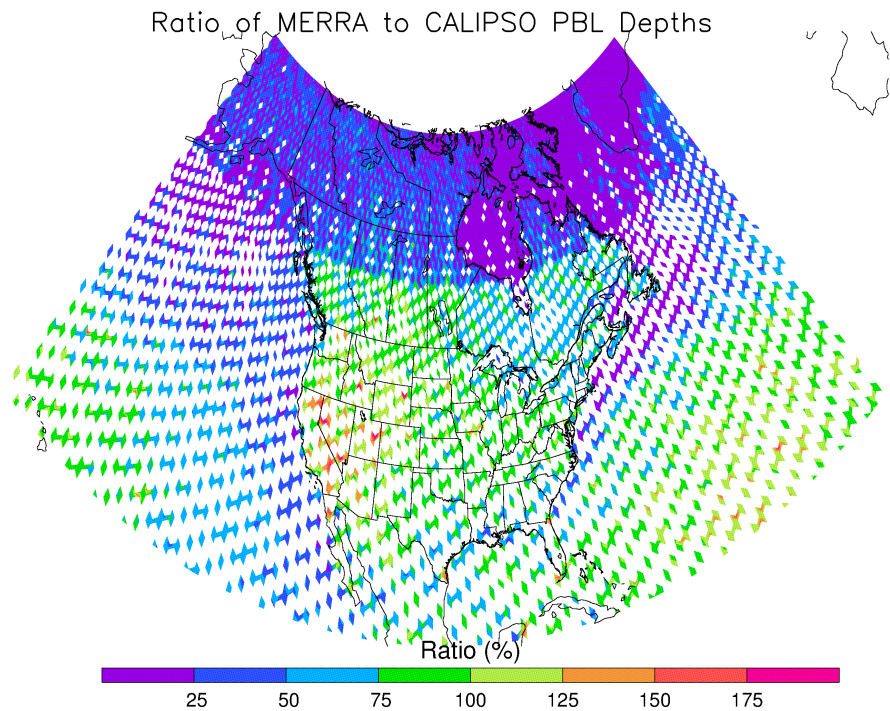
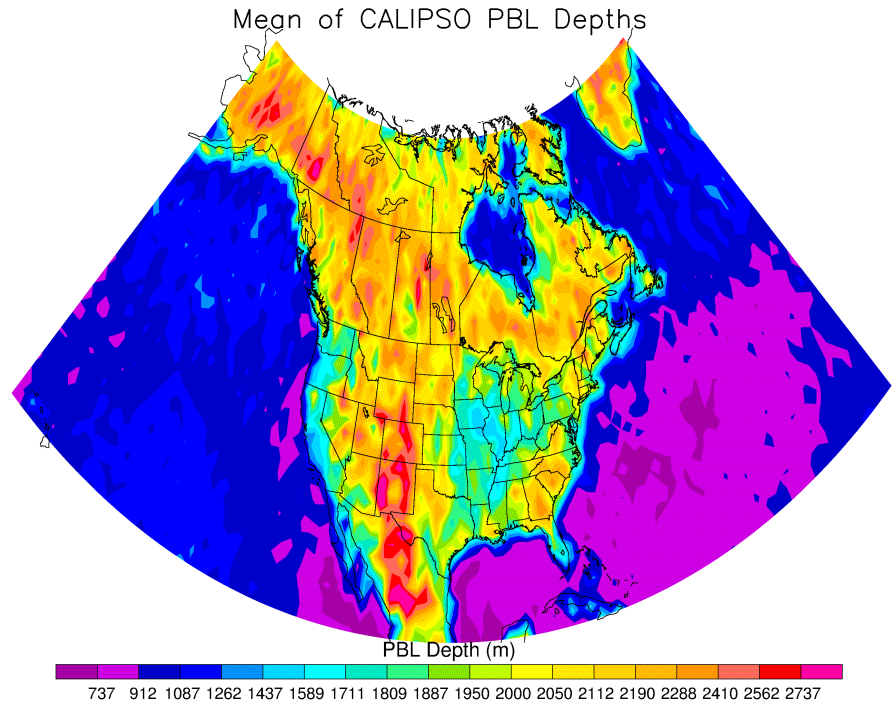


Figure 5.6 2006-2010 JJA mean PBL depths derived from the CALIPSO LIDAR data (top) and the ratio of MERRA reanalysis PBL depths to CALIPSO PBL depths averaged to the MERRA grid (bottom).

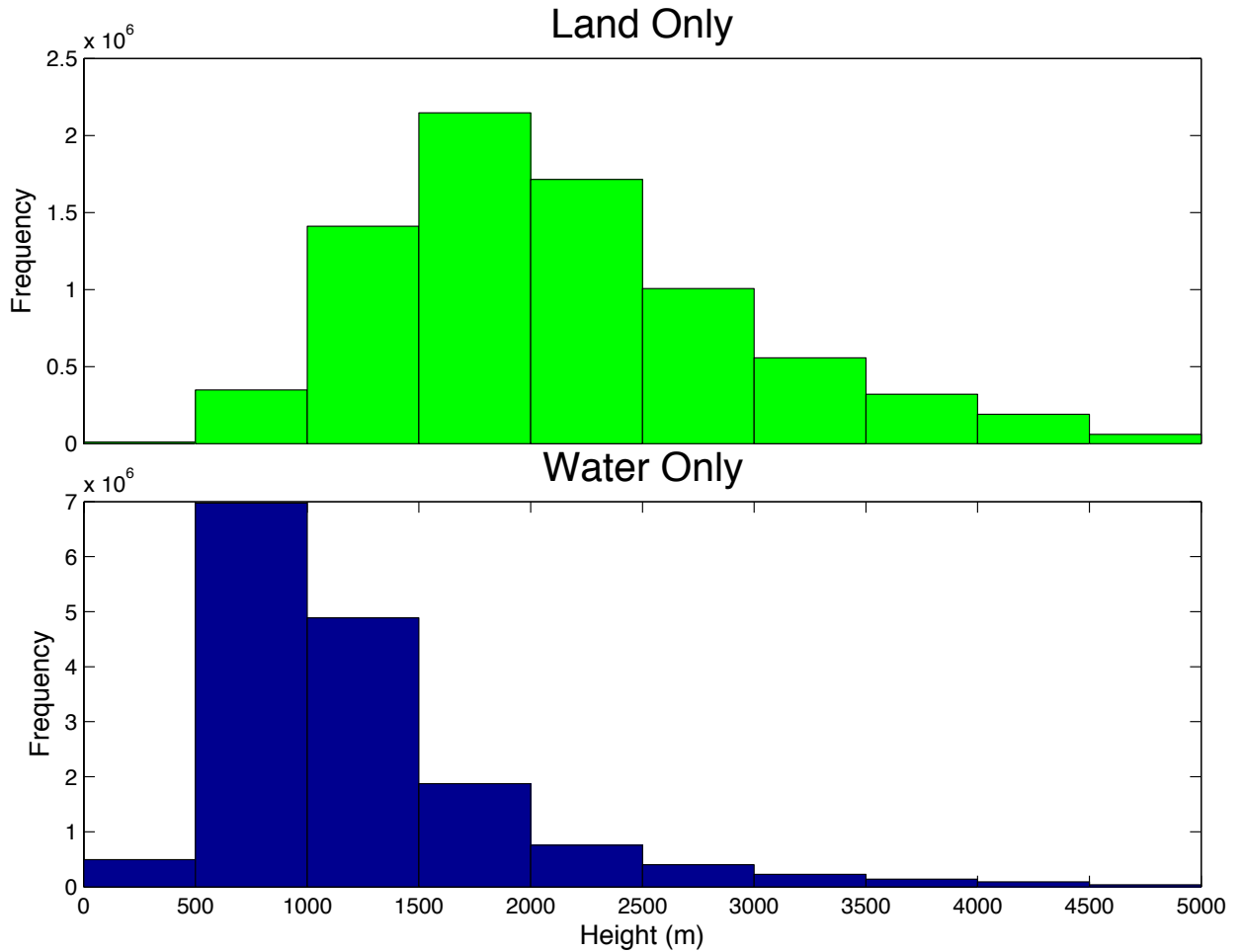


Figure 5.7 Histogram of backscatter feature depths derived from CALIPSO over land (top) and over water (bottom). The depths are from JJA 2006 – 2010.

5.4 Conclusions

The CALIPSO retrieval is successful over 75% of the time over the subtropical oceans, less than 40% over the Southwestern deserts and around 50% over the majority of the North American continent. The results show that the CALIPSO backscatter climatology is deeper over the oceans than estimates of PBL depth from reanalyses. Areas of the boreal forest with deep daytime summer PBL depths are also underestimated

in the MERRA reanalysis as compared to CALIPSO. Over the arid and semiarid complex terrain of the Southwestern United States and the Rocky Mountain region, the CALIPSO retrievals estimate a shallower PBL depth.

Initial estimates of a PBL depth using the methodology of Jordan et al. (2010) seem qualitatively reasonable. The success rate of deriving backscatter features from the CALIPSO satellite is high enough that there are millions of available observations within the limited spatial and temporal domain examined here. With enough computer resources, this analysis could be extended to provide a global PBL climatology.

Chapter 6

Conclusions

Planetary boundary layer (PBL) processes are important for air pollution, cloud formation, and precipitation among other land-atmosphere interactions and atmospheric processes. Scalars with surface sources and sinks are trapped within the daytime PBL and this produces a gradient between the PBL and the free troposphere. In addition, fluxes of carbon occur into and out of the PBL (Wofsy et al., 1988; Baker et al., 2003) and are mixed by turbulent eddies. This means that the response of carbon dioxide (CO₂) concentrations to fluxes is inversely proportional to the PBL depth (Denning et al., 1995; Yi et al., 2001; 2004) and an incorrect simulation of PBL depth can lead to errors in estimates of CO₂ fluxes in inverse models since most CO₂ measurements are made in the PBL. Therefore, understanding PBL processes is important for understanding the vertical and horizontal distribution of CO₂ (Wofsy et al., 1988; Denning et al., 1995; Yi et al., 2001; 2004; Chen et al., 2005).

However, modeling the boundary layer is hard. Most processes are unresolved by the model grid (Ayotte et al., 1996; Gerbig et al., 2003) and we do not have enough observations (temporally, spatially, or type) to compare our simulations to anyway. These observations are difficult and expensive and so they are limited. In addition, there is not yet a consensus as to how we define the boundary layer. Definitions depend on what is being used to evaluate the PBL (radiosondes, wind profilers, models, etc.) and the

person doing the evaluating. For example, radiosonde data can be evaluated by finding a temperature inversion or by finding the height at which a surface parcel becomes neutrally buoyant (among others, Seidel et al., 2010). Sometimes these methods agree, but not always.

Seemingly small processes can have large impacts and these processes depend on both the atmosphere and the surface, necessitating accurate modeling of both. If either is incorrect, the complex, nonlinear interactions feed back on one another making the other also incorrect. Because of this, more work should be done to obtain more observations of PBL processes and depth. In the meantime, simulations of vertical mixing should be optimized using the observations we do have. These challenges provide an opportunity to learn more about surface-atmosphere interactions while also producing better models of weather, climate, and the carbon cycle!

The focus of this study was to implement and evaluate an entrainment parameterization in a coupled ecosystem-atmosphere model based on a closure assumption for the heat flux at the base of the capping inversion at the top of the PBL. In addition, an observation-based measurement of PBL depth to which models can be compared was developed using data from the Cloud-Aerosol LIDAR and Infrared Pathfinder Satellite Observations (CALIPSO) satellite launched in April 2006 (Winker et al., 2007; 2009). The onboard LIDAR is sensitive to aerosols trapped within the PBL and boundary layer clouds and is therefore able to detect features that are highly correlated with the PBL top.

Chapter 2 discussed idealized simulations using the enhanced entrainment parameterization. In these simulations, the PBL was found to be warmer, drier, and

deeper when the parameterization was implemented. The changes in temperature and water vapor were found to affect surface fluxes through physiological processes in the plant canopy (McGrath-Spangler et al., 2009). These complex land-atmosphere interactions feed back on each other to dilute the surface fluxes and affect the surface conditions to which the vegetation respond.

In a realistic simulation for the late summer 1999 when PBL depth observations were available near the WLEF tower in northern Wisconsin, warmer, drier, and deeper PBL depths were found compared to a control. The simulation including enhanced entrainment also better simulated the monthly mean diurnal cycle of PBL depth. In addition, the Bowen ratio was shifted due to changes in the surface sensible and latent heat fluxes because of the vegetative response and the incoming solar radiation. The model estimate of midday PBL depth was increased by an increased morning growth rate and a 7 ppm CO₂ change over 1000 km was produced.

Chapter 4 discussed the model sensitivity to the enhanced entrainment parameterization in a realistic simulation of June 2007. The tunable parameter within the parameterization was adjusted from 0.05 to 0.4 to account for variations in the strength of entrainment. Subtle differences in the spatial patterns of atmospheric and ecological variables were found between the different simulations. The advection pattern was also altered contributing to lower CO₂ concentrations in the southeastern United States. These changes contributed to a CO₂ change of 3.5 ppm over 280 km on average over the month.

Finally, the CALIPSO satellite was used to analyze spatial patterns of 5 year mean midday summertime PBL depths. This was done by automating the Jordan et al. (2010) algorithm. The retrieval success rate was greatest over the subtropical oceans and

limited over regions with high rates of summertime convection. The retrieved PBL depths were deeper than reanalysis over the oceans and the boreal forests and shallower over the semiarid southwestern United States.

In order to understand the impact of anthropogenic carbon fluxes on natural surface sources and sinks carbon budget studies will continue to be important in the future. It is therefore important to better simulate PBL processes and vertical mixing. This work strives to better explain the impact of one PBL process on the carbon budget and the complex land-atmosphere interactions associated with the PBL. An observation-based PBL depth dataset will be able to constrain models in order to improve their simulations of the carbon budget in the future.

Possible future directions using the CALIPSO satellite include comparing the derived PBL depth to other observations, evaluating the depth globally and in different seasons, and comparing the CALIPSO PBL depth to aerosol distributions in models.

REFERENCES

- André, J., D. Moor, P. Lacarrère, G. Therry, and R. du Vachat (1978), Modeling the 24-hour evolution of the mean and turbulent structures of the planetary boundary layer, *Journal of the Atmospheric Sciences*, 35(10), 1861-1883.
- Andres, R. J., G. Marland, I. Fung, and E. Matthews (1996), A $1^\circ \times 1^\circ$ distribution of carbon dioxide emissions from fossil fuel consumption and cement manufacture, 1950 - 1990, *Global Biogeochem. Cycles*, 10(3), 419-429.
- Angevine, W. M., S. K. Avery, W. L. Ecklund, and D. A. Carter (1993), Fluxes of Heat and Momentum Measured with a Boundary-Layer Wind Profiler Radar-Radio Acoustic Sounding System, *Journal of Applied Meteorology*, 32(1), 73-80.
- Angevine, W. M., A. B. White, and S. K. Avery (1994), Boundary-layer depth and entrainment zone characterization with a boundary-layer profiler, *Boundary-Layer Meteorology*, 68(4), 375-385.
- Angevine, W. M., R. J. Doviak, and Z. Sorbjan (1994), Remote Sensing of Vertical Velocity Variance and Surface Heat Flux in a Convective Boundary Layer, *Journal of Applied Meteorology*, 33(8), 977-983.
- Angevine, W. M., P. S. Bakwin, and K. J. Davis (1998), Wind Profiler and RASS Measurements Compared with Measurements from a 450-m-Tall Tower, *Journal of Atmospheric and Oceanic Technology*, 15(3), 818-825.
- Avissar, R., and R. A. Pielke (1989), A Parameterization of Heterogeneous Land Surfaces for Atmospheric Numerical Models and Its Impact on Regional Meteorology, *Mon. Weather Rev.*, 117(10), 2113-2136.
- Avissar, R. (1991), A statistical-dynamical approach to parameterize subgrid-scale land-surface heterogeneity in climate models, *Surveys in Geophysics*, 12(1), 155-178.
- Ayotte, K. W., et al. (1996), An evaluation of neutral and convective planetary boundary-layer parameterizations relative to large eddy simulations, *Boundary-Layer Meteorology*, 79(1-2), 131-175.
- Baker, I., A. Denning, N. Hanan, L. Prihodko, M. Uliasz, P. Vidale, K. Davis, and P. Bakwin (2003), Simulated and observed fluxes of sensible and latent heat and CO₂ at the WLEF-TV tower using SiB2.5, *Global Change Biology*, 9(9), 1262-1277.

- Baker, D., et al. (2006), TransCom 3 inversion intercomparison: Impact of transport model errors on the interannual variability of regional CO₂ fluxes, 1988-2003, *Global Biogeochemical Cycles*, 20(1).
- Bakwin, P. S., P. P. Tans, D. F. Hurst, and C. Zhao (1998), Measurements of carbon dioxide on very tall towers: results of the NOAA/CMDL program, *Tellus B*, 50(5), 401-415.
- Ball, J. T., I. E. Woodrow, and B. J. A. (1987), A model predicting stomatal conductance and its contribution to the control of photosynthesis under different environmental conditions, in *Progress in Photosynthesis Research*, edited by J. Biggins, pp. 221-224, Martinus Nijhoff Publishers, Dordrecht, The Netherlands.
- Beljaars, A. C. M., and A. K. Betts (1992), Validation of the boundary layer representation in the ECMWF model, paper presented at ECMWF Seminar Proceedings: Validation of models over Europe, 7-11 September 1992.
- Berger, B. W., K. J. Davis, C. Yi, P. S. Bakwin, and C. L. Zhao (2001), Long-Term Carbon Dioxide Fluxes from a Very Tall Tower in a Northern Forest: Flux Measurement Methodology, *Journal of Atmospheric and Oceanic Technology*, 18(4), 529-542.
- Betts, A. K. (1973), Non-precipitating cumulus convection and its parameterization, *Quarterly Journal of the Royal Meteorological Society*, 99(419), 178-196.
- Betts, A. K., J. H. Ball, A. C. M. Beljaars, M. J. Miller, and P. A. Viterbo (1996), The land surface-atmosphere interaction: A review based on observational and global modeling perspectives, *J. Geophys. Res.*, 101(D3), 7209-7225.
- Beyrich, F. (1997), Mixing height estimation from sodar data--A critical discussion, *Atmospheric Environment*, 31(23), 3941-3953.
- Bonan, G. B., S. Levis, L. Kergoat, and K. W. Oleson (2002), Landscapes as patches of plant functional types: An integrating concept for climate and ecosystem models, *Global Biogeochem. Cycles*, 16(2), 1021.
- Brooks, I. M. (2003), Finding boundary layer top: application of a wavelet covariance transform to lidar backscatter profiles, *Journal of Atmospheric and Oceanic Technology*, 20(8), 1092-1105.
- Carson, D. J. (1973), The development of a dry inversion-capped convectively unstable boundary layer, *Quarterly Journal of the Royal Meteorological Society*, 99(421), 450-467.
- Chen, B., J. M. Chen, and D. E. J. Worthy (2005), Interannual variability in the atmospheric CO₂ rectification over a boreal forest region, *J. Geophys. Res.*, 110, D16301.

- Cohn, S. A., and W. M. Angevine (2000), Boundary Layer Height and Entrainment Zone Thickness Measured by Lidars and Wind-Profiling Radars, *Journal of Applied Meteorology*, 39(8), 1233-1247.
- Collatz, G. J., J. T. Ball, C. Grivet, and J. A. Berry (1991), Physiological and Environmental Regulation of Stomatal Conductance, Photosynthesis and Transpiration-A Model that Includes a Laminar Boundary Layer, *Agric. For. Meteorol.*, 54(2-4), 107-136.
- Collatz, G. J., M. Ribas-Carbo, and J. A. Berry (1992), Coupled Photosynthesis-Stomatal Conductance Model for Leaves of C4 Plants, *Australian Journal of Plant Physiology*, 19(5), 519-538.
- Conway, T. J., P. P. Tans, L. S. Waterman, K. W. Thoning, D. R. Kitzis, K. A. Masarie, and N. Zhang (1994), Evidence for interannual variability of the carbon cycle from the National Oceanic and Atmospheric Administration/Climate Monitoring and Diagnostics Laboratory Global Air Sampling Network, *J. Geophys. Res.*, 99(D11), 22831-22855.
- Corbin, K. D., A. S. Denning, L. Lu, J.-W. Wang, and I. T. Baker (2008), Possible representation errors in inversions of satellite CO₂ retrievals, *J. Geophys. Res.-Atmos.*, 113(D2).
- Corbin, K. D., A. S. Denning, E. Y. Lokupitiya, A. E. Schuh, N. L. Miles, K. J. Davis, S. Richardson, and I. T. Baker (2010), Assessing the impact of crops on regional CO₂ fluxes and atmospheric concentrations, *Tellus B*, 62(5), 521-532.
- Cotton, W. R., et al. (2003), RAMS 2001: Current status and future directions, *Meteorology and Atmospheric Physics*, 82(1), 5-29.
- Davis, K. J., D. H. Lenschow, S. P. Oncley, C. Kiemle, G. Ehret, A. Giez, and J. Mann (1997), Role of entrainment in surface-atmosphere interactions over the boreal forest, *J. Geophys. Res.*, 102(D24), 29219-29230.
- Davis, K. J., N. Gamage, C. Hagelberg, C. Kiemle, D. Lenschow, and P. Sullivan (2000), An objective method for deriving atmospheric structure from airborne lidar observations, *Journal of Atmospheric and Oceanic Technology*, 17(11), 1455-1468.
- Davis, K. J., P. S. Bakwin, C. Yi, B. W. Berger, C. Zhao, R. M. Teclaw, and J. Isebrands (2003), The annual cycles of CO₂ and H₂O exchange over a northern mixed forest as observed from a very tall tower, *Global change biology*, 9, 1278 - 1293.

- Deardorff, J. W. (1974), Three-dimensional numerical study of the height and mean structure of a heated planetary boundary layer, *Boundary-Layer Meteorology*, 7(1), 81-106.
- Denning, A. S., I. Y. Fung, and D. Randall (1995), Latitudinal gradient of atmospheric CO₂ due to seasonal exchange with land biota, *Nature*, 376(6537), 240-243.
- Denning, A. S., G. Collatz, C. Zhang, D. Randall, J. Berry, P. Sellers, G. Colello, and D. Dazlich (1996a), Simulations of terrestrial carbon metabolism and atmospheric CO₂ in a general circulation model. Part 1: Surface carbon fluxes, *Tellus Ser. B-Chem. Phys. Meteorol.*, 48(4), 521-542.
- Denning, A. S., D. A. Randall, G. J. Collatz, and P. J. Sellers (1996b), Simulations of terrestrial carbon metabolism and atmospheric CO₂ in a general circulation model Part 2: Simulated CO₂ concentrations, *Tellus B*, 48(4), 543-567.
- Denning, A. S., T. Takahashi, and P. Friedlingstein (1999), Can a strong atmospheric CO₂ rectifier effect be reconciled with a "reasonable" carbon budget?, *Tellus Ser. B-Chem. Phys. Meteorol.*, 51(2), 249-253.
- Denning, A. S., M. Nicholls, L. Prihodko, I. Baker, P. Vidale, K. Davis, and P. Bakwin (2003), Simulated variations in atmospheric CO₂ over a Wisconsin forest using a coupled ecosystem-atmosphere model, *Global Change Biology*, 9(9), 1241-1250.
- Denning, A. S., N. Zhang, C. Yi, M. Branson, K. Davis, J. Kleist, and P. Bakwin (2008), Evaluation of modeled atmospheric boundary layer depth at the WLEF tower, *Agric. For. Meteorol.*, 148(2), 206-215.
- Ecklund, W. L., D. A. Carter, and B. B. Balsley (1988), A UHF Wind Profiler for the Boundary Layer: Brief Description and Initial Results, *Journal of Atmospheric and Oceanic Technology*, 5(3), 432-441.
- Farquhar, G., S. Cammerer, and J. Berry (1980), A Biochemical-Model of Photosynthetic CO₂ Assimilation in Leaves of C₃ Species, *Planta*, 149(1), 78-90.
- Freitas, S. R., K. Longo, M. Silva Dias, P. Silva Dias, R. Chatfield, A. Fazenda, and L. F. Rodrigues (2006), The coupled aerosol and tracer transport model to the Brazilian developments on the Regional Atmospheric Modeling System: Validation using direct and remote sensing observations, paper presented at International Conference on Southern Hemisphere Meteorology and Oceanography (ICSHMO).
- Friedlingstein, P., et al. (2006), Climate-Carbon Cycle Feedback Analysis: Results from the C4MIP Model Intercomparison, *Journal Of Climate*, 19(14), 3337-3353.
- Gerbig, C., J. C. Lin, S. C. Wofsy, B. C. Daube, A. E. Andrews, B. B. Stephens, P. S. Bakwin, and C. A. Grainger (2003), Toward constraining regional-scale fluxes of

- CO₂ with atmospheric observations over a continent: 1. Observed spatial variability from airborne platforms, *J. Geophys. Res.-Atmos.*, 108(D24).
- Gerbig, C., J. Lin, S. Wofsy, B. Daube, A. Andrews, B. Stephens, P. Bakwin, and C. Grainger (2003), Toward constraining regional-scale fluxes of CO₂ with atmospheric observations over a continent: 2. Analysis of COBRA data using a receptor-oriented framework, *J. Geophys. Res.*, 108(4757), 10.1029.
- Gerbig, C., S. Körner, and J. C. Lin (2008), Vertical mixing in atmospheric tracer transport models: error characterization and propagation, *Atmospheric Chemistry and Physics*, 8(3), 591-602.
- Gurney, K., et al. (2002), Towards robust regional estimates of CO₂ sources and sinks using atmospheric transport models, *Nature*, 415(6872), 626-630.
- Gurney, K., et al. (2003), TransCom 3 CO₂ inversion intercomparison: 1. Annual mean control results and sensitivity to transport and prior flux information, *Tellus Ser. B-Chem. Phys. Meteorol.*, 55(2), 555-579.
- Gurney, K. R., D. L. Mendoza, Y. Zhou, M. L. Fischer, C. C. Miller, S. Geethakumar, and S. de la Rue du Can (2009), High Resolution Fossil Fuel Combustion CO₂ Emission Fluxes for the United States, *Environmental Science and Technology*, 43(14), 5535-5541.
- Hansen, M. C., R. S. Defries, J. R. G. Townshend, and R. Sohlberg (2000), Global land cover classification at 1 km spatial resolution using a classification tree approach, *International Journal of Remote Sensing*, 21(6), 1331-1364.
- Harrington, J. Y. (1997), The effects of radiative and microphysical processes on simulated warm and transition season Arctic stratus, Dissertation thesis, 289 pp, Colorado State University, Fort Collins.
- Houghton, R. (1999), The annual net flux of carbon to the atmosphere from changes in land use 1850-1990, *Tellus Ser. B-Chem. Phys. Meteorol.*, 51(2), 298-313.
- Jordan, N. S., R. M. Hoff, and J. T. Bacmeister (2010), Validation of Goddard Earth Observing System-version 5 MERRA planetary boundary layer heights using CALIPSO, *J. Geophys. Res.*, 115(D24), D24218.
- Kawa, S., D. Erickson III, S. Pawson, and Z. Zhu (2004), Global CO₂ transport simulations using meteorological data from the NASA data assimilation system, *J. Geophys. Res.*, 109, D18312.
- Liu, Y., C. P. Weaver, and R. Avissar (1999), Toward a parameterization of mesoscale fluxes and moist convection induced by landscape heterogeneity, *J. Geophys. Res.*, 104(D16), 19515-19533.

- Lokupitiya, E., S. Denning, K. Paustian, I. Baker, K. Schaefer, S. Verma, T. Meyers, C. J. Bernacchi, A. Suyker, and M. Fischer (2009), Incorporation of crop phenology in Simple Biosphere Model (SiBcrop) to improve land-atmosphere carbon exchanges from croplands, *Biogeosciences*, 6(6), 969-986.
- Margolis, H. A., and M. G. Ryan (1997), A physiological basis for biosphere-atmosphere interactions in the boreal forest: an overview, *Tree Physiology*, 17(8-9), 491-499.
- Marland, G., T. A. Boden, and R. J. Andres (2005), Global, regional and national CO₂ emissions, in *Trends: A compendium of Data on Global Change*, edited, Carbon Dioxide Inf. Anal. Cent., Oak Ridge Natl. Lab., U.S. Dep. of Energy, Oak Ridge, Tennessee.
- Martins, J. P. A., J. Teixeira, P. M. M. Soares, P. M. A. Miranda, B. H. Kahn, V. T. Dang, F. W. Irion, E. J. Fetzer, and E. Fishbein (2010), Infrared sounding of the trade-wind boundary layer: AIRS and the RICO experiment, *Geophys. Res. Lett.*, 37(24), L24806.
- Mattis, I., D. Müller, A. Ansmann, U. Wandinger, J. Preißler, P. Seifert, and M. Tesche (2008), Ten years of multiwavelength Raman lidar observations of free-tropospheric aerosol layers over central Europe: Geometrical properties and annual cycle, *J. Geophys. Res.*, 113, D20202.
- McGrath-Spangler, E. L., A. S. Denning, K. D. Corbin, and I. T. Baker (2009), Sensitivity of land-atmosphere exchanges to overshooting PBL thermals in an idealized coupled model, *Journal of Advances in Modeling Earth Systems*, 1(Art. #14), 13 pp.
- McGrath-Spangler, E. L., and A. S. Denning (2010), Impact of entrainment from overshooting thermals on land-atmosphere interactions during summer 1999, *Tellus B*, 62(5), 441-454.
- Medvigy, D., P. Moorcroft, R. Avissar, and R. Walko (2005), Mass conservation and atmospheric dynamics in the Regional Atmospheric Modeling System (RAMS), *Environmental Fluid Mechanics*, 5(1), 109-134.
- Melfi, S. H., J. D. Spinhirne, S.-H. Chou, and S. P. Palm (1985), Lidar Observations of Vertically Organized Convection in the Planetary Boundary Layer over the Ocean, *Journal of Climate and Applied Meteorology*, 24(8), 806-821.
- Mellor, G. L., and T. Yamada (1982), Development of a turbulence closure model for geophysical fluid problems, *Reviews of geophysics and space physics*, 20(4), 851-875.

- Mesinger, F., et al. (2006), North American Regional Reanalysis, *Bull. Amer. Meteor. Soc.*, 87(3), 343 - 360.
- Nicholls, M., A. Denning, L. Prihodko, P. Vidale, I. Baker, K. Davis, and P. Bakwin (2004), A multiple-scale simulation of variations in atmospheric carbon dioxide using a coupled biosphere-atmospheric model, *J. Geophys. Res.-Atmos.*, 109(D18).
- Okamoto, H., et al. (2007), Vertical cloud structure observed from shipborne radar and lidar: Midlatitude case study during the MR01/K02 cruise of the research vessel Mirai, *J. Geophys. Res.*, 112(D8), D08216.
- Palm, S. P., A. Benedetti, and J. Spinhirne (2005), Validation of ECMWF global forecast model parameters using GLAS atmospheric channel measurements, *Geophys. Res. Lett.*, 32(22), L22S09.
- Parazoo, N. C., A. S. Denning, S. R. Kawa, K. D. Corbin, R. S. Lokupitiya, and I. T. Baker (2008), Mechanisms for synoptic variations of atmospheric CO₂ in North America, South America and Europe, *Atmospheric Chemistry and Physics*, 8(23), 7239-7254.
- Pielke, R. A. (1974), A Three-Dimensional Numerical Model of the Sea Breezes Over South Florida, *Mon. Weather Rev.*, 102(2), 115-139.
- Pielke, R. A., and R. Avissar (1990), Influence of landscape structure on local and regional climate, *Landscape Ecology*, 4(2), 133-155.
- Pielke, R. A. (1991), Overlooked scientific issues in assessing hypothesized greenhouse gas warming, *Environmental Software*, 6(2), 100-107.
- Pielke, R. A., et al. (1992), A comprehensive meteorological modeling system—RAMS, *Meteorology and Atmospheric Physics*, 49(1), 69-91.
- Randall, D. A., Q. Shao, and M. Branson (1998), Representation of clear and cloudy boundary layers in climate models, in *Clear and Cloudy Boundary Layers*, edited by A. A. M. Holtslag and P. G. Duynkerke, pp. 305-322, Royal Netherlands Academy of Arts and Sciences, Amsterdam.
- Rayment, R., and C. J. Readings (1974), A case study of the structure and energetics of an inversion, *Quarterly Journal of the Royal Meteorological Society*, 100(424), 221-233.
- Sarmiento, J. L., J. C. Orr, and U. Siegenthaler (1992), A Perturbation Simulation of CO₂ Uptake in an Ocean General Circulation Model, *J. Geophys. Res.*, 97(C3), 3621-3645.

- Sarmiento, J. L., and E. T. Sundquist (1992), Revised budget for the oceanic uptake of anthropogenic carbon dioxide, *Nature*, 356(6370), 589-593.
- Saylor, B. J., and R. E. Breidenthal (1998), Laboratory simulations of radiatively induced entrainment in stratiform clouds, *Journal of Geophysical Research*, 103, 8827 - 8837.
- Schimel, D., I. G. Enting, M. Heimann, T. Wigley, D. Raynaud, D. Alves, and U. Siegenthaler (1995), CO₂ and the carbon cycle, in *Climate Change 1994, Radiative Forcing of Climate Change and Evaluation of the IPCC IS92 Emission Scenarios*, edited by J. T. Houghton, L. G. Meira Filho, J. Bruce, H. Lee, B. A. Callander, E. Haites, N. Harris and K. Maskell, pp. 35-71, Cambridge University Press, New York, NY.
- Seibert, P., F. Beyrich, S.-E. Gryning, S. Joffre, A. Rasmussen, and P. Tercier (2000), Review and intercomparison of operational methods for the determination of the mixing height, *Atmospheric Environment*, 34(7), 1001-1027.
- Seidel, D. J., C. O. Ao, and K. Li (2010), Estimating climatological planetary boundary layer heights from radiosonde observations: Comparison of methods and uncertainty analysis, *J. Geophys. Res.*, 115(D16), D16113.
- Sellers, P. J., Y. Mintz, Y. C. Sud, and A. Dalcher (1986), A Simple Biosphere Model (SiB) for use within General-Circulation Models, *Journal of the Atmospheric Sciences*, 43(6), 505-531.
- Sellers, P., S. Los, C. Tucker, C. Justice, D. Dazlich, G. Collatz, and D. Randall (1996), A revised land surface parameterization (SiB2) for atmospheric GCMs .2. The generation of global fields of terrestrial biophysical parameters from satellite data, *Journal of Climate*, 9(4), 706-737.
- Sellers, P., D. Randall, G. Collatz, J. Berry, C. Field, D. Dazlich, C. Zhang, G. Collelo, and L. Bounoua (1996), A revised land surface parameterization (SiB2) for atmospheric GCMs .1. Model formulation, *Journal of Climate*, 9(4), 676-705.
- Sellers, P., et al. (1997), Modeling the exchanges of energy, water, and carbon between continents and the atmosphere, *Science*, 275(5299), 502-509.
- Smagorinsky, J. (1963), General Circulation Experiments with the Primitive Equations, *Mon. Weather Rev.*, 91(3), 99-164.
- Solomon, S., D. Qin, M. Manning, Z. Chen, M. Marquis, K. B. Averyt, M. Tignor, and H. L. Miller (Eds.) (2007), *Contribution of Working Group I to the Fourth Assessment Report of the Intergovernmental Panel on Climate Change*, Cambridge University Press, Cambridge, United Kingdom and New York, NY, USA.

- Stevens, D. E., and C. S. Bretherton (1999), Effects of resolution on the simulation of stratocumulus entrainment, *Quarterly Journal of the Royal Meteorological Society*, 125(554), 425-439.
- Stull, R. B. (1976), The Energetics of Entrainment Across a Density Interface, *Journal of the Atmospheric Sciences*, 33(7), 1260-1267.
- Stull, R. B. (1988), An introduction to boundary layer meteorology, 666 pp., Kluwer Academic Publishers, Norwell, MA.
- Sullivan, P. P., C.-H. Moeng, B. Stevens, D. H. Lenschow, and S. D. Mayor (1998), Structure of the Entrainment Zone Capping the Convective Atmospheric Boundary Layer, *Journal of the Atmospheric Sciences*, 55(19), 3042-3064.
- Takahashi, T., et al. (2002), Global sea-air CO₂ flux based on climatological surface ocean pCO₂, and seasonal biological and temperature effects, *Deep Sea Research Part II: Topical Studies in Oceanography*, 49(9-10), 1601-1622.
- Tans, P. P., I. Y. Fung, and T. Takahashi (1990), Observational Constraints on the Global Atmospheric CO₂ Budget, *Science*, 247(4949), 1431-1438.
- Tripoli, G., and W. Cotton (1982), The Colorado State University three-dimensional model-1982. Part I: General theoretical framework and sensitivity experiments, *J. Rech. Atmos*, 16, 185-220.
- Walko, R. L., C. J. Tremback, J. Panetta, S. R. Freitas, and A. Fazenda (2002), RAMS Regional Atmospheric Modeling System version 5.0 model input namelist parameters, edited.
- Wang, J.-W., A. S. Denning, L. Lu, I. T. Baker, K. D. Corbin, and K. J. Davis (2007), Observations and simulations of synoptic, regional, and local variations in atmospheric CO₂, *J. Geophys. Res.-Atmos.*, 112(D4).
- Weaver, C. P., and R. Avissar (2001), Atmospheric Disturbances Caused by Human Modification of the Landscape, *Bulletin of the American Meteorological Society*, 82(2), 269-281.
- White, A. B., C. W. Fairall, and D. W. Thomson (1991), Radar Observations of Humidity Variability in and above the Marine Atmospheric Boundary Layer, *Journal of Atmospheric and Oceanic Technology*, 8(5), 639-658.
- Wiegner, M., S. Emeis, V. Freudenthaler, B. Heese, W. Junkermann, C. Münkler, K. Schäfer, M. Seefeldner, and S. Vogt (2006), Mixing layer height over Munich, Germany: Variability and comparisons of different methodologies, *J. Geophys. Res.*, 111(D13), D13201.

- Willis, G. E., and J. W. Deardorff (1974), A Laboratory Model of the Unstable Planetary Boundary Layer, *Journal of the Atmospheric Sciences*, 31(5), 1297-1307.
- Winker, D. M., W. H. Hunt, and M. J. McGill (2007), Initial performance assessment of CALIOP, *Geophys. Res. Lett.*, 34(19), L19803.
- Winker, D. M., M. A. Vaughan, A. Omar, Y. Hu, K. A. Powell, Z. Liu, W. H. Hunt, and S. A. Young (2009), Overview of the CALIPSO Mission and CALIOP Data Processing Algorithms, *Journal of Atmospheric and Oceanic Technology*, 26(11), 2310-2323.
- Wofsy, S. C., R. C. Harriss, and W. A. Kaplan (1988), Carbon Dioxide in the Atmosphere Over the Amazon Basin, *J. Geophys. Res.*, 93(D2), 1377-1387.
- Yi, C., K. Davis, P. Bakwin, B. Berger, and L. Marr (2000), Influence of advection on measurements of the net ecosystem-atmosphere exchange of CO₂ from a very tall tower, *Journal of Geophysical Research*, 105(D8), 999.
- Yi, C., K. Davis, B. Berger, and P. Bakwin (2001), Long-term observations of the dynamics of the continental planetary boundary layer, *Journal of the Atmospheric Sciences*, 58(10), 1288-1299.
- Yi, C., K. Davis, P. Bakwin, A. Denning, N. Zhang, A. Desai, J. Lin, and C. Gerbig (2004), Observed covariance between ecosystem carbon exchange and atmospheric boundary layer dynamics at a site in northern Wisconsin, *J. Geophys. Res.-Atmos.*, 109(D8).
- Zhang, N. (2002), Observations and simulations of the planetary boundary layer at a tall tower in northern Wisconsin, Master's thesis, 71 pp, Colorado State University, Fort Collins.
- Zupanski, D., A. S. Denning, M. Uliasz, M. Zupanski, A. E. Schuh, P. J. Rayner, W. Peters, and K. D. Corbin (2007), Carbon flux bias estimation employing maximum likelihood ensemble filter (MLEF), *J. Geophys. Res.-Atmos.*, 112(D17).